Generating mammalian mitochondrial disease models with mitochondrial DNA mutations

INAUGURAL-DISSERTATION

zur
Erlangung des Doktorgrades
der Mathematisch-Naturwissenschaftlichen
der Universität zu Köln

vorgelegt von

Johanna Heta Katariina Kauppila, geborene Lampinen

Aus Valkeakoski, Finnland

Köln 2018

I

Berichterstatter:

Prof. Dr. Nils-Göran Larsson
Prof. Dr. Aleksandra Trifunovic

Tag der mündlichen Prüfung: 20.6.2018

II

Table of Contents

ABBREVATIONS

2D-AGE	Two-dimensional agarose gel electrophoresis
3'	3' end
5'	5' end
5'dRP	5'deoxyribose phosphate
8-oxo-dG	8-oxoguanine
AP	Abasic site
APE1	Human apurinic/apyrimidinic (AP) endonuclease
ATP	Adenosine triphosphate
B[a]P	Benzo[a]pyrene
BER	Base excision repair
BN-PAGE	Blue native polyacrylamide gel electrophoresis
bp	Base pair
BSA	Bovine serum albumin
CI	Complex I, NADH dehydrogenase
CII	Complex II, succinate dehydrogenase
CIII	Complex III, Cytochrome c reductase
CIV	Complex IV, Cytochrome C oxidase
CoRR	Colocalization for redox regulation
COX	Cytochrome c oxidase
CPEO	Chronic progressive external ophthalmoplegia
cryo-EM	Cryo electron microscopy
CS	Citrate synthase
CSB	Cockayne Syndrome group B
CV	Complex V, ATP synthetase
CytC	Cytochrome C
D-loop	Displacement loop
DNA	Deoxyribonucleic acid
dNTP	Deoxyribonucleotide
dsDNA	Double-stranded DNA
EDTA	(Ethylenedinitrilo)tetraacetic acid
EGTA	Ethylene-bis(oxyethylenenitrilo)tetraacetic acid
ENU	N-ethyl-N-nitrosourea
ESC	Embryonic stem cell
EtBr	Ethidium bromide
ETF	Electron-transferring-flavoprotein
FEN1	Flap endonuclease 1
FRT	FRT Flippase recognition site
HSP	Heavy-strand promoter
kB	Kilobase
LHON	Leber's hereditary optic neuropathy
LSP	Light strand promoter
MB	Megabase
MELAS	Mitochondrial myopathy, encephalopathy, lactic acidosis, and stroke-like episodes
MERRF	Myoclonic epilepsy and ragged-red fibers
MGME1	Mitochondrial genome maintenance exonuclease 1
MIDD	Maternally inherited diabetes and deafness
MMR	Mismatch repair
mRNA	Messenger RNA
MRO	Mitochondrion-related organelles
MRPP1	Mitochondrial ribonuclease P protein 1
MRPS34	Mitochondrial ribosomal protein S34
mtDNA	Mitochondrial DNA
MTERF1	Mitochondrial transcription termination factor 1
MTS	Mitochondrial targeting sequence
mtSSB	Mitochondrial single-stranded DNA binding protein
MUTYH	MutY homolog
NADH	Nicotinamide adenine dinucleotide

ND6	NADH dehydrogenase 6
NEIL1	Endonuclease VIII-like 1
NEIL2	Endonuclease VIII-like 2
NER	Nucleotide excision repair
NHEJ	Non-homologous end joining
NTH1	Endonuclease III-like protein 1
NTP	Ribonucleotide
NuMTs	Nuclear mitochondrial DNA segment
OGG1	8-oxoguanine DNA glycosylase 1
OriH	Origin of heavy strand replication
OriL	Origin of light strand replication
OXPHOS	Oxidative phosphorylation system
PAGE	Polyacrylamide gel electrophoresis
PAM	Presequence translocase-associated motor
pAM1	Plasmid with mouse mitochondrial DNA
PCR	Polymerase chain reaction
PEN	Polyethylenenaphthalate
PFA	Paraformaldehyde
PMG	Pyruvate glutamate malate
PNKP	Polynucleotide phosphatase /kinase
Pol G	DNA polymerase γ
POLRMT	DNA-directed RNA polymerase, mitochondrial
PVDF	Polyvinylidene difluoride
RITOLS	Ribonucleotide incorporated through the lagging strand
RMC	Random mutation capture assay
RNA	Ribonucleic acid
ROS	Reactive oxygen species
rRNA	Ribosomal RNA
SDH	Succinate dehydrogenase
SDS	Sodium dodecyl sulfate
SDS-PAGE	Sodium dodecyl sulfate polyacrylamide gel electrophoresis
SOD1	Superoxide dismutase 1
SOD2	Superoxide dismutase 2
ssDNA	Single-stranded DNA
SUCC	Succinate
TALEN	Transcription activator-like effector nuclease
TAS	Termination associated sequence
TBS	Tris-buffered saline
TE	Tris-EDTA
TEFM	Mitochondrial transcription elongation factor
TFAM	Mitochondrial transcription factor A
TFB2M	Mitochondrial transcription factor B2
TIM23	Presequence translocase of the inner membrane
TOM20	Translocase of the outer membrane
Tris	Tris(hydroxymethyl)aminomethane
tRNA	Transfer RNA
TRNT1	TRNA-nucleotidyltransferase 1
Tween 20	Polysorbate 20
TWINKLE	Mitochondrial DNA helicase
UNG1	Uracil-DNA glycosylase
WANCY-COX1	Region with $tRNA^W$, $tRNA^A$, $tRNA^N$, $tRNA^C$, $tRNA^Y$ $cox1$ genes in mitochondrial DNA

Amino Acid	Abbreviation	Symbol
Alanine	Ala	A
Arginine	Arg	R
Asparagine	Asn	N
Aspartate	Asp	D
Cysteine	Cys	C
Glutamate	Glu	E
Glutamine	Gln	Q
Glycine	Gly	G
Histidine	His	H
Isoleucine	Ile	I
Leucine	Leu	L
Lysine	Lys	K
Methionine	Met	M
Phenylalanine	Phe	F
Proline	Pro	P
Serine	Ser	S
Threonine	Thr	T
Tryptophan	Trp	W
Tyrosine	Tyr	Y
Valine	Val	V

ZUSAMMENFASSUNG

Mitochondrien sind lebenswichtige zelluläre Organellen, die bei einer Vielzahl zellulärer Prozesse, wie zum Beispiel bei der Energieumwandlung, der Synthese von Eisen-Schwefel-Clustern und der β-Oxidation von Fettsäuren eine wichtige Rolle spielen. Obwohl die überwiegende Mehrzahl mitochondrialer Proteine durch die nukleäre DNA codiert und post-translational in Mitochondrien transportiert wird, enthalten Mitochondrien ihre eigene DNA, die sogenannte mitochondriale DNA (mtDNA), welche für die Funktion der Mitochondrien unerlässlich ist. Die mtDNA von Säugetieren codiert für 2 rRNAs und 22 tRNAs, die für die Translation von 11 Protein-codierenden mRNAs benötigt werden, die ebenfalls durch die mtDNA codiert werden. Die so codierten Proteine sind zentraler Bestandteil des Prozesses der oxidativen Phosphorylierung (OXPHOS), von daher können pathogene mtDNA-Mutationen zu drastischen Energiestoffwechsel-Defizit-Erkrankungen, den sogenannten Mitochondriopathien, führen. Diese sind durch pleiotrope Symptome, wie zum Beispiel progressive Neurodegeneration, Muskelschwäche, Epilepsie, Schlaganfall und diverse Arten von Myopathien gekennzeichnet.

Trotz intensiver Forschung ist die Genotyp-Phänotyp-Korrelation und die Gewebesspezifität mitochondrialer Erkrankungen bisher noch ungeklärt. Ein umfassendes molekulares Verständnis dieser Erkrankungen wurde durch die limitierte Anzahl adäquater Tiermodelle erschwert. Da eine effiziente Modifizierung der mtDNA mittels gängiger molekularbiologischer Techniken nicht möglich ist, wurden diese Tiermodelle durch die Einführung von in Zelllinien entdeckten Mutationen in murine embryonale Stammzellen generiert. In der vorliegenden Dissertation werden zwei genetische Methoden zur Einführung endogener Mutationen in die mtDNA vorgestellt. Für beide Strategien wurden natürliche Quellen möglicher mtDNA Mutationen verwendet, zum einen Replikationsfehler und zum anderen die oxidative Schädigung der mtDNA. Im ersten Ansatz wird eine mutierte Version der DNA-Polymerase γ mit reduzierter Korrekturlesefunktion eingesetzt um die mtDNA zu mutieren. Im zweiten Ansatz wird die mitochondriale DNA-Reparatur vermindert um so einen Anstieg der mtDNA-Mutationen zu erreichen, die durch oxidativen Stress verursacht werden. Hierbei wird die mitochondriale DNA-Reparaturmaschinerie durch die fehlende mitochondriale Lokalisation der zwei Basen-Exzisions-Reparaturenzyme OGG1 und MUTYH beeinträchtigt.

Im ersten Ansatz wurden maternale Linien mit einer limitierten Anzahl von mtDNA-Mutationen generiert, indem heterozygote weibliche Mäuse mit reduzierter Korrekturlesefunktion der DNA-Polymerase γ (mtDNA-Mutator-Mäuse) für eine Generation gezüchtet wurden. Die Identifizierung der induzierten pathogenen mtDNA-Mutationen erfolgte mittels einer neuen Strategie, einem Screening auf Funktionsstörungen der Atmungskette in Colonkrypten der *Founder*-Mäuse. mtDNA-Mutationen können in den Colonkrypten schnell klonal expandieren und erreichen so Heteroplasmie-Level, die ausreichend hoch sind, um eine

OXPHOS-Funktionsstörung hervorzurufen. Dies ermöglicht einen einfachen und frühzeitigen Nachweis von Mauslinien, die pathogene mtDNA-Mutationen tragen. Mit diesem experimentellen Ansatz wurde eine Maus identifiziert, die eine C5024T Mutation im mitochondrialen *tRNA^{ALA}*-Gen aufwies. Diese tRNA^{ALA}-Mäuse zeigen die für die klassischen mitochondrialen Erkrankungen üblichen charakteristischen molekularen Phänotypen, wie zum Beispiel eine verringerte Stabilität des mutierten tRNA^{ALA}-Transkripts, eine Beeinträchtigung der mitochondrialen Translation sowie das Vorhandensein von Zellen mit Atmungskettendefekten. Zusammengefasst ist festzustellen, dass die Verwendung heterozygoter mtDNA-Mutator-Mäuse in Kombination mit dem Screening für pathogene Mutationen in Colonkrypten ein erfolgreicher Ansatz ist um Mausmodelle zur Erforschung der Mitochondrien zu erzeugen.

Erstaunlicherweise führte der zweite erbgutverändernde Ansatz, die Beeinträchtigung der Basen-Exzisions-Reparatur (BER) in Mitochondrien, zu keinem Anstieg der mtDNA-Mutationen, auch nicht bei älteren Mäusen. Da vermutet wird, dass die DNA-Reparatur in Keimzellen von besonderer Bedeutung ist, wurden die BER-defizienten Mäuse für fünf konsekutive Generationen als homozygote maternale Linie gezüchtet. Jedoch wurde auch in diesen Mäusen kein Anstieg der mtDNA-Mutationen festgestellt. Zur Erhöhung des oxidativen Stresses in diesen Tieren wurden sie mit gewebsspezifischen Superoxid Dismutase 2 (SOD2) *Knockout*-Mäusen verpaart. Die Herz-spezifischen *Sod2-Knockout*-Mäuse zeigen einen eindeutigen Anstieg der Superoxid-Konzentration, der sich in Form eines Aktivitätsverlusts der Aconitase und einer Vielzahl von Veränderungen der mitochondrialen Funktion zeigt. In den BER-defizienten, Herz-spezifischen *Sod2 Knockout*-Mäusen wurde jedoch kein Anstieg der mtDNA- oder mtRNA-Mutationen festgestellt. Diese Ergebnisse zeigen, dass zum einen die BER-Defizienz kein praktikabler Ansatz ist um Mutationen in der mtDNA zu induzieren. Zum anderen sollte die Bedeutung des oxidativen Stresses für die Entstehung von mtDNA-Mutationen neu bewertet werden. Als Hauptursache für mtDNA-Mutationen sollte der Fokus auf Replikationsfehler gerichtet werden, sowohl in der Alternsforschung als auch in Modellen mitochondrialer Erkrankungen.

ABSTRACT

Mitochondria are vitally important cellular organelles that are instrumental to many cellular functions such as energy conversion, iron-sulfur cluster synthesis and β-oxidation of fatty acids. Although, the vast majority of mitochondrial proteins are encoded by the nuclear DNA and transported into mitochondria post-translationally, mitochondria also contain their own DNA, mitochondrial DNA (mtDNA), which is essential for mitochondrial function. Mammalian mtDNA encodes 2 rRNAs and 22 tRNAs that are required to translate the 11 protein-coding mRNAs encoded by mtDNA. The encoded proteins are essential components of the oxidative phosphorylation system (OXPHOS) and therefore pathogenic mtDNA mutations can lead to drastic energy deficiency disorders with typically pleiotropic symptoms including progressive neurodegeneration, muscle weakness, epilepsy, stroke and different type of myopathies.

Despite extensive research, the genotype-phenotype correlations and tissue specificity of mitochondrial disorders remain still an enigma. Comprehensive molecular understanding of these diseases has been hindered by the limited number of animal models available for research. Because mtDNA cannot be efficiently modified with molecular-biology techniques, the main strategy to generate these animal models has been a to introduce mutations found in cell lines into mouse ES cells. In this thesis, two genetic approaches are presented to introduce endogenous mutations to mtDNA. These strategies utilized both natural sources of mtDNA mutations, namely replication errors and oxidative damage to mtDNA. In the first approach, proofreading-deficient DNA polymerase γ is utilized to mutate mtDNA and in the second approach, mitochondrial DNA repair is impaired to increase the prevalence of oxidative stress driven mutations. The repair is impaired by abolishing the mitochondrial localization of two base-excision repair glycosylases, OGG1 and MUTYH.

In the first approach, maternal lineages carrying limited number of mtDNA mutations were generated by breeding the heterozygous proofreading deficient female mice (mtDNA mutator mice) for one generation. Next, the induced pathogenic mtDNA mutations were identified via a new strategy, by screening the colonic crypts of the founder mice for respiratory chain dysfunction. The mtDNA mutations can rapidly clonally expand in colonic crypts to reach heteroplasmy levels high enough to induce OXPHOS dysfunction, which allows a straight-forward and early detection of mouse lineages that carry pathogenic mtDNA mutations. With this approach, a founder mouse was identified that carried a C5024T mutation in mitochondrial *tRNA*^{ALA} gene. These tRNA^{ALA} mice display typical molecular phenotypes seen in classical mitochondrial diseases, i.e. decreased stability of the mutated tRNA^{ALA} transcript, impaired mitochondrial translation and presence of respiratory chain deficient cells. In summary, the results show that heterozygous mtDNA mutator mice in combination with colonic-crypt screening for pathogenic mutations, is a successful approach to generate mouse models for mitochondrial research.

Surprisingly, the second mutagenic approach, using dysfunctional base-excision repair (BER) in mitochondria, did not result into an increase in mtDNA mutation load even when the mice were aged. As DNA repair is suggested to be especially important in the germ line and the BER deficient mice were therefore bred for five consecutive generation as a homozygote maternal line. However, no increase mtDNA mutation load was detected also in these mice. To increase prevalence of oxidative stress in these animals they were bred with tissue specific superoxide dismutase 2 (SOD2) knockout mice. The heart *Sod2* knockout mice show a clear increase in superoxide levels demonstrated by loss of aconitase activity and a plethora of changes in mitochondrial function. However, no increase in mtDNA or mtRNA mutation load was detected in the repair deficient heart *Sod2* knockout mice. These results demonstrate that firstly BER deficiency is not a feasible approach to introduce mutations to mtDNA and secondly that the importance of oxidative stress as a contributor to mtDNA mutation load should be re-evaluated. Instead, in both ageing research and mitochondrial disease models, we should focus on replication errors as the source of mtDNA mutations.

INTRODUCTION

1.1 MITOCHONDRIA AND MITOCHONDRIAL DNA: EVOLUTION AND ORIGIN

The mitochondrion is a cellular organelle that was formed when an α-proteobacterium fused with another cell, likely of archaeal origin (Gray, 2012). According to the commonly accepted hydrogen hypothesis (Martin and Müller, 1998) the symbiotic nature was maintained because the facultative proteobacterium provided hydrogen as the byproduct of anaerobic respiration to the hydrogen dependent host. The ancestral α-proteobacterium was likely Rickettsiales, current representative of which have a small circular genome, suggesting that the fusing bacterium could also have had one (Lavrov and Pett, 2016).

With time mtDNA has evolved to various sizes in different organisms. In most bilaterians mtDNA is a so called "typical animal DNA", i.e. a single small circular molecule with almost fixed gene content and order. In mammals, mtDNA is an ~16kb double-stranded circle that encodes two rRNAs, 22 tRNAs and 11 mRNAs containing 13 protein-coding open reading frames (Figure 1.1). Mammalian mtDNA is typically intronless and contain only a small amount of noncoding material (Lavrov and Pett, 2016). However, in different life forms the size of mtDNA can vary from few kb up to several Mb, e.g. in cucumber the mtDNA is an impressive molecule of ~1.6 Mb (Smith and Keeling, 2015). Additionally, mtDNA can be linear or circular, and it can consist of one or multiple separate molecules. Some genomes have large introns that encompass even other mitochondrial genes such as ND5 in hexacorals (Emblem et al., 2014). Furthermore, one gene can even be separated into two chromosomal molecules such as the gene encoding for the large subunit ribosomal RNA (rRNA) in some sponges (Lavrov and Pett, 2016).

Through evolution the gene content of mtDNA has decreased extensively from the genome of ancestral α-proteobacterium. Naturally, a genetic endosymbiont does not require all the genes that are present in a free-living bacterium e.g. genes that encode for the bacterial cell wall (Adams and Palmer, 2003). In most species encodes mitochondrial rRNAs, at least some tRNAs and a few mRNAs encoding core components of the respiratory chain. (Lavrov and Pett, 2016). Most proteobacterial genes have either been lost or transferred to the nucleus and, thus more than 99% of the mitochondrial proteins are encoded by nuclear DNA and imported into mitochondria after cytosolic translation (Foster et al., 2006; Pagliarini et al., 2008). Only around 35 % of the imported proteins in mice and humans are encoded from genes with proteobacterial origin (Pagliarini et al., 2008). Others are of nuclear origin or have emerged through horizontal gene transfer like many mtDNA maintenance proteins (Shutt and Gray, 2006). In some species, almost all mitochondrial tRNA genes are encoded from the nuclear

DNA and therefore need to be imported into mitochondria for functional translation to occur (Wang and Lavrov, 2008).

Figure 1.1 Mammalian mitochondrial DNA. Mammalian mtDNA is small, circular genome. It encodes for 11 mRNAs, 22 tRNAs and two ribosomal RNAs. Annual review of biochemistry by ANNUAL REVIEWS. Reproduced with permission of ANNUAL REVIEWS in the format Thesis/Dissertation via Copyright Clearance Center. License Number: 4365500499308.

One could ask why it is beneficial to maintain the genes of mitochondrial proteins in nuclear DNA instead of mtDNA? Many reasons have been put forward (Adams and Palmer, 2003) and they commonly include the avoidance of irreversible buildup of deleterious mutations to a uniparentally inherited genome (Müllers ratchet) (Blanchard and Lynch, 2000; Muller, 1964), protection from mitochondrial mutagens such as the byproducts of the respiration chain function and more efficient fixation of beneficial mutations (Adams and Palmer, 2003). The other obvious question is then, why respiring mitochondria have retained their own genome? It seems rather wasteful to import the whole machinery to maintain, transcribe and translate only 13 protein-coding genes. Just the mitochondrial ribosome alone contains around 80 proteins (Greber and Ban, 2016). Several, non-mutually exclusive, hypotheses have been put forward to explain the retention of mtDNA (Adams and Palmer, 2003; Allen, 2015). One of them suggests that mtDNA gene loss is a random ongoing process and the present mitochondrial gene content is only coincidental (Johnston and Williams, 2016). An argument against this hypothesis is the notion that most mitochondrially encoded proteins are highly hydrophobic, which is also one of the hypothesis explaining why they are still encoded from the mtDNA. It has been suggested that due to their hydrophobicity their import and sorting across the

2

membrane could be difficult (Popot and de Vitry, 1990). Experiments with complex IV (COX) protein COX2 from soybean are supporting this hypothesis (Daley et al., 2002). Soybean contains two active *cox2* genes one in nuclear and one in mtDNA. When the mtDNA-coded COX2 variant was produced *in vitro* its mitochondrial import was successful only when the hydrophobicity of the first transmembrane helix was decreased through mutagenesis. Interestingly, import of the nuclear DNA-coded COX2 variant was additionally blocked if the amino acids in the first transmembrane helix were changed to those found in the mitochondrial variant. This suggests that decreasing hydrophobicity could enable successful gene transfer to nucleus. Another hypothesis for mtDNA retention suggests that the difference in genetic code retains some genes in mtDNA (Adams and Palmer, 2003). Accordingly, some nonfunctional nuclear copies of mitochondrial genes can be found in nuclear DNA. They are called NuMTs (nuclear mitochondrial DNA segment) and their co-amplification during PCR amplification for mitochondrial genes is an issue.

The most recent hypothesis for gene retention in mitochondria is the co-localization for redox regulation (CoRR)-hypothesis (Allen, 2015). The CoRR hypothesis builds on the notion that the retained protein-coding genes encode the core components of the respiratory chain. Therefore, when these genes are retained in mtDNA, it enables localized redox driven gene expression of the crucial components of OXPHOS (oxidative phosphorylation system). Furthermore, this hypothesis suggests that mtDNA retention allows specific and dynamic optimization of the mitochondrial network in changing situations.

After discussing the retention of mtDNA, it should be mentioned that there are mitochondria that lack mtDNA altogether. These organelles are called mitochondrion-related organelles (MROs). Even without mtDNA, some MROs are still able to generate ATP albeit not through respiration (Gray, 2012). A common feature among MROs is the maintenance of Fe-S cluster formation that is thus considered the most critical function of mitochondria (Tovar et al., 2003).

1.2 MITOCHONDRIA: ARCHITECTURE AND FUNCTION

Mitochondria are surrounded by two phospholipid bilayers called inner and outer membrane. The inner membrane folds and forms invaginations, called cristae, which protrude to the mitochondrial matrix and extend the available membrane space (Figure 1.2). As mtDNA has only 13 protein-coding genes, the vast majority of the ~1500 mitochondrial proteins are encoded from the nuclear DNA, translated in cytosol and imported into mitochondria in a precursor form (Figure 1.2) (Foster et al., 2006; Pagliarini et al., 2008). Currently, five protein-import pathways have been described which transport proteins into different mitochondrial compartments, i.e. outer membrane, inner membrane, intermembrane space and matrix (reviewed in (Wiedemann and Pfanner, 2017)). These pathways have been initially characterized in yeast but they are conserved in higher eukaryotes as well (Dudek et al., 2013). The classical protein import pathway (TOM20-TIM23-PAM) translocates proteins with a cleavable N-terminal presequence to matrix and inner membrane (Wiedemann and Pfanner,

2017). Vast majority of matrix and some intermembrane proteins contain this N-terminal presequence (mitochondrial targeting sequence, MTS) (Calvo et al., 2017; Vögtle et al., 2009). Other mitochondrial proteins harbor an internal targeting signal and they are imported into mitochondria with the other import pathways. The imported proteins are highly important not only to ATP production through OXPHOS but also to other vital mitochondrial functions such as iron-sulfur cluster biosynthesis, initiation of apoptosis, amino acid metabolism, β-oxidation, TCA cycle and membrane lipid biosynthesis. In addition to protein import, mitochondrial protein content in a given mitochondrion can also be mixed through fusion with other mitochondria. Mitochondria are not separate cellular organelles (reviewed in (Chan, 2012)), but rather they form a dynamic mitochondrial network that is in constant state of fission and fusion. This dynamic nature of mitochondria allows mixing of metabolic, proteomic and genomic content.
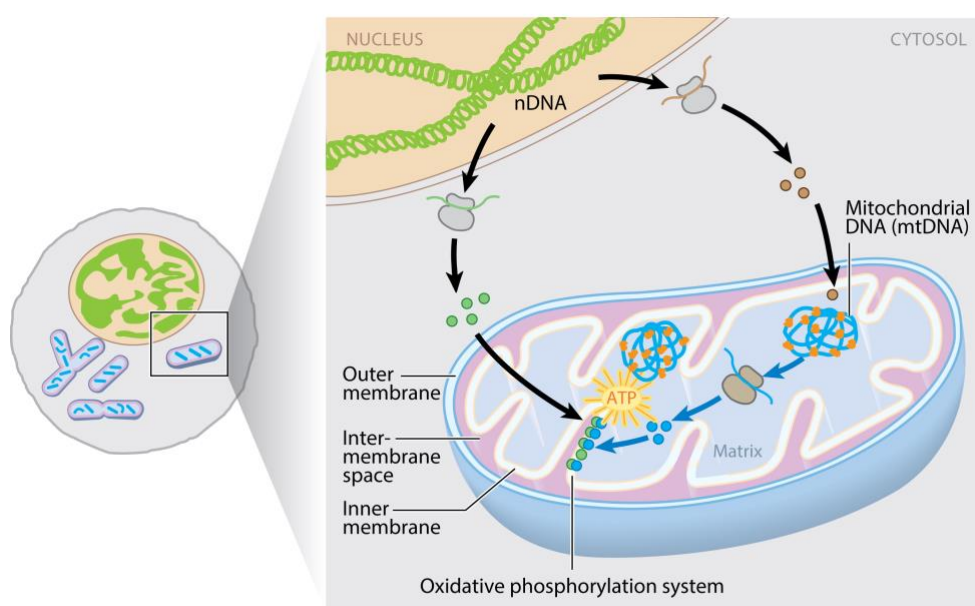
Gustafsson CM, et al. 2016.
Annu. Rev. Biochem. 85:133–60

Figure 1.2 Mitochondrial proteome. Majority of mitochondrial proteins are encoded by nuclear genes and imported into mitochondria post translationally (~1500 proteins). Only core components of the oxidative phosphorylation system are encoded in mtDNA and translated on mitochondrial ribosome. Annual review of biochemistry by ANNUAL REVIEWS. Reproduced with permission of ANNUAL REVIEWS in the format Thesis/Dissertation via Copyright Clearance Center. License Number: 4365501099330.

1.2.1 Oxidative phosphorylation system

ATP production through the oxidative phosphorylation system is one of the key functions of mitochondria. The process in well-established and reviewed for example in these papers (Hatefi, 1985; Schultz and Chan, 2001). It can be divided into two parts; respiratory chain function and ATP production. In the respiratory chain, the respiratory chain complexes, (I to IV) form a chain, as indicated by their name, where electrons are transferred from the initial substrate (NADH or succinate) to molecular oxygen with the help of electron carrier molecules (coenzyme Q, and cytochrome C) (Figure 1.3). In each respiratory chain complex, apart from

4

complex II, the substrate oxidation is coupled with proton extrusion from mitochondrial matrix to the intermembrane space. This extrusion builds up electrochemical gradient (ΔpH and proton gradient), which is then used by the ATP synthetase (complex V) to convert ADP to ATP. Complexes I, III, IV and V are under dual genetic control as their subunits are encoded in both mitochondrial and nuclear DNA.
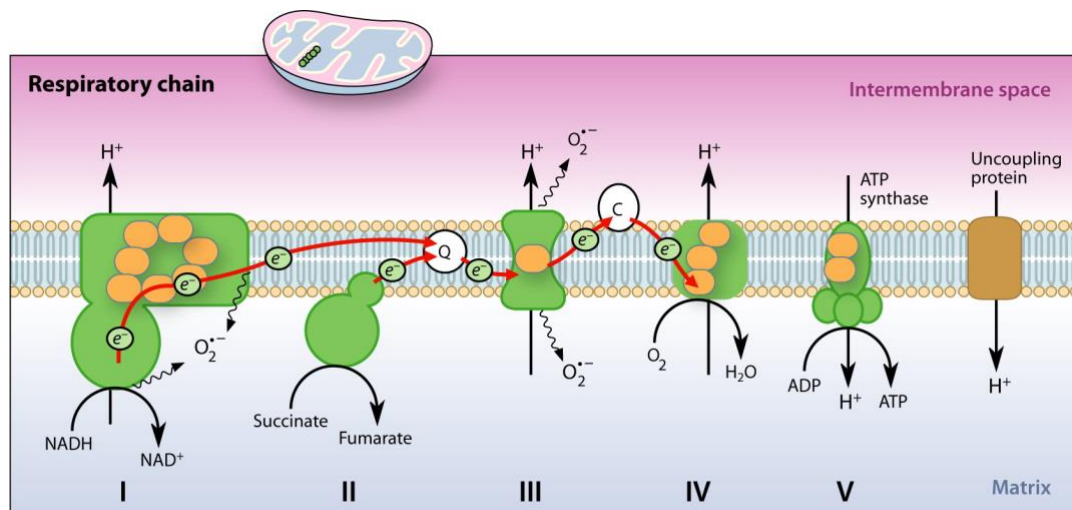
Figure 1.3 Oxidative phosphorylation system. The electron transfer is coupled with proton extrusion to the intermembrane space to build up electrochemical gradient, which is then used by the ATP synthase to convert ADP to ATP. OXPHOS complexes I, III, IV and V are under dual genetic control. Most of their subunits are encoded in the nuclear DNA but the core subunits (marked in orange) are encoded in mtDNA. Annual review of biochemistry by ANNUAL REVIEWS. Reproduced with permission of ANNUAL REVIEWS in the format Thesis/Dissertation via Copyright Clearance Center. License Number: 4365500499308.

The first complex in the respiratory chain is complex I (NADH dehydrogenase), which oxidizes mitochondrial NADH and transfers electrons through series of iron-sulfur clusters to coenzyme Q. Alternatively, electrons can enter respiratory chain at the level of coenzyme Q from oxidation of succinate by complex II (succinate dehydrogenase), from cytosolic NADH through glycerol-3-phosphate dehydrogenase and from β-oxidation through ETF dehydrogenase (Alcázar-Fabra et al., 2016). Reduced coenzyme Q then carries the electrons to complex III (cytochrome c reductase), which further delivers them to the cytochrome c electron carrier. Cytochrome c transfers then the electrons to complex IV (cytochrome c oxidase), which finally reduces molecular oxygen to water.

Studies with Blue-Native PAGE has revealed that the respiratory complexes are not only single entities in mitochondrial inner membrane but a fraction of them are organized into supercomplexes (Schägger and Pfeiffer, 2000), composed of various combinations of respiratory complexes such as CI/CIII$_2$/ CIV$_{1-4}$ and CIII$_2$/CIV$_{1-2}$. It is still debated why complexes are organized this way. The most common argument is that the close proximity of the complexes would enhance catalysis through substrate channeling. However, recently published cryo-EM structures do not strongly support this theory (Milenkovic et al., 2017).

1.3 REACTIVE OXYGEN SPECIES

1.3.1 Formation in mitochondria

A small fraction of the transferred electrons leak during OXPHOS and react with free oxygen leading to formation of superoxide ($O_2^{\bullet-}$). Superoxide can be converted either spontaneously, enzymatically or though reaction with other radicals to other reactive oxygen species (ROS) such as hydrogen peroxide (H_2O_2) or peroxynitrate (NOO^-) (Table 1.1). It was previously proposed that ~1-2% of all oxygen used during OXPHOS was converted into H_2O_2 (Boveris et al., 1972), but this is likely an overestimation and the levels of H_2O_2 production during respiration are probably at least an order of magnitude lower (Hansford et al., 1997). The main superoxide production sites are complex I and complex III (Murphy, 2009) (Figure 1.3). Even though the respiratory chain is considered to produce largest fraction of cellular ROS, it should be mentioned that OXPHOS is not the only electron transfer reaction that can produce ROS in the cell, e.g. monoamine oxidases and α-ketoglutarate dehydrogenase complex are also potential electron donors (Andreyev et al., 2005). Additionally, NADPH oxidases produce superoxide even enzymatically in a response to cellular stimuli (Meitzler et al., 2014).

Table 1.1 Various reactive oxygen species (ROS) and their properties. Table modified from (Das and Roychoudhury, 2014). Additional reference (Halliwell, 2006).

ROS	$t_{1/2}$	Migration distance	Mode of action	Reaction with DNA	Reaction with protein
Superoxide ($O_2^{\bullet-}$)	1-4 μs	30 nm	Reacts with other radicals and Fe-S clusters	no	Via the Fe-center
Hydroxyl radical ($OH^{\bullet}$)	1 μs	1 nm	Extremely reactive with all biomolecules	Rapidly reacting	Rapidly reacting
Hydrogen peroxide (H_2O_2)	1 ms	1 μm	Oxidizes redox sensitive proteins, forms $OH^{\bullet}$ through Fenton reaction	no	Reactions with redox sensitive proteins, e.g. on Cys-residues

Adapted from Das et al., 2014

Many lines of defense are in place in cell to neutralize ROS before they can react uncontrollably with cellular macromolecules. In mitochondria, superoxide dismutase enzymes (SOD) quickly dismutate the produced superoxide to H_2O_2 and thus provide an important ROS defense mechanism (Murphy, 2009). SOD2 dismutates the superoxide that has been produced to the matrix side and SOD1 the one in the intermembrane space (Weisiger and Fridovich, 1973). If superoxide persists, it can react with [4Fe-4S] clusters resulting in the release of iron (Flint et al., 1993). The released iron can then, in turn, react with H_2O_2 through Fenton chemistry resulting in the production of hydroxyl radical, $OH^{\bullet}$ (Halliwell and Gutteridge, 1992) (Table 1.1). $OH^{\bullet}$ is extremely reactive radical, it is able to react with any cellular macromolecule and its

reactivity is only restricted by diffusion. Reactions between DNA and hydroxyl radical, can result in oxidized guanosine, single-stranded breaks, DNA-DNA intrastrand adducts, abasic sites and DNA-protein crosslinks (Cadet et al., 1999). Superoxide and hydrogen peroxide, in turn, are rather unreactive towards DNA (Halliwell and Aruoma, 1991). However, they can be converted to more reactive radicals such as $OH^\bullet$. Accordingly, when cells were incubated with H_2O_2, damage in nuclear and mtDNA was reported (Yakes and VanHouten, 1997). Furthermore, incubation with rotenone, which increases superoxide production from complex I, induced single-stranded breaks to mtDNA (Shokolenko et al., 2009). To decrease H_2O_2 involved damage, it can be further converted to water by mitochondrial scavenging enzymes, glutathione peroxidase 1 (GPX1) (Esworthy et al., 1997) and thioredoxin-dependent peroxiredoxin 3 (PRDX3) (Chae et al., 1999).

Additionally, H_2O_2 is known to function as a redox signaling molecule. This signaling can, for example, modify the thiol groups in the target protein, which can lead to various changes in the protein function such as enzyme activity, binding affinity or location (Murphy, 2012).

1.4 MAINTENANCE AND EXPRESSION OF MTDNA

1.4.1 Transcription

Mammalian mitochondrial gene expression occurs polycistronically from two promoters, namely light-strand promoter (LSP) and heavy-strand promoter (HSP). These promoters are both situated in the noncoding region of mtDNA. To initiate transcription from these sites, transcription factor A (TFAM) binds the promoter region and bends the DNA to a stable U-turn, which allows mtDNA directed RNA polymerase (POLRMT) binding to the DNA. POLRMT then undergoes a conformational change that facilitates mitochondrial transcription factor 2 (TFB2M) binding and transcription initiation. (Gustafsson et al., 2016; Morozov et al., 2014; 2015; Posse et al., 2014; Yakubovskaya et al., 2014). For high processivity, POLRMT requires mitochondrial transcription elongation factor (TEFM) (Minczuk et al., 2011) that interacts with POLRMT already at the initiation complex (Agaronyan et al., 2015; Posse et al., 2015). In addition to processivity, TEFM allows transcription through strong secondary structures such as G-quadraplexes and oxidative lesions such as 8-oxo-dG (Posse et al., 2015). Transcription from LSP is terminated prior to the ribosomal RNA genes at tRNA[LEU(UUR)] by mitochondrial transcription termination factor 1 (MTERF1) (Terzioglu et al., 2013). HSP transcription termination occurs close to the noncoding region but the process is not currently fully understood. The produced polycistronic transcripts are then processed to release the individual mRNAs, tRNAs and rRNAs. Almost every mRNA is surrounded by tRNAs and thus as the punctuation model (Ojala et al., 1981) suggests, the folded tRNAs serve as a recognition sites for the processing machinery. The 5' end of each tRNA is cleaved by RNaseP and the 3' end by RNaseZ (Ferreira et al., 2017). Upon processing tRNAs are methylated by RNase P component MRPP1 at nucleotide A9 or G9, which is important for the proper formation of the

cloverleaf fold (Vilardo et al., 2012). CCA-sequence is also added to their 3' end by TRNT1, (Nagaike et al., 2001). The CCA is required for the recognition by aminoacyl synthetases for amino acid charging. Some tRNAs have additional modifications especially in the anti-codon stem loop such as 5-taurinomethyl-(2-thio)uridine at the wobble position in tRNA Leu[UUR] (Suzuki et al., 2011).

1.4.2 REPLICATION

1.4.2.1 Replisome

MtDNA is present in hundreds to thousands of copies per cell. It is replicated throughout life without cell cycle control, in a relaxed fashion (Bogenhagen and Clayton, 1977). The mitochondrial replisome consists of four components: the replicative DNA polymerase gamma holoenzyme (Pol γ), DNA helicase (TWINKLE), single-stranded DNA binding protein (mtSSB) and POLRMT. Pol γ, is the sole replicative DNA polymerase found in mitochondria. It belongs to family A DNA polymerases and it is structurally most similar with bacteriophage T7 DNA polymerase (Kaguni, 2004). Pol γ holoenzyme is a heterodimer consisting of one catalytic subunit Pol γ-α and a dimer of accessory subunits (Pol γ-β). The catalytic subunit (140kDa) contains C-terminal 5' to 3' DNA synthesis activity and N-terminal 3' to 5' exonuclease proofreading activity. Additionally, it has been reported to have 5'deoxyribose phosphate (5'dRP) lyase activity, but the catalytic amino acids involved have not been identified (Longley et al., 1998). The lyase activity would be important for base-excision repair (BER), enabling the direct removal of 5'dRP prior to gap-filling. However, the efficiency of this reaction has been questioned as *in vitro* experiments have demonstrated that the dRP release from Pol γ is slower than in Pol β (Pinz and Bogenhagen, 2000). In DNA synthesis, the catalytic subunit is relatively processive on its own, replicating *in vitro* ~50-100 nucleotides per DNA binding event (Fan et al., 2006; Graves et al., 1998), but the processivity is markedly increased upon accessory subunit binding. This interaction increases DNA binding and rate of polymerization while decreasing the exonuclease activity (Farge et al., 2007; Johnson et al., 2000; Lim et al., 1999). The accessory subunit (55 kDa) resembles class II aminoacyl-tRNA synthetase but the catalytically active sites are not conserved (Fan et al., 2006).

Wild-type Pol γ has no strand-displacement activity (Macao et al., 2015) and for successful replication it requires DNA helicase TWINKLE, which unwinds the DNA 5' to 3'. The unwound single-stranded DNA is coated and stabilized by mtSSB, which is a small (16kDa) protein that binds DNA as a tetramer in a cooperative fashion (Li and Williams, 1997; Yang et al., 1997). In addition to ssDNA stabilization, mtSSB also stimulates the helicase activity of TWINKLE (Korhonen et al., 2003; Oliveira and Kaguni, 2011) and enhances processivity and primer recognition of Pol γ (Kaguni, 2004). Even though TWINKLE is homologous to bacteriophage T7 helicase it lacks primase activity and DNA replication in mitochondria is instead primed by RNA polymerase POLRMT (Fusté et al., 2010; Wanrooij et al., 2008). In

addition to the core components of replication machinery, a successful replication requires topoisomerase activity to relax the supercoiling initiated by the replication. Mitochondrial topoisomerase 1 (TOP1mt) catalyzes transient single-stranded breaks and it can relax the induced supercoiling in DNA (Sobek et al., 2013; Zhang et al., 2007).

1.4.2.2 Replication: Strand-displacement mode of replication

The strand-displacement mode of mtDNA replication is well established (Figure 1.4) and recently reviewed in (Gustafsson et al., 2016). First, POLRMT primes DNA replication by creating a RNA primer that extends from the light-strand promoter (LSP) until the origin of heavy-strand replication (OriH) (Chang and Clayton, 1985; Fusté et al., 2010). At OriH Pol γ takes over and replicates new a heavy strand. The resulting displaced long single-stranded stretch of DNA is coated and stabilized by mtSSB. The initiated replication is, however, frequently stopped at termination association sequence (TAS) (Figure 1.4) creating only ~650 bp long aberrant replication product called 7S DNA. Together with the complimentary noncoding region, 7S DNA creates a triple-stranded region called displacement loop (D loop). If replication proceeds successfully beyond the TAS region, it continues unidirectionally around two thirds of mtDNA until it passes origin of light-strand replication (OriL). When OriL is single-stranded it is able to form a stem-loop structure, allowing POLRMT binding and priming of light strand replication. After replication is finished and full-length molecules are formed, the ends of the newly synthesized strands are ligated together by DNA ligase 3 (Gao et al., 2011; Shokolenko et al., 2013). Recently, topoisomerase 3α was also found in mitochondria and it was reported to enable the decatenation of the formed daughter molecules after replication (Nicholls et al., 2018).

A debate has stirred over the mode of mtDNA replication. The above described replication model is called the strand-displacement model or Clayton's model (Berk and Clayton, 1974; Bogenhagen and Clayton, 2003; Clayton, 1991). Neutral 2D agarose gel electrophoresis (2D-AGE) analysis of replication intermediates, however, suggests that instead of the asymmetrical initiation of replication, replication would occur bidirectionally from a broad origin of replication (Bowmaker et al., 2003). These observations gave rise to strand coupled replication model. However, it has been reported that these replication intermediates on 2D-AGE analysis could have also been formed though strand-displacement replication (Brown et al., 2005). In favor of the strand-displacement mode of replication, OriL has been conserved in all vertebrates underlining the important role of this sequence. Furthermore, saturation mutagenesis in mouse shows that the correct sequence of the stem-loop structure is required for mtDNA replication (Wanrooij et al., 2012). Moreover, strand displacement replication model is supported by atomic force electron microscopy (Brown et al., 2005) and has been reconstituted *in vitro* (Wanrooij et al., 2008).
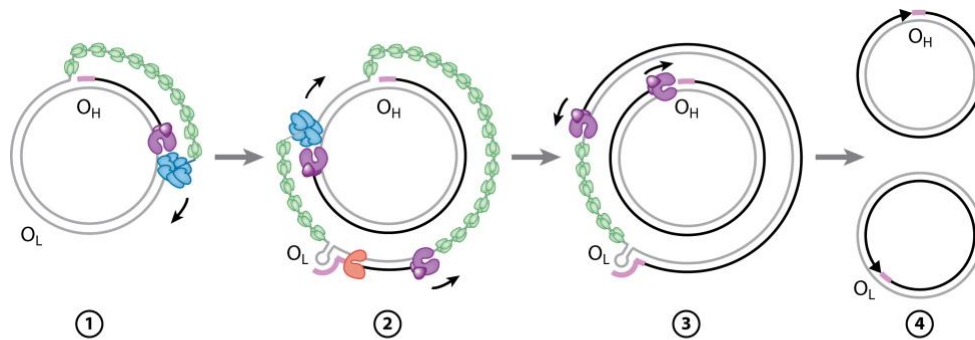
Figure 1.4 Strand displacement mode of replication. Heterotrimeric DNA polymerase γ (violet) initiates replication from noncoding region from an RNA primer (violet) to replicate the heavy strand of mtDNA. Twinkle helicase (blue) unwinds the DNA ahead of DNA polymerase γ and the displaced single-stranded DNA is covered with tetrameric mitochondrial single-stranded DNA bring protein (green). When the replication machinery has passed the origin of light strand replication (O_L, OriL), it folds into a stem-loop structure, which allows RNA polymerase, POLRMT, (orange) binding. POLRMT then makes RNA primer which is extended by DNA polymerase γ to replicate the light strand of mtDNA. The replicated molecules are resolved by Topo 3α and the ends of the new strands are ligated together by DNA ligase 3. Annual review of biochemistry by ANNUAL REVIEWS. Reproduced with permission of ANNUAL REVIEWS in the format Thesis/Dissertation via Copyright Clearance Center. License Number: 4365501099330.

Another alternative replication model is a modification of the strand-displacement model, where the unwound ssDNA would be coated by RNA instead of mtSSB because fraction of the replication intermediates were sensitive to RNAH1 treatment in 2D-AGE (Yasukawa et al., 2006). This model is called the ribonucleotide incorporated through the lagging strand (RITOLS) model or its further modification called the bootlace mechanism (Holt and Jacobs, 2014). However, it has been demonstrated that these RNA coated replication intermediates can be formed *in vitro* by mixing purified mtDNA and processed mitochondrial transcripts (Miralles Fusté et al., 2014), questioning the validity of bootlace and RITOLS models. Additionally, it is difficult to envision how the strongly structured tRNAs and rRNAs could be melted to bind the single stranded stretches of DNA (Gustafsson et al., 2016). As a summary, data fairly convincingly supports that at least currently, strand-displacement mode of replication.

1.5 DNA DAMAGE IN MITOCHONDRIA

1.5.1 Nucleoid

Upon discovery, mtDNA was initially thought to be naked (Nass and Nass, 1963; Nass et al., 1965) – devoid of protective packaging proteins such as the histones in nucleus. It is now firmly established that mtDNA is protein coated and it exists in a DNA-protein complex, called the nucleoid. The detailed characterization of nucleoid composition is still ongoing but it is clear that the main building block is the mitochondrial transcription faction A protein, (TFAM) (Kaufman et al., 2007; Kukat et al., 2015), which binds and condenses mtDNA. Additionally, packaging mtDNA into a nucleoid will likely make it less accessible to external assaults.

1.5.2 Oxidative damage to mtDNA

MtDNA can be damaged in various ways, leading to the formation of large variety of lesions, such as UV initiated thymidine dimers, S-adenosyl methionine induced alkylation damage, abasic sites or cytosine deamination (Alexeyev et al., 2013). The most studied and possibly the prevalent type of damage to mtDNA is induced by ROS. Reaction with ROS can cause various base modifications, abasic sites or single-stranded breaks (Pogozelski and Tullius, 1998; Shokolenko et al., 2009). As mtDNA is situated in relatively close proximity to the superoxide producing respiratory chain, mtDNA was initially thought to harbor more lesions than nuclear DNA (Richter et al., 1988). Later, it was reported that the levels of damaged bases were comparable between the two compartments and some lesion were even more frequent in nuclear DNA such as 8-oxo-dG, FAPy guanosine, 5-hydroxyl cytosine (Anson et al., 2000; Lim et al., 2005). The most common oxidative base modification on a pyrimidine is likely thymine glycol (Cadet et al., 1999; Wang et al., 1998) and on purine 8-oxo-dG (Alexeyev et al., 2013; De Bont and van Larebeke, 2004). Thymine glycol is thought not to be a mutagenic lesion, but rather a replication-blocking lesion, since its presence hinders stacking of the upcoming nucleotide (Aller et al., 2007; Hayes et al., 1988; McNulty et al., 1998). 8-oxo-dG has induced a lot of interest in the field of oxidative stress, since it can form a Hoogsteen base pair with adenosine during DNA replication leading to G to T transversion mutations (Brieba et al., 2004; Kouchakdjian et al., 1991). It is present at a frequency of $\sim 10^{-5}$ -10^{-6} per dG in extracted DNA (de Souza-Pinto et al., 2001; Gedik et al., 2005). However, it can be easily induced artificially during DNA extraction and further DNA preparation steps (Anson et al., 2000; Chen et al., 2017; Costello et al., 2013; Schmitt et al., 2012) which complicates the analysis of its prevalence and relevance. Even with the same sample and standardized DNA isolation and processing methods, the measurements for 8-oxo-dG steady-state levels varied ~13-fold between different laboratories (Gedik et al., 2005). Despite the mutagenic potential of 8-oxo-dG in nucleus, the extent of G:C>T:A transversions in mtDNA could still be infrequent in mitochondria as *in vitro* assays have shown that Pol γ has a decreased efficiency in incorporating nucleotides opposite to 8-oxo-dG during mtDNA replication (Graziewicz et al., 2007; Hanes et al., 2006; Stojkovič et al., 2016). Moreover, when Pol γ was able to replicate 8-oxo-dG, the addition of cytosine opposite to 8-oxo-dG was much more likely than the incorrect adenosine (Graziewicz et al., 2007; Hanes et al., 2006). Interestingly, similar decrease in mutagenicity in mtDNA in comparison with nuclear DNA has been seen when mice were treated with daily doses of benzo[a]pyrene (B[a]P) and N-ethyl-N-nitrosourea (ENU). These mutagenic compounds increased the nuclear DNA mutation load whereas the mtDNA mutation load remained unchanged despite the fact that B[a]P adducts were formed on mtDNA (Valente et al., 2016). These studies suggest that Pol γ has distinct replication properties and therefore direct correlations between nuclear DNA damage and mtDNA mutagenicity cannot be directly drawn.

1.5.3 Other type of damage to DNA

Already in 1973 it was shown that alkylation treatment caused single-stranded nicks in mtDNA, which is a sign of ribonucleotide presence (Grossman et al., 1973). Based on the nick kinetics it was estimated that there are maximum of 10 ribonucleotides incorporated to each mtDNA molecule (Grossman et al., 1973). Recently, the ribonucleotide presence was additionally verified with RNase H2 digestions from purified mtDNA (Reijns et al., 2012). Even though Pol γ shows strong preference for dNTPs over NTPs (Kasiviswanathan and Copeland, 2011), ribonucleotide incorporation can be favorable when the nucleotide pools are highly biased towards NTPs, e.g. ATP concentration evaluated to be ~1000 higher than dATP (Wheeler and Mathews, 2011). The high ration of ATP to dATP inside mitochondria actually suggests that for every 6-7th dATP incorporated, an ATP could be added instead (Kasiviswanathan and Copeland, 2011). Ribonucleotide incorporation makes DNA susceptible to hydrolysis in alkali pH and could cause single-stranded breaks. However, no pathway for ribonucleotide removal is known for mitochondria. RNase H2 has the activity to remove single ribonucleotides incorporated to DNA possible serving a function in ribonucleotide removal in nucleus (Cerritelli and Crouch, 2009), but RNase H2 has not been found in mitochondria. It is currently unknown whether ribonucleotide incorporation induces mtDNA instability also *in vivo*. However, it is likely that single ribonucleotides are not blocking lesions for Pol γ, since *in vitro* assays have demonstrated that Pol γ can extend incorporated ribonucleotides and utilize RNA sequence as a template (Kasiviswanathan and Copeland, 2011; Murakami et al., 2003).

Another type of damage to DNA is the spontaneous hydrolytic deamination of bases, cytosine to uracil, adenosine to hypoxanthine and guanosine to xanthine. All of these base changes are mutagenic as hypoxanthine and xanthine pair with cytosine and thymine, respectively, in DNA replication leading to C:G>T:A and T:A>C:G transitions. Accordingly, mtDNA sequencing from aged flies and humans demonstrates that C:G>T:A and T:A>C:G transitions are the most common type of mutations (Itsara et al., 2014; Kennedy et al., 2013). It should be mentioned, however, that the same mutation pattern is compatible with replication errors and therefore the source of these mutations is not clear (Zheng et al., 2006). Interestingly, the signs of spontaneous deamination can be seen in the base composition of the fourfold degenerative sites of protein coding genes in mtDNA (Reyes et al., 1998). Single-stranded DNA is ~ 200 times more susceptible to spontaneous deamination than double-stranded DNA (Lindahl, 1993) and during DNA replication, the heavy strand is kept single stranded until light strand replication is initiated from OriL. Consistently, a gradient of thymine (cytosine deamination) and guanine (adenosine deamination) can be detected from the single-stranded strand. The gradient is consistent with the duration of single-stranded state during replication (Reyes et al., 1998). Interestingly, in some fishes with inverted the noncoding region the gradient is also inverted (Fonseca et al., 2014). Even though cytosine is most sensitive to deamination (Lindahl, 1993) the gradient is suggested to be formed by adenosine to hypoxanthine deamination as cytosine deamination saturates the system quickly (Faith and Pollock, 2003; Raina et al., 2005).

1.6 MITOCHONDRIAL DNA REPAIR

It was initially thought that mitochondria are devoid of DNA repair as mitochondrial extracts were unable to remove or repair substrates of nucleotide excision repair (NER) pathway, such as thymidine dimers (Clayton et al., 1975), cisplatin-intrastrand crosslinks and complex alkylation damage (Ledoux et al., 1992; Pascucci et al., 1997). Later, it was found that mitochondria actually lack NER but they are able to repair various other lesions. The most studied and possibly the main repair pathway found in mitochondria is the base excision repair (BER) pathway, in which the damaged base is recognized and removed by a specific DNA glycosylase followed by gap tailoring, filling and ligation steps. Many of the nuclear BER pathway proteins have been found to localize into mitochondria in the same or alternatively processed forms (OGG1 (Nishioka et al., 1999; Takao et al., 1998) UNG1 (Nilsen et al., 1997), MUTYH (Takao et al., 1999), DNA Ligase 3 (Lakshmipathy and Campbell, 1999a)) in humans. In the absence of experimental objections, BER pathway is assumed to work similarly in mitochondria as in nucleus (Figure 1.5). BER can be divided into two subcategories namely long- and short-patch BER. In short-patch BER only one nucleotide is removed upon damage repair whereas in long-patch BER commonly >2 nucleotides are digested to remove 5' blocking groups through 5' flap processing (Copeland and Longley, 2014).

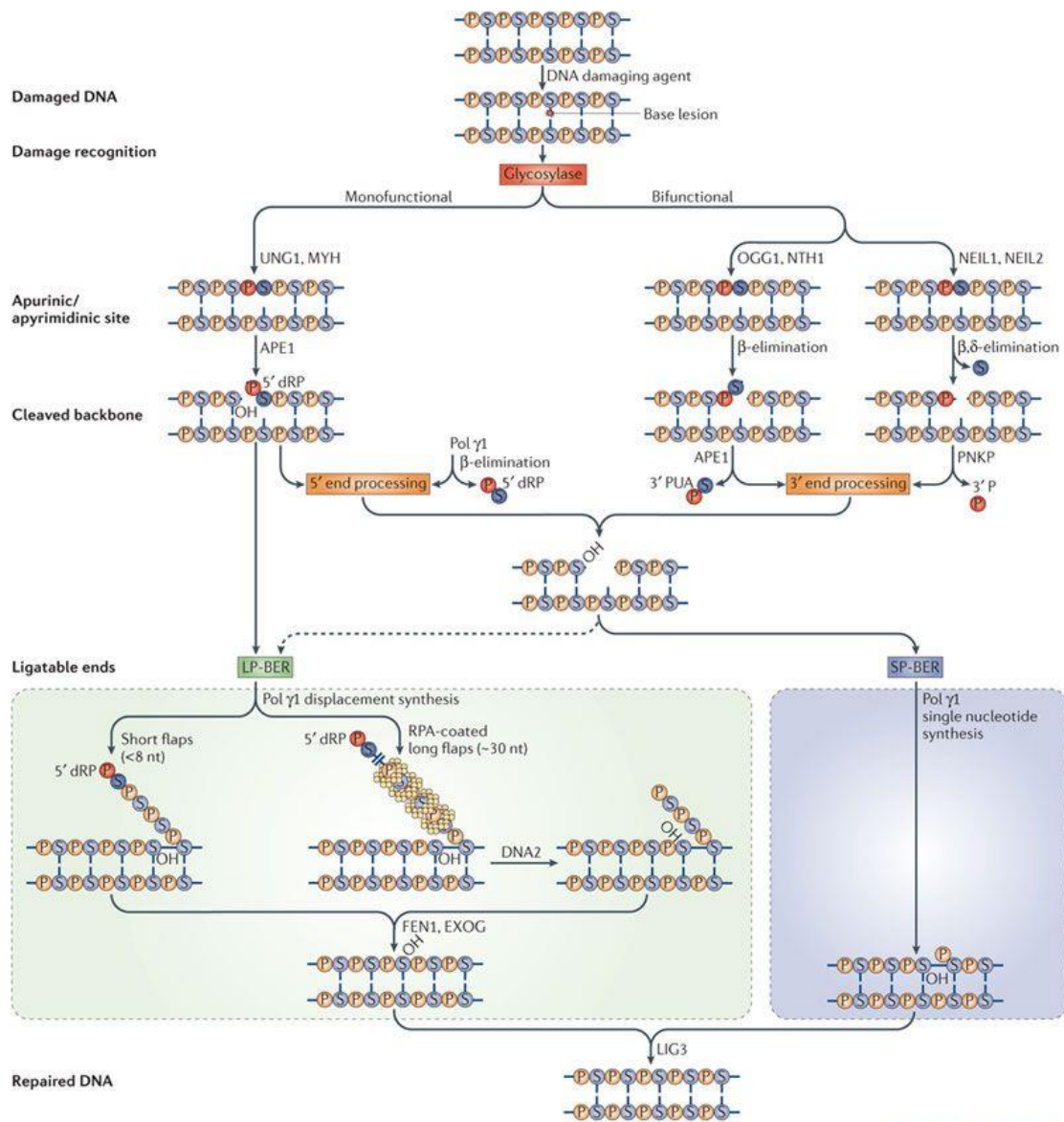### 1.6.1 Base excision repair (BER)

The first step in BER is the removal of the damaged base by a specific DNA glycosylase. These glycosylases can be divided into two groups based on their catalytic properties, namely, monofunctional and bifunctional glycosylases (Figure 1.5). Monofunctional glycosylases are only able to remove the damaged base leaving behind an abasic site (David and Wiliams, 1998). These glycosylases include *E. coli* MutY homolog, MUTYH, that removes the adenosine that has been erroneously paired with 8-oxo-dG (Slupska et al., 1999; Takao et al., 1999) and Uracil DNA glycosylase I (UNG1) that removes the end product of spontaneous deamination of cytosine, uracil (Nilsen et al., 1997; Slupphaug et al., 1995). The abasic site, formed by the activity of these enzymes, is further processed by APE1 (Chattopadhyay et al., 2006). APE1 leaves behind a 5'dRP site that needs to be further processed before ligation. Mitochondrial DNA polymerase γ has been shown (Longley et al., 1998; Pinz and Bogenhagen, 2000) to harbor 5' dRP lyase activity and is thus suggested to remove the remaining 5'dRP. However, the lyase activity has a slow turnover rate in Pol γ (Pinz and Bogenhagen, 2000) and it is therefore possible that the 5'dRP group is instead removed through the long-patch BER pathway.

In addition to the glycosylase activity, bifunctional glycosylases contain AP lyase activity. After base removal, they cleave the N-glycosidic bond leaving behind a single-stranded break. There are four described bifunctional glycosylases in mitochondria, 8-oxoguanine DNA glycosylase 1 (OGG1), three homologues of *E. coli* glycosylases, endonuclease III (NTH1),

13

endonuclease IIIV (NEIL1) and (NEIL2). All of these glycosylases repair oxidized damage induced DNA lesions. As the name entails, OGG1 removes 8-oxo-dG and possibly the ring opened form of guanosine, FAPy G, from double stranded DNA (Hu et al., 2005; Rosenquist et al., 1997). NTH1 has mostly been associated with thymine glycol removal (Ikeda et al., 1998; 2002; Karahalil et al., 2003), whereas NEIL1 removes thymine glycol, FAPy G and 5-hydroxyuracil and has a small activity towards 8-oxo-dG removal (Bandaru et al., 2002; Hazra et al., 2002a). NEIL2 is involved in removing 5-hydroxyuracil and other oxidized derivatives of cytosine (Hazra et al., 2002b; Mandal et al., 2012). OGG1 and NTH1 are beta-functional glycosylases (Ikeda et al., 1998; Rosenquist et al., 1997) and leave behind 3' phosphor-αβ-unsaturated aldehyde that is further processed by APE1. Both NEIL 1 and 2 are βδ functional glycosylases (Bandaru et al., 2002), and leave behind 5'phosphate and 3'phosphate nonligatable ends that need to further be processed by bifunctional polynucleotide phosphatase /kinase (PNKP) (Mandal et al., 2012; Tahbaz et al., 2012). After gap tailoring by either APE1 or PNKP, Pol γ fills the nucleotide gap and DNA Ligase 3 (Gao et al., 2011; Shokolenko et al., 2013) ligates the DNA strand back together. Interestingly, NEIL1 and 2 are observed to be most active on DNA-bubble structures (Dou et al., 2003) thus possibly indicating redundancy in the BER glycosylases and explaining the lack of strong phenotype in OGG1 knockout (Klungland et al., 1999) or OGG1 NTH1 double knockout mice (Karahalil et al., 2003). Additionally, NEIL1 knockout mice were reported to have increased mtDNA damage and deletions indicating their importance to mtDNA maintenance (Vartanian et al., 2006).

1.6.1.1 Long-patch BER

Long-patch repair activity has been found from purified mitochondria from human lymphoblast, mouse liver and kidney (Akbari et al., 2008; Liu et al., 2008; Szczesny et al., 2008). As mentioned, in long-patch repair the 5' replication blocking groups are removed through strand displacement and flap processing (Copeland and Longley, 2014). The pathway is suggested to be highly important for mitochondrial functionality, as it removes 5'deoxyribolactone, which is one of the common oxidative lesions to sugar-phosphate backbone (Roginskaya et al., 2005; 2014). FEN1 protein is responsible for the flap processing in nucleus (Sung et al., 2005) but mitochondrial long-patch BER was only marginally afflicted in FEN1 knockdown mitochondrial extracts, suggesting that other proteins might be involved in the process in mitochondria (Szczesny et al., 2008). The involvement of DNA2, EXOG and MGME1 (Duxin et al., 2009; Kornblum et al., 2013; Tann et al., 2011) have been proposed but none has been conclusively confirmed.

Kazak et al., 2012

Figure 1.5. Base-excision (BER) repair in mammalian mitochondria. Specific DNA glycosylase recognizes and removes the damaged base, followed by gap-tailoring of the site to allow gap filling by DNA polymerase γ and ligation by DNA ligase 3. Depending on the lesion, gap tailoring occurs either through long-patch repair (LP-BER) or short-patch repair (SP-BER). In LP-BER the gap tailoring requires flap processing that occurs through a currently unknown enzyme but the involvement of FEN1, EXOG or MGME1 has been suggested. In yeast, longer flaps are coated with RPA, but it is currently unclear if this occurs in the mammalian system as well. Reprinted by permission from Springer Nature: Nature Reviews Molecular Cell Biology. Minimizing the damage: repair pathways keep mitochondrial DNA intact, Kazak et al., (2012) License Number: 4362980778596.

1.6.2 Other repair pathways

In addition to the main repair pathway, base excision repair, also indications of other repair pathways are found in mitochondria such as mismatch repair, single and double-stranded break repair. However, it is clear that nucleotide excision repair (NER) pathway is not present in mammalian mitochondria, since the mitochondrial extracts are unable to remove most common substrates of nucleotide-excision repair such as thymidine dimers (Clayton et al., 1975), cispatin intrastrand crosslinks, complex alkylation damage and others (Ledoux et al., 1992;

Pascucci et al., 1997). However, rather recently a protein involved with NER in nucleus, Cockayne syndrome B, has been reported to be involved in oxidative DNA damage repair, such as 8-oxo-dG removal, through stimulation of repair (Stevnsner et al., 2002). The relevance of this is still unclear as CSB and OGG1 double knockout mice showed no strong phenotype and did not accumulate 8-oxo-dG in intact mtDNA (Trapp et al., 2007).

1.6.2.1 Mismatch repair

DNA Mismatch repair (MMR) focuses on recognizing and repairing base-base mismatches and small loops. In nucleus this pathway involves the coordinated functions of mismatch recognizing proteins MutSα and MutSβ (Kunkel and Erie, 2005). So far, these proteins have not been found in mammalian mitochondria. However, mitochondrial specific MMR activity has been found from rat mitochondrial lysates and mitoplasts of human cell lines (de Souza-Pinto et al., 2009; Mason et al., 2003) suggesting that mitochondrial MMR could be using a different set of proteins. A caveat is that this activity is not strand biased and lower than in the nucleus (Mason et al., 2003). A potent MMR protein in mitochondria, YB-1, that has been found to bind mismatched DNA and its knock-down decreases MMR activity in mitochondria (de Souza-Pinto et al., 2009). However, so far it is not known how this protein could act in mitochondrial MMR. Additionally, after the initial report there has been no follow-up studies on the YB-1 protein.

1.6.2.2 DNA-strand break repair

Single-stranded breaks are suggested to be more common than base damage upon oxidative insult in mitochondria and even 1000-fold more common than double-stranded breaks (Shokolenko et al., 2009). Single-stranded break can be formed either indirectly by e.g. oxidative insult or directly by e.g. aborted topoisomerase activity. (Alexeyev et al., 2013). The repair involves some of the same enzymes as BER, such as APE1 and DNA Ligase 3 in addition to some specific tailoring enzymes such as aprataxin and tyrosyl-DNA-phosphodiesterase (TDP1) (Kazak et al., 2012).

Double stranded breaks can be repaired with either non-homologous end joining (NHEJ) or homologous recombination in nucleus. The occurrence of homologous recombination repair in mammalian mitochondria is highly controversial subject. Currently, it seems that if occurring, mtDNA recombination is a highly rare event (Hagström et al., 2014). However, there are indications of NHEJ existence. Mitochondrial protein extracts have been reported to ligate linearized plasmid DNA with 5', 3' overhangs and blunt ends, where the ligation frequency was lowest for the latter. Most of the ligation events occurred correctly (Lakshmipathy and Campbell, 1999b). On the contrary, experiments with mitochondrially-targeted restriction enzymes demonstrated that the mtDNA molecules with double-stranded breaks are digested rapidly, leading to a decrease in mtDNA copy number (Moretton et al., 2017; Srivastava and Moraes, 2001). This suggests that if NHEJ is present in mitochondria, it is either extremely active or it is extremely faithful so that the ligated molecules are digested

again after ligation. For a polyploidic genome, repairing linear-DNA fragments might even be unnecessary and even dangerous if executed unfaithfully.

1.7 MTDNA MUTATIONS AND AGEING

Mitochondrial dysfunction with age has been considered one of the hallmarks of ageing (López-Otín et al., 2013). Indeed, the prevalence of mtDNA mutations increases with age in multiple tissues such as skeletal muscle, heart, brain and colon (Bua et al., 2006; Cortopassi and Arnheim, 1990; Greaves et al., 2014a; Kennedy et al., 2013). However, it is not known whether these mutations are causal or they merely correlate with aging. Evidence from mice with proofreading-deficient Pol γ, suggest that mutations could at least contribute to ageing phenotypes. These mice, called mutator mice, accumulate high number of mutations in mtDNA and show several symptoms of premature ageing such as reduced fertility, anemia, osteoporosis, hair loss and reduced lifespan (Kujoth et al., 2005; Trifunovic et al., 2004). Even wild-type mice that that have inherited mutations from their heterozygous mutator mothers, recapitulate signs of premature ageing such as premature death, hair loss, reduced body size and curvature of the spine (Ross et al., 2014; 2013). Accordingly, mtDNA point mutations have been observed to accumulate in clonal populations in human liver (Fellous et al., 2009), stomach (McDonald et al., 2008) and colonic crypts. In colonic crypts and hepatocytes, these mutations have been associated with complex IV (COX) deficiency in differentiated cell types and the presence of the COX-deficient colonic crypts increases with age (Taylor et al., 2003), suggesting that the clonal expansion of mtDNA point mutations in stem cells could contribute to aging. With age these OXPHOS deficient focal sites are detected in various tissues, such as brain, heart, skeletal muscle and colonic crypts (Brierley et al., 1998; Bua et al., 2006; Cortopassi and Arnheim, 1990; Greaves et al., 2014b; Müller-Höcker, 1989; Taylor et al., 2003) but, in these tissues, except in colonic crypts, the dysfunction is more commonly associated with mtDNA deletions rather than point mutations.

1.8 POINT MUTATIONS IN MTDNA

1.8.1 Origin

The mutation rate in mtDNA has been reported to be two orders of magnitude higher than in nuclear DNA (Khrapko et al., 1997). Currently, there are two, not mutually exclusive, hypotheses explaining the source of these point mutations, namely, replication errors and oxidative stress induced base lesions that are converted to mutations.

Oxidative stress induced base damage was considered to be the main source of mtDNA point mutations, since 1970s, when Harman first proposed that ageing is driven by oxidative damage to mitochondrial macromolecules (Harman, 1956; 1972). As DNA is the most stable macromolecule in mitochondria, it is said to serve as the biological clock, and damage accumulation to mtDNA causes ageing. This line of thinking is known as the mitochondrial (free

radical) theory of ageing (Miquel et al., 1980) (reviewed in (Alexeyev, 2009)). This theory suggests that mitochondria produce the largest fraction of cellular ROS and this oxidative stress induces damage on mtDNA, which leads to mtDNA mutations. The mutated, mtDNA encoded proteins then in turn make the OXPHOS leakier, which leads to increase in ROS in a 'vicious cycle manner'. Initially, the idea of oxidative damage-driven ageing seemed logical when considering that mtDNA was thought to be 'naked' unprotected, almost devoid of DNA repair, in close proximity of respiratory chain that produces extensive amounts of ROS and oxidative base damages were reported to be much more common in mtDNA than in nuclear DNA. As discussed in previous sections, each of these ideas have later been proven to be inaccurate. The mtDNA resides protein-coated in a nucleoid (Kaufman et al., 2007; Kukat et al., 2015). Mitochondria do lack nucleotide excision repair but they harbor base excision repair (Kazak et al., 2012). The estimates of ROS production from the respiratory chain has been overestimated (Hansford et al., 1997). Lastly, many oxidative base lesions are equal or even more common in a nuclear than mitochondrial DNA (Lim et al., 2005). Additionally, there is no clear correlation between oxidative damage levels and lifespan (Barja and Herrero, 2000; Lei et al., 2016). In mice, neither mild increase in oxidative damage ($Sod2^{+/-}$) nor deficit or decreased levels of antioxidant enzymes ($Trx2^{+/-}$, $Gpx1^{-/-}$) limited lifespan (Pérez et al., 2009a; Van Remmen et al., 2003). Additionally, overexpression of antioxidative enzymes (SOD1 or SOD2) did not extend lifespan (Pérez et al., 2009b).

Experiments with the mutator mice have demonstrated that increase in mtDNA mutation load does not induce an increase in superoxide levels or protein carbonylation in mitochondria (Trifunovic et al., 2005). At the end stage of mutator lifespan, an increase in H_2O_2 levels was reported in heart and kidney while no increase was found in liver and skeletal muscle or in any analyzed tissue at a young age (Logan et al., 2014). These experiments support the notion that mtDNA point mutations do not lead to a 'leakier' respiratory chain that would produce more ROS, which would in turn initiate more mtDNA mutations in a vicious cycle manner, as suggested in the mitochondrial (free radical) theory of ageing (Alexeyev, 2009).

Oxidative stress driven mutations are mainly considered to be caused by the erroneous replication against oxidized guanosine, 8-oxo-dG, leading to C:G>A:T transversion mutations. Interestingly, mutations in aged flies (Itsara et al., 2014) and humans (Kennedy et al., 2013), are transitions rather than transversions. Similar results were also obtained from human tumor cell lines (Ericson et al., 2012; Polyak et al., 1998) and tumors (Ju et al., 2014; Stewart et al., 2015). Therefore, the mutation pattern of naturally occurring mutations is more consistent with spontaneous deamination and replication errors than mutagenic oxidative base lesions. Consistently, the mutational pattern of mtDNA seen in ageing human tissues can be recreated in aged heterozygous mtDNA mutator mice (Baines et al., 2014). These mice have decreased proofreading activity in Pol γ inducing modest increase in mtDNA mutation load, resulted in clonally expanded point mutations that lead to COX deficiency in colonic crypts similar to what is seen in ageing humans (Baines et al., 2014). These results suggest that mtDNA mutations, which are detected with age, are largely induced by replication errors. *In vitro* analyses have

demonstrated that mammalian Pol γ has an unexpectedly high fidelity, on average 7.4×10^{-6} mutations/bp, (Johnson and Johnson, 2001; Kunkel, 1985; Kunkel and Loeb, 1981; Longley et al., 2001; Lynch, 2011; Ponamarev et al., 2002; Pursell et al., 2008; Song et al., 2005). Therefore, Pol γ is more accurate than the nuclear replicative polymerases Pol δ and Pol ε (Lynch, 2011). Even with high fidelity, mutations will occur as mtDNA goes through an extensive number of replication cycles through life. In primordial germ cells mtDNA copy number drops to around 200 copies per cell (Cree et al., 2008) that are then propagated to establish all the mtDNA copies of an adult individual.

1.8.2 Mitochondrial DNA point mutations in disease

Pathogenic mutations in mtDNA or in genes that encode mitochondrial proteins can lead to mitochondrial disease. These disorders are a diverse group of diseases with typically pleiotropic symptoms, which can involve symptoms such as severe progressive neurodegeneration (e.g. Leigh syndrome), stroke, hearing loss, infantile multisystem disorders (e.g. Pearson´s syndrome), myopathy, optic atrophy, cardiomyopathy, blindness and myoclonic epilepsy (Larsson and Clayton, 1995; Lightowlers et al., 2015). The underlying molecular defect is often a dysfunctional respiratory chain and thus these disorders mainly affect the high energy demanding tissues such as brain, skeletal muscle and heart. Even though the involved genetic components are known, genotype-phenotype correlations of mitochondrial diseases are poorly understood. This is emphasized by the observation that mutations in different tRNAs are associated with specific symptoms, e.g. mutations in tRNA^{SER} are typically associated with deafness, tRNA^{LYS} with myoclonic epilepsy and tRNA^{LEU} mutations with diabetes, hearing loss, early strokes and cardiomyopathy (Tyynismaa and Suomalainen, 2009). In theory, mutations in tRNA genes should have a common effect of impairing translation leading to similar clinical outcomes. Even the same A3243G mutation in the *tRNA$^{LEU(UUR)}$* gene can lead to different clinical presentations, namely maternally inherited diabetes and deafness (MIDD) (Nesbitt et al., 2013); mitochondrial myopathy, encephalopathy, lactic acidosis, and stroke-like episodes (MELAS) syndrome (Goto et al., 1990); or to chronic progressive external ophthalmoplegia (CPEO) (Moraes et al., 1992). Currently, over 200 pathogenic mtDNA mutations have been reported over half of which reside in mitochondrial tRNA genes (Suzuki et al., 2011). As only palliative treatment is currently available to these disorders, there is a demanding need for animal models to unravel the genotype-phenotype correlations of these diseases.

1.8.3 Heteroplasmy, biochemical threshold, bottleneck phenomenon and purifying selection

MtDNA is present in hundreds to thousands of copies per cell and therefore a mutation can be present in all of the copies of mtDNA, in a condition referred to as homoplasmy, or just in a fraction of all copies, a condition called heteroplasmy. To cause a dysfunction, a pathogenic mtDNA mutation needs to be present in a large enough fraction of mtDNA molecules to induce

biochemical phenotype. This so called biochemical threshold depends on the mutation type and the bioenergetics demand of the tissue, and the threshold is often ~ 60-80% (Boulet et al., 1992; Larsson et al., 1992; Rossignol et al., 2003; Stewart and Chinnery, 2015). Computational modeling and sequence analysis have demonstrated that given sufficient time somatically occurring mtDNA mutations can reach these thresholds in a subset of cells through random segregation and clonal expansion (Elson et al., 2001; Greaves et al., 2014b). After passing their biochemical threshold, they cause focal respiration chain dysfunction as seen more commonly with age. Examples of this have been found in certain tissues such as brain, colonic crypts and heart (Brierley et al., 1998; Bua et al., 2006; Cortopassi and Arnheim, 1990; Greaves et al., 2014b; Müller-Höcker, 1989; Taylor et al., 2003).

When a mutation is present in germline, the relative heteroplasmy level of a mutation can also vary extensively between generations due to the well-known bottleneck phenomenon, whereby the mtDNA copy number drops (~200 copies per cell in mice) during primordial germ cell development. The few mtDNA copies in primordial germ cells are replicated to populate the female germ cells (~1500 in mice) that have a very high copy number of mtDNA (1-2x 10^6 copies of mtDNA per oocyte) (Stewart and Larsson, 2014). This subsampling can lead to large sifts in the relative heteroplasmy level of a mutation. In most extreme cases, one variant could even become dominant in a generation, like in Holstein cows (Olivo et al., 1983). The size of the bottleneck determines how big of a shift in heteroplasmy levels that can occur in one generation. For example, when the bottleneck is large, as in *Drosophila melanogaster,* the shifts between generations are small (Bratic et al., 2015). It has been shown that the ten most common pathogenic mtDNA mutations are present 1 in 200 healthy individuals (Elliott et al., 2008), suggesting that mtDNA diseases could arise in a subpopulation quite unexpectedly. In addition to the bottleneck phenomenon, a selection against unwanted mutations occurs in female germline, a phenomenon called purifying selection. When mtDNA was mutated with proofreading deficient Pol γ and the clonally expanded mutations were sequenced from the offspring, a strong decrease in number of mutations at first and second codon position was found in comparison with third codon position in protein-coding genes (Stewart et al., 2008b). However, the fact that diseases caused by pathogenic mtDNA mutations still exist, suggests that the purifying selection is not effective in removing all mutations that are present at a high relative heteroplasmy level in the germline. It should be mentioned that pathogenic mtDNA mutations can be also homoplasmic albeit they are less frequent than the heteroplamic disease-causing mutations. For example, three common point mutations, G117784A, G34604A and T14484TC, which cause Leber's Hereditary Optic Neuropathy (LHON) are often homoplasmic (Russell and Turnbull, 2014).

1.8.4 Methods to detect mtDNA point mutation

There are various techniques available to detect mtDNA point mutations through sequencing. For diagnostic purposes Sanger sequencing is sufficient as it detects a mutation that constitutes ~15-30% of the signal on studied position (Hancock et al., 2005; Rohlin et al., 2009). Mutations

that are present at a lower relative level are most likely not relevant for disease diagnostics as they do not exceed the biochemical threshold. Sanger sequencing alone is not sensitive enough to detect the low-level mutations in a sample, as most of the somatic *de novo* mutations have not clonally expanded sufficiently to reach the 15-30% detection limit. To study the somatic mutation load, different detection methods can be applied such as post-PCR cloning, next-generation sequencing and random mutation capture assay (RMC).

In post-PCR cloning technique total DNA is extracted followed by PCR amplification of a selected mtDNA region (~1kb) with a high-fidelity DNA polymerase (Wanrooij et al., 2012). Next, the amplified fragment is cloned into a bacterial vector, amplified and the plasmid carrying the mtDNA fragment is purified and sequenced. Each bacterial clone represents, in theory, a single mtDNA molecule, which allows mutation load detection per base pair when large number of clones are sequenced. However, the PCR amplification step in the method has encountered some criticism as it is impossible to distinguish a true mutation from a PCR-induced error, leading to a possible overestimation of the mutation load. However, clone of a clone experiments have demonstrated that the background error rate of the method is only ~3.48 $\times 10^{-6}$ mutations/base pair (Wanrooij et al., 2012). Alternative method for post-PCR cloning is RMC in which the enriched mtDNA is digested with a restriction enzyme prior to PCR amplification, thus only molecules that carry a mutation in the restriction site are amplified (Greaves et al., 2009; Vermulst et al., 2007). RMC is not sensitive to PCR induced errors but the drawback of this technique is that the DNA concentration needs to be quantified with qPCR to calculate the mutation load per base. Additionally, the method only detects mutations that disrupt the restriction site, which might not represent the mutation load in the whole mtDNA.

Additional commonly used mtDNA sequencing methods are the various next-generation sequencing techniques such as sequencing-by-synthesis analysis e.g. Illumina sequencing. The Illumina sequencing method allows analysis of the whole mtDNA with high coverage. One analysis requires ~50 ng of pure mtDNA and creates Gb of sequence data that needs to be analyzed in a cluster bioinformatically. The method has a higher error rate (~ 0.1%) than other sequencing methods (Fox et al., 2014) but the deep coverage of the data alleviates this issue. Prior to sequencing the DNA is first fragmented to few hundred-base pair long DNA fragments, and thus the sample should be clean from nuclear contaminants or otherwise reads from NuMTs can be erroneously aligned to mtDNA and lead to an inaccurate mutation load assessment.

1.9 DISEASE MODELS CARRYING MTDNA MUTATIONS

As previously discussed, mitochondrial diseases that originate from pathogenic mtDNA mutations do not show clear genotype-phenotype correlations. To better understand these diseases, efforts have been made to produce mouse models that carry pathogenic mtDNA mutations. Currently, methods to robustly transfect mitochondria are lacking and therefore these studies are limited to pre-existing mtDNA mutations, which are already present in cell lines or somatic tissues.

The first strategy to produce these transmitochondrial mice involved a fusion between female karyotype embryonic stem cell (ESC) and preexisting mitochondria with a mtDNA mutation. The first pathogenic mutation introduced into mice via this technique was a mutation in large ribosomal RNA (16S), which conferred resistance to chloramphenicol toxicity (Levy et al., 1999; Marchington et al., 1999; Watanabe et al., 1978). The efficiency of the mutation transmission was subsequently improved by removing the endogenous mitochondria from the ESC cells prior to the fusion with rhodamine 6G treatment (Sligh et al., 2000). The resulting high relative levels of the pathogenic mutation were, however, lethal and the mice died as embryos or as newborn pups shortly after birth.

Later, the ESC method has been used to introduce mutations in tRNA (Shimizu et al., 2015; 2014) and mRNA genes (Fan et al., 2008). Additionally, transmitochondrial mice with duplicated/deleted mtDNA has been produced though fusion of enucleated cytoplasm and fertilized oocytes (Inoue et al., 2000; Nakada et al., 2004). Some of these transmitochondrial mice developed symptoms associated with mitochondrial disease including anemia, cardiomyopathy and muscle atrophy (Fan et al., 2008; Inoue et al., 2000; Nakada et al., 2004; Shimizu et al., 2015; Sligh et al., 2000). The drawback in cytoplasmic fusion techniques is that it is limited to mtDNA mutations present in existing cell and tissue models and it is highly laborious. Additionally, some of the introduced mutations are not stable in the mouse lines because they are selected against in the female germline (Fan et al., 2008; Stewart and Larsson, 2014).

1.10 AIMS OF THE THESIS

Mutations of mtDNA cause drastic mitochondrial disorders with diverse, commonly pleiotropic symptoms. Despite that these diseases have been studied for over 30 years, their enigmatic phenotype-genotype correlations are still not completely understood and only symptomatic treatment is available to patients with mitochondrial disease. Comprehensive molecular understanding of these diseases has been hindered by the limited number of animal models available for research. Therefore, the aim of this thesis is to generate mitochondrial disease models with mtDNA mutations and analyze their molecular phenotype. Because mtDNA cannot be efficiently modified with molecular biology techniques, two genetic approaches were designed to introduce endogenously mutations to mtDNA.

Generating mouse models for mitochondrial disease with two different approaches:

1. **Proofreading deficient replicative mitochondrial DNA polymerase**

2. **Impairment of mitochondrial DNA repair by abolishing the mitochondrial localization of base-excision repair DNA glycosylases**

GENERATING MTDNA POINT MUTATIONS WITH PROOFREADING DEFICIENT MITOCHONDRIAL DNA POLYMERASE

2.1 INTRODUCTION

Mitochondrial diseases that originate from a pathogenic mtDNA mutation do not always show clear genotype-phenotype correlation (Tyynismaa and Suomalainen, 2009). It is currently unknown, for example, why certain tissues are affected with one pathogenic tRNA mutation but remain unaffected with another. In order to understand and treat these diseases effectively, more comprehensive understanding of the underlying genotype-phenotype correlation is required. Currently, few transmitochondrial mouse models have been created through cytoplasmic fusion techniques (Fan et al., 2008; Inoue et al., 2000; Nakada et al., 2004; Shimizu et al., 2015; Sligh et al., 2000). Unfortunately, these techniques are highly laborious and limited by the availability of mtDNA mutations in cell models and somatic tissues.

One way to induce new mutations to mtDNA is through proofreading deficient mitochondrial replicative DNA polymerase, Pol γ. When a catalytically important amino acid is mutated from aspartate to alanine (D257A) in the exonuclease active site, the proofreading activity of Pol γ is reduced extensively (Trifunovic et al., 2004). *In vitro* assays in yeast, with corresponding mutants, have demonstrated that the fidelity of Pol γ is decreased around 100-200 fold (Foury and Vanderstraeten, 1992). These proofreading-deficient 'mutator mice' have been used successfully to introduce stable and transmissible mtDNA mutations to both the germline and somatic tissues (Ross et al., 2013; Stewart et al., 2008b). When homozygous $Pol\gamma A^{MUT/MUT}$ mice were used to establish wild-type lineages, it was noticed that the wild-type progeny carried ~14 mutations per mtDNA molecule (Ross et al., 2013). While these mice are an important tool for saturation mutagenesis (Wanrooij et al., 2012) and purifying selection studies (Freyer et al., 2012; Stewart et al., 2008b), with such a high number of linked mutations, they are of limited use in establishing genotype-phenotype correlations. Therefore, to establish mouse models for mitochondrial disease a new breeding approach was needed.

2.2 RESULTS

2.2.1 Breeding to establish mouse lines with pathogenic mtDNA mutations

Proofreading-deficient Pol γ introduces equal mutation load to both somatic tissues and germline (Ross et al., 2013; Stewart et al., 2008b). It can be thus estimated that heterozygous mutator mice ($Pol\gamma A^{+/MUT}$) with somatic mutation load of $\sim 2 \times 10^{-4}$ mutations/bp (Ross et al., 2013), would introduce on average 3 mutations per transmitted mtDNA molecule. This low-level mutagenesis can be utilized to establish wild-type mouse lineages that carry only few linked mtDNA mutations. To this end, we established female lineages (n=12: Figure 2.1) in the following way, first we crossed $Pol\gamma A^{+/MUT}$ males with wild-type C57BL/6N females to obtain $Pol\gamma A^{+/MUT}$ females with reintroduced wild-type mtDNA. Then we bred these $Pol\gamma A^{+/MUT}$ females with wild-type males (N1) to generate the founder females, which carry maternally inherited mtDNA mutations in a wild-type nuclear background. To clonally expand and segregate the

maternally transmitted mutations, maternal lineages were established from these founders, with subsequent breeding with wild-type males.
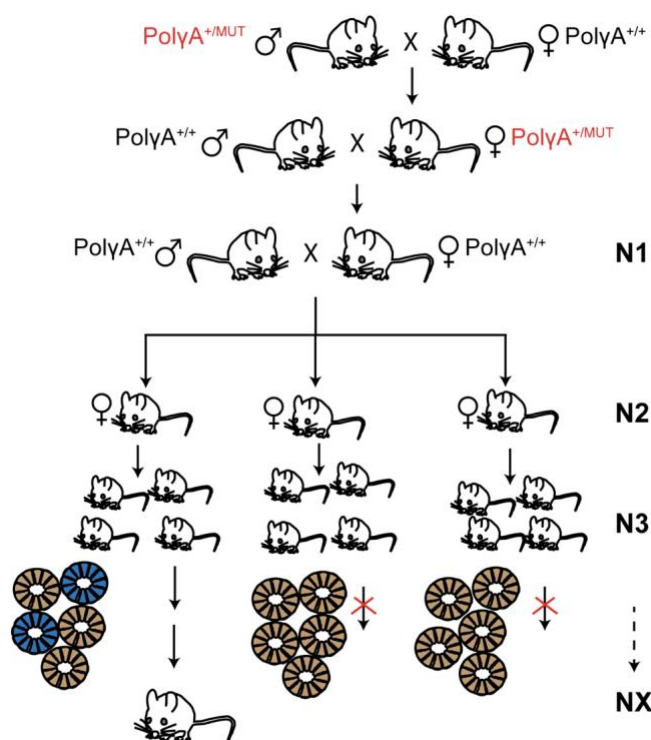
Figure 2.1 Breeding strategy to generate and identify lineages that carry pathogenic mtDNA mutations. Heterozygous mutator mice ($Polg\gamma A^{MUT}$) with clean mitochondrial background were utilized to generate and transmit mtDNA mutations to their offspring. These wild-type offspring were further bred with wild-type males to generate female lineages that harbor mtDNA mutations. Rapid clonal expansion in colonic crypts allows fast segregation of the mutation to high heteroplasmy levels that impair respiration. The lineages that carry a pathogenic mtDNA mutation were identified by screening the colonic crypts for complex IV (COX) dysfunction from the founder mice from third generation (N3) on. The lineages with normal mitochondrial function were discontinued and the lineages with mitochondrial dysfunction (additional blue, COX negative crypts) were bred further and the COX negative crypts were microdissected and their mtDNA was sequenced. N1-NX, indicates the generation number.

2.2.2 Identification of pathogenic mutations from colonic crypts

The epithelial layer of an individual colonic crypt originates from single stem cell at the base of the crypt (Humphries and Wright, 2008). The clonal nature of the crypts allows mtDNA mutations to undergo clonal expansion. If a pathogenic mutation is present in high enough relative level, it can cause focal respiratory chain deficiency in a crypt, which has been detected in both humans (Greaves et al., 2010; Taylor et al., 2003) and mice (Baines et al., 2014). In postmitotic tissues, clonal expansion of a given mutation to a level which induces respiratory chain deficiency, can take years, which makes *in vivo* identification of low-level pathogenic mtDNA mutations difficult and time consuming. Therefore, this rapid clonal expansion in colonic crypts could be a powerful tool to identify low-level pathogenic mtDNA mutations and establish their pathogenicity. To test this approach, we performed COX/SDH enzyme histochemistry to the colonic epithelium of the founder individual from each of the 12 mouse lineages (N3

onwards). This well-established staining technique is used to detect respiratory chain dysfunction that stems from mtDNA mutations. This technique stains all the crypts to detect functional COX (complex IV) brown and counter-stains the COX-deficient crypts blue with succinate dehydrogenase (SDH, complex II) activity. SDH is entirely nuclearly encoded, thus it is not affected by mitochondrial translational dysfunctions or direct mutations in mitochondrial *cox* genes, unlike COX activity. Many mtDNA mutations affect tRNA genes and thus impair translation when present in high enough relative levels. With COX/SDH staining we detected respiratory-chain-deficient colonic crypts in three out of the twelve founders. To further analyze these COX-deficient crypts, we laser-dissected them individually and sequenced the complete mtDNA after PCR amplification. In one out of the three COX-deficient lines (Figure 2.2 A), we detected high levels of a heteroplasmic C5024T mutation which resides in *tRNA^{ALA}* gene (Figure 2.2 B). To quantify the level of this mutation in tissues, we developed quantifying pyrosequecing protocol and measured the levels of mutated mtDNA in individual colonic crypts and observed significant correlation between occurrence of respiratory chain deficiency and levels of the *tRNA^{ALA}* mutation (Figure 2.2 C).

In mouse, the C5024T mutation disrupts a base pair in the acceptor stem of tRNA^{ALA}. This same base pair is disrupted in human patients with pathogenic G5650A mutation (Figure 2.2 D), which causes mitochondrial disease (Finnila et al., 2001; McFarland et al., 2008). The C5024T mouse mutation introduces a C-A mismatch next to a U-U mismatch in the acceptor stem, in turn, the human G5650A mutation generates a second G-U wobble base pair. Despite these similarly located structural changes, the effects of these mutations to the stability of tRNA^{ALA} could be different.

The *tRNA^{ALA}* mutation is additionally linked with C1375T mutation, which causes glycine 119 to aspartate mutation in ND6 protein. The 1375 site is poorly conserved in rodents (Figure 2.3 A), and additionally the C1375T mutation has low predicted-pathogenicity score (MUTPRED, general pathogenicity score of 0.473 (http://mutpred.mutdb.org/)). To study whether the C1375T mutation contributes to the detected respiratory chain dysfunction, we analyzed the steady-state level of complex I with NDUFB8 antibody from colonic crypts of mice with high relative levels of C5024T and C1375T mtDNA molecule. The analysis revealed slightly more crypts with decreased complex I than COX deficiency, which is more consistent with general translation dysfunction than compound effect from C1375T mutation with translational dysfunction (Figure 2.3 B) (Rocha et al., 2015). mtDNA encodes seven complex I mRNAs and only three COX mRNAs explaining the slightly more afflicted complex I steady-state levels with dysfunctional translation.

Pathogenic mutations in mitochondrially encoded complex I proteins lead commonly to subassembled complex I and strong decrease in complex I steady-state level (Bai and Attardi, 1998; Leman et al., 2015; Leshinsky-Silver et al., 2010; Lim et al., 2016; Lin et al., 2012; Ugalde et al., 2007). When we performed Blue Native PAGE analysis from mouse mitochondria with high relative levels of C5024T and C1375T mtDNA molecule, we saw no decrease in the steady-state levels of CI or partially assembled CI (Figure 2.3 C). Additionally, in gel activity

assay did not reveal biochemical complex I dysfunction (Figure 2.3 C). In summary, we did not see any evidence for pathogenicity of the C1375T mutation and therefore we conclude that the mouse line harbors single pathogenic mutation in *tRNA^ALA* gene, which causes the observed respiratory chain deficiency.
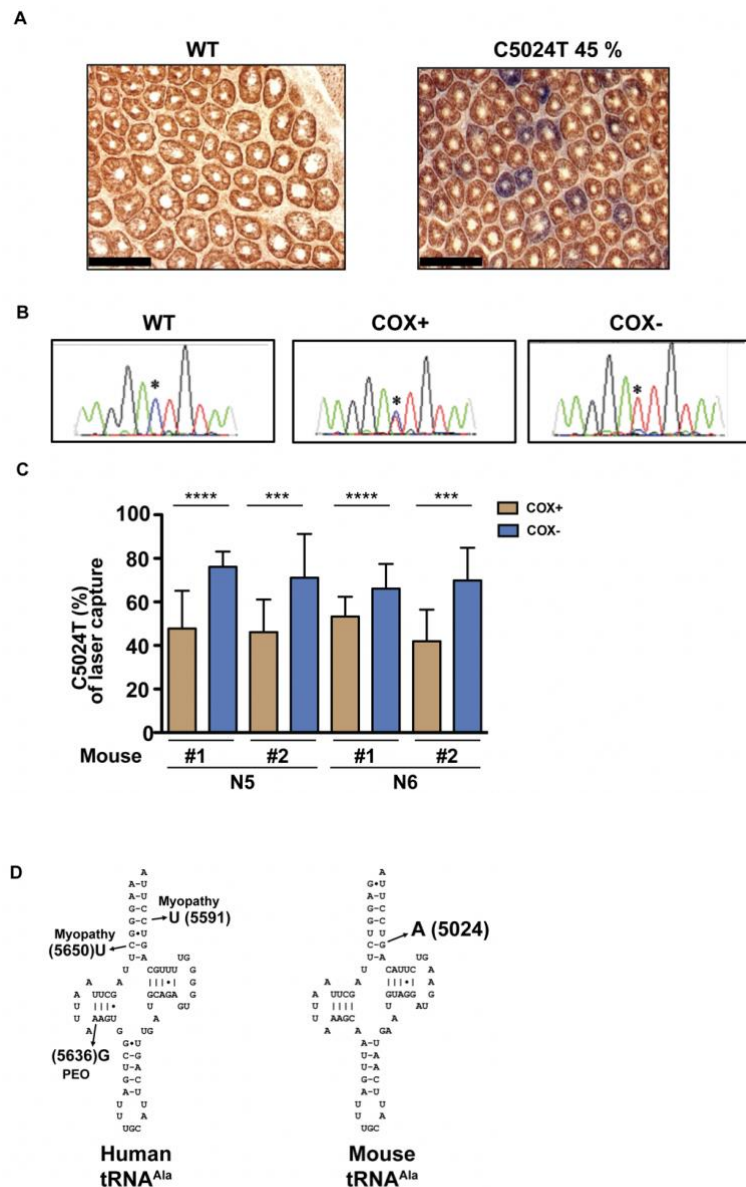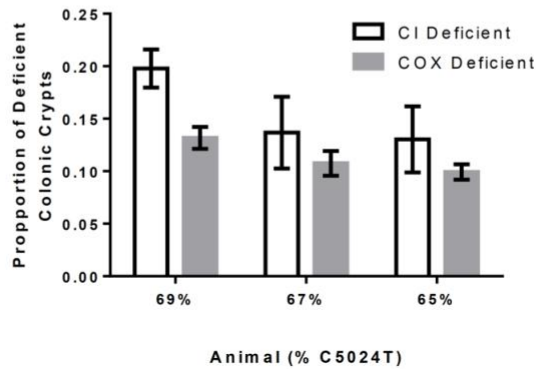

Adapted from Kauppila et al., 2016

Figure 2.2 Identification of the pathogenic C5024T mutation in *tRNA^ALA* gene in mtDNA. A. Representative image of histological section of COX/SDH enzyme histochemistry from colon of wild-type (WT) mouse and a mouse with 45 % heteroplasmy level of C5024T mutation. Brown crypts have normal COX activity whereas blue crypts have COX dysfunction. Black bar represents 100 mm. **B**. Electropherograms from *tRNA^ALA* gene region from isolated colonic crypts. Position 5024 is indicated with an asterisk. Crypts with normal mitochondrial function (COX positive) shows lower relative level of C5024T mutation than crypts with mitochondrial dysfunction (COX negative). **C.** Relative level of C5024T mutation from individually dissected colonic crypts, shows that COX negative crypts have high relative level of C5024T mutation. Error bars indicate SD. ***p < 0.001; ****p < 0.0001 (Mann-Whitney *U* test). **D.** Clover-leaf presentation of tRNA^ALA from humans and mice with indicated positions of known pathogenic mutations and C5024T mutation.
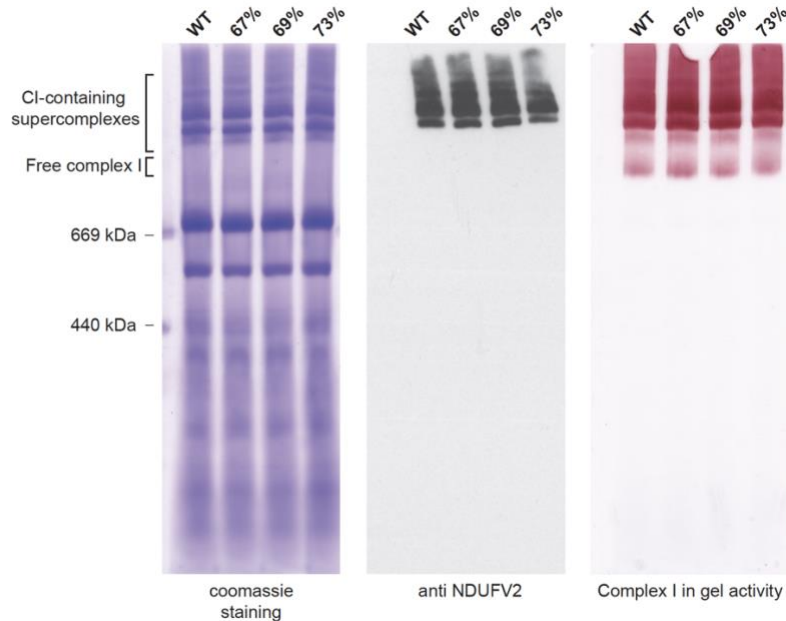
**Figure 2.3 Co-segregating C1375T NAD6 mutation. A.** A snapshot of an alignment with 240 rodent mitochondrial ND6 protein sequences (GenBank). Out of the 240 genomes, 22 variants in the ND6 amino acid sequence were found at site 119 (marked with red box), thus the site is poorly conserved, arguing for low pathogenicity for the G119D (C1375T) mutation. **B.** Quantification of immunohistochemical CI staining with anti-NDUF8 antibody and COX/SDH enzyme histochemistry staining from the same individual. n=3. Error bars indicate SD. **C.** A representative Blue-Native PAGE analysis from mice with high relative level of C5024T/C13715T mtDNA. Coomassie staining, NDUFV2 steady-state levels and complex I in gel activity do not reveal a subassembled or less active complex I in the presence of C1375T mutation.

2.2.3 The transmission of C5024T $tRNA^{ALA}$ mutant allele is not neutral

When breeding mice with $tRNA^{ALA}$ mutation, we did not observe an individual with more than 80 % relative level of the $tRNA^{ALA}$ mutation, quantified from tail biopsy collected at 3 weeks of age (Figure 2.4 A). Females, which harbored low relative levels of the $tRNA^{ALA}$ mutation (<51%), showed a transmission patter that was fully consistent with neutral drift (Figure 2.4 B, +supplementary), when Kimura model was used as a null hypothesis for neutral transmission. In turn, the relative level of $tRNA^{ALA}$ mutation in progeny from females that harbored high relative levels of the $tRNA^{ALA}$ mutation (>55%), did not follow the Kimura model, because the number of pups with high relative level of $tRNA^{ALA}$ mutation was lower than the expected value. We did not observe a change in the litter size from females with high relative levels of $tRNA^{ALA}$ mutation (Figure 2.4 C), which suggests that the source of this selection is a cellular or organellar phenomenon and not death at embryo stage.

2.2.4 $tRNA^{ALA}$ mutant mice show cardiomyopathy and reduced body mass

MtDNA mutations can cause tissue specific symptoms. To this end, we carried out COX/SDH enzyme histochemistry analysis from various tissues of the $tRNA^{ALA}$ mice. At 20 weeks of age, COX deficiency was detected only in the epithelial cells of colonic crypts, in turn, at 40 weeks of age and older, COX deficiency was detected frequently in the smooth muscle that aligns the colon and occasionally in cardiomyocytes from mice with >60% relative level of C5024T mutation (Figure 2.5 A, C). Moreover, $tRNA^{ALA}$ mutation levels and COX deficiency showed a significant correlation in the colonic smooth muscle cells (Figure 2.5 B). This correlation confirms the pathogenicity of the C5024T $tRNA^{ALA}$ mutation. Additionally, we observed a decrease in total body mass, lean mass and fat content in male mice that carry $tRNA^{ALA}$ mutation in comparison with control males, while the female mice remained unaffected (Figure 2.5 D). Additionally, an increase in heart mass was observed in both female and male mice with high relative level of the $tRNA^{ALA}$ mutation (Figure 2.5 E).
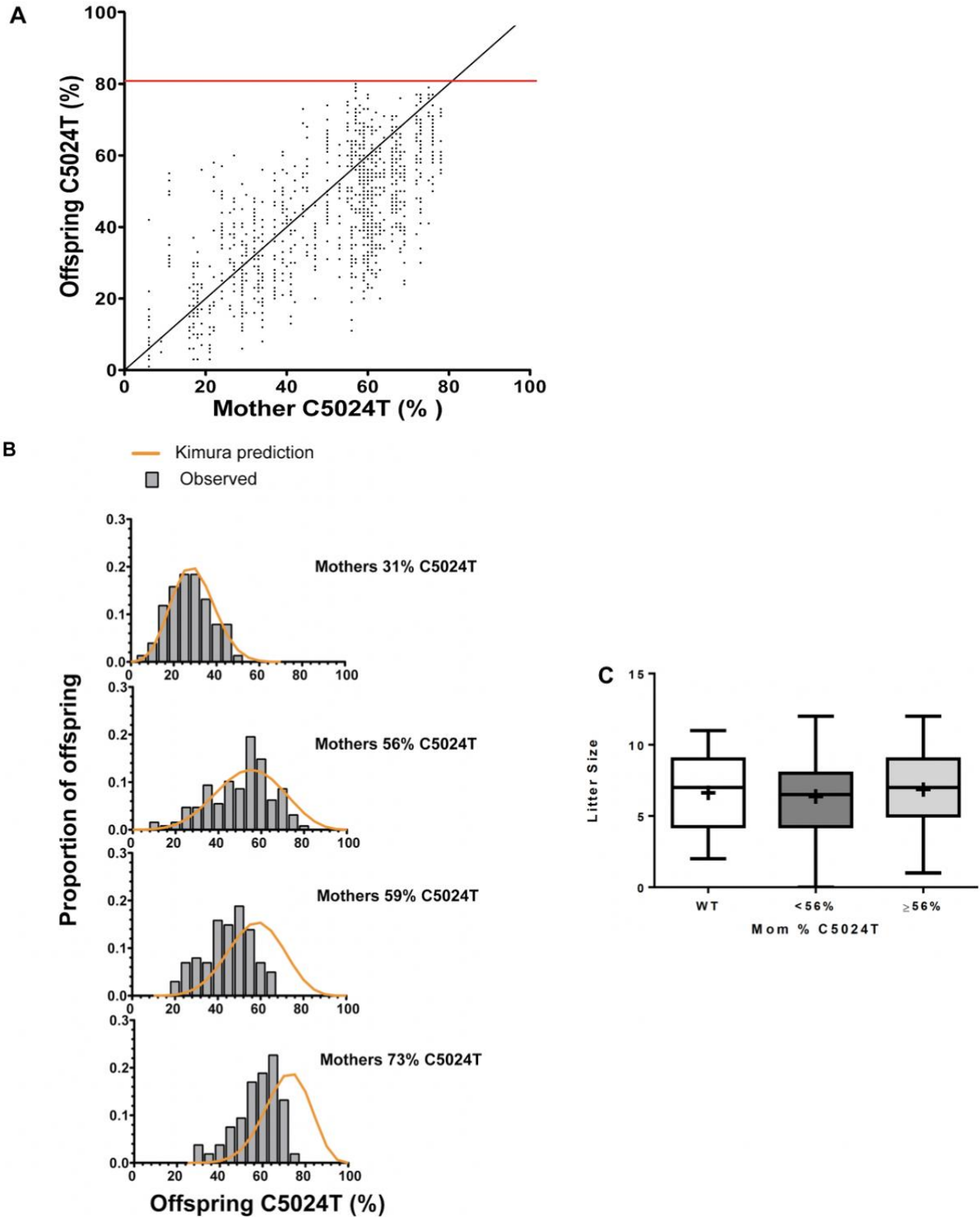
Figure 2.4 C5024T mutation is not neutrally transmitted. A. Relative level of C5024T mutation in 1,105 offspring in comparison with their heteroplasmic mothers. The maximum level of C5024T mutation detected is indicted with red line. **B.** Four representative tests for neutral segregation using Kimura distribution (Wonnapinij et al., 2008). Expected level of mutation is depicted with orange line and the observed with grey bars. The segregation of C5024T mutation was neutral until the mother carries 59% relative level of C5024T mutation. **C.** Litter size from mothers carrying more or less than 56 % heteroplasmy level of C5024T mutation did not differ from age matched wild-type control. >56% n=102 litters, <56% n=80, WT n=84. Not significant, 1 way ANOVA, with Dunn's correction multiple comparisons between all groups. Bars indicate data range, + indicates mean, line indicates median, box indicates 25-75th percentile of the data. All tests for neutral segregation are included in Supplement section.
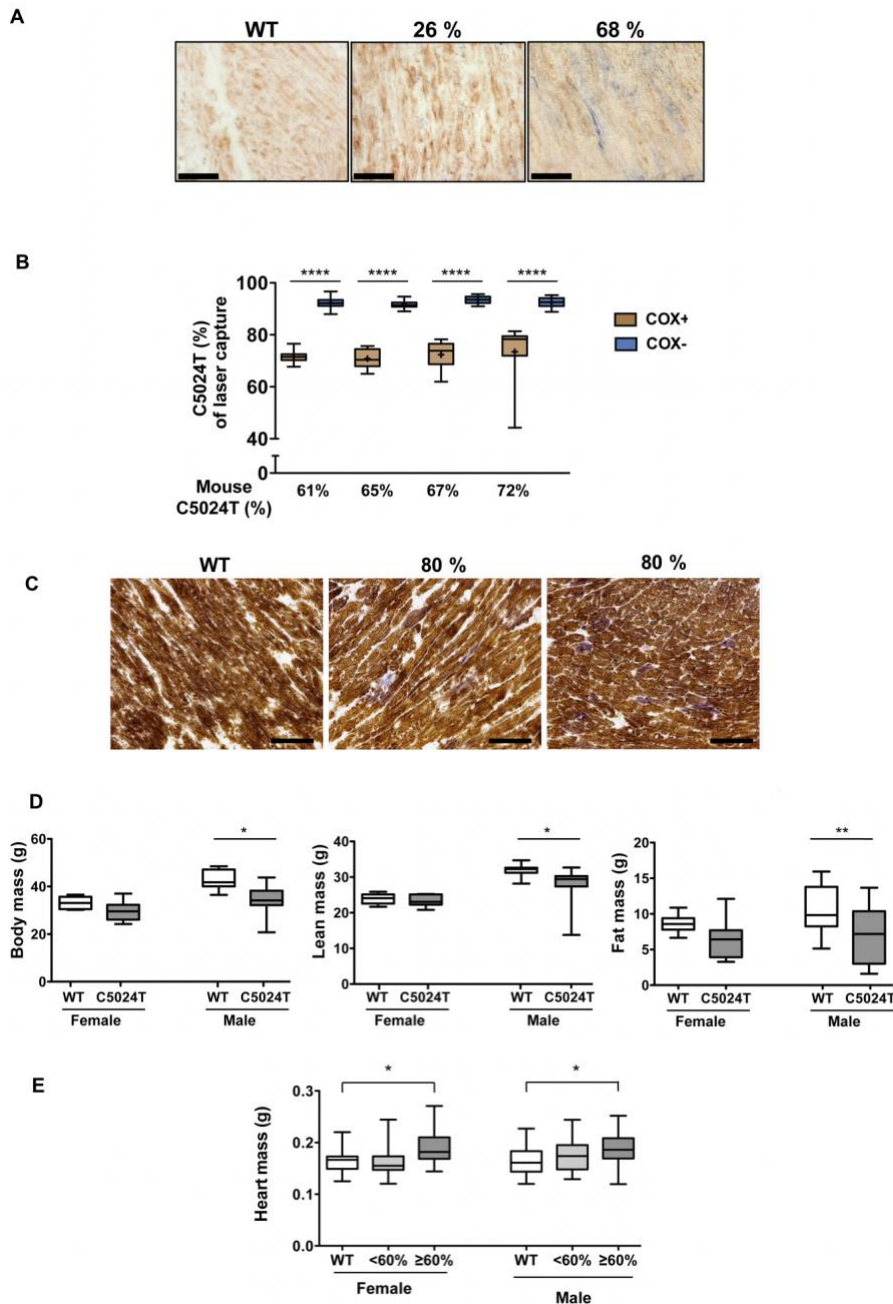
Figure 2.5 Physiological changes in mice with high levels of C5024T mutation. A. COX deficientl cells are observed in mice with a high relative level of the C5024T mutation after 40 weeks of of age. Black bar represents 50 mm. **B.** C5024T mutation level and COX deficiency from colonic smooth muscle cells. The COX negative cells have significantly higher C5024T heteroplasmy level. n = 15–22 per group. ****$p < 0.0001$ (Mann-Whitney *U* test). **C**. Occasional COX dysfunctional cardiomyocytes can be detected from mice with high C5024T heteroplasmy level. Black bar represents 100 μm. **D.** Male mice with C5024T mutation are smaller in body mass, lean mass and fat mass than the age matched controls. n=10-14 per group. Two independent cohorts were analyzed. *$p < 0.05$; **$p < 0.01$ (Dunn's multiple comparison test). **E.** Mice with high relative level of C5024T mutation show increase in heart mass, which is an indication of cardiomyopathy. *$p < 0.05$ (Mann-Whitney *U* test).   For box-and-whisker plots, bars represent data range, + represents mean, line represents median, and box shows 25th–75th percentile of the data.

2.2.5 High mutation levels of *tRNA^ALA* are selected against in proliferating tissues

At young ages (~20 weeks), the levels of *tRNA^ALA* mutation remain similar in all analyzed tissues and are consistent with the levels quantified from the tail biopsy at weaning. (~3 weeks) (Figure 2.6 A). Interestingly, at older ages (>40 weeks) the relative levels of the *tRNA^ALA* mutation decrease in the highly proliferative colonic epithelium in comparison with the surrounding smooth muscle (Figure 2.6 B). Consistently, a decrease in the mutation levels with age was also detected in peripheral blood (Figure 2.6 C). These observations suggest that highly proliferative tissues can select against high levels of the *tRNA^ALA* mutation, while in postmitotic tissues, the levels remain constant over time. Similar patterns of selection have been detected in human mtDNA mutation diseases e.g. the A3243G MELAS mutation (Ciafaloni et al., 1991) and CPEO (Larsson and Clayton, 1995). However, this is not a common phenomenon in all mtDNA diseases, for example, G8344A mutation which causes MERRF syndrome, shows consistent levels in skeletal muscle and peripheral blood (Larsson et al., 1992).
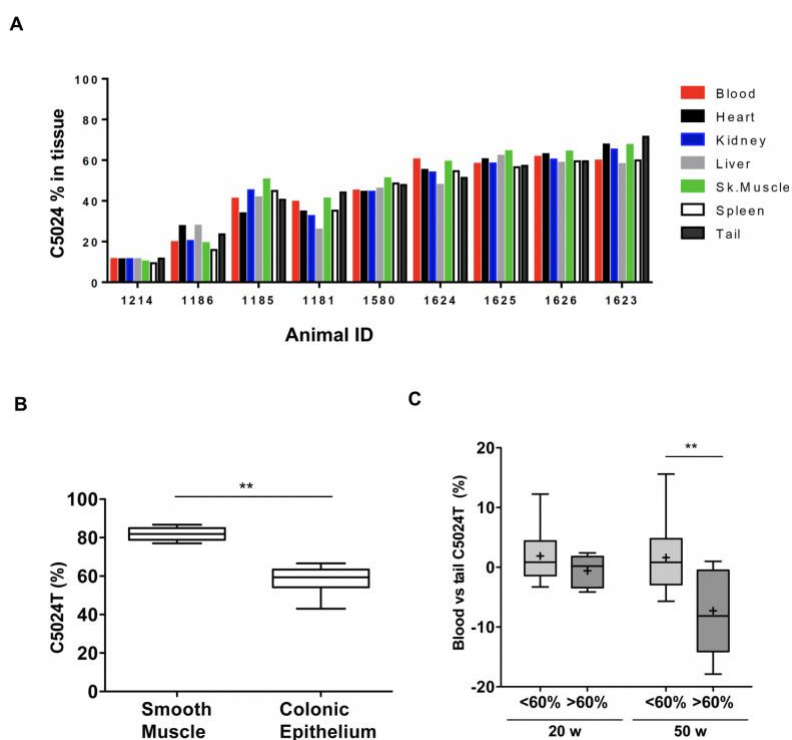
Adapted from Kauppila et al., 2016

Figure 2.6 High levels of C5024T mutation is selected against in highly proliferative tissues A. At 20 weeks of age, C5024T heteroplasmy level is similar between various tissues. n=9 **B.** At 40 weeks of age and older, the relative heteroplasmy level of laser-capture microdissected colonic epithelium decreases in comparison with its surrounding smooth muscle in the same individual n = 8. **$p < 0.01$ (Wilcoxon matched-pairs signed rank test). **C.** Relative levels of C5024T decreases with older age in peripheral blood in mice that carry high levels of C5024T mutation. **$p < 0.01$ (Mann-Whitney *U* test). For box-and-whisker plots, bars represent data range, + represents mean, line represents median, and box shows 25th–75th percentile of the data.

2.2.6 The *tRNA^ALA* mutation leads to dysfunctional mitochondrial translation

We carried out northern blot analysis on the steady-state levels of mitochondrially encoded RNA species from heart of mice with *tRNA^ALA* mutation (Figure 2.7 A, B) and found strong decrease in tRNA^ALA levels in the tRNA^ALA mutant mice. The steady-state levels of the other analyzed tRNAs were either slightly decreased (tRNA^GLN) or unaffected (tRNA^CYS, tRNA^ASN and tRNA^TRP). In turn, the steady-state levels of ribosomal RNAs (12S rRNA, 16S rRNA) were slightly elevated and the analyzed mRNAs were either normal (cox1) or slightly elevated (nad2, nad6). Interestingly, the steady-state level of tRNA^ALA correlated inversely with the relative level of C5024T *tRNA^ALA* mutation, which is consistent with the idea that C5024T mutation impairs the stability of tRNA^ALA (Figure 2.7 C).

Next, we analyzed whether the decreased steady-state levels of tRNA^ALA affects mitochondrial translation. We observed reduction in *in organello* translation from mitochondria that harbored high relative levels of C5024T mutation, demonstrating that *tRNA^ALA* mutation indeed impairs translation (Figure 2.8). The decrease in translation is detected with high relative heteroplasmy levels of *tRNA^ALA* mutation, which is consistent with the observation that mitochondrial translation is only impaired, when the mutation reaches certain threshold level (Hayashi et al., 1991; Larsson et al., 1992). Alanine amino acid constitutes ~5% of all amino acids in every mitochondrially encoded protein, explaining the general decrease in mitochondrial translation in mice with high relative levels of the *tRNA^ALA* mutation. Additionally, we observed occasional aberrant low-molecular weight translation products, which could be consistent with translational stalling or premature termination of translation (Figure 2.8).

2.3 DISCUSSION

We present here a phenotype-driven method to generate mouse models of mitochondrial disease. The approach utilizes the proofreading-deficient mutator mice (*PolγA^{+/MUT}*) to establish maternal mouse lineages that carry limited number of mtDNA mutations in wild-type nuclear background. Next, the lineages, which carry pathogenic mtDNA mutations, are detected with respiratory chain analysis from the colonic crypts of the founder mice and the pathogenic mutation in question is identified with laser-capture dissection and mtDNA sequencing. The pathogenicity of the identified mutation is additionally verified by comparing its heteroplasmy levels in crypts with normal or dysfunctional respiration. Mutations commonly clonally expand in highly proliferative tissues such as colonic crypts (Baines et al., 2014; Greaves et al., 2010; Taylor et al., 2003), which allows their detection before the onset of any obvious disease phenotypes and when they are still present in a low relative heteroplasmy levels in other tissues and would not be detected with normal Sanger sequencing of tissue samples. The alternative strategy of pathogenic mutation detection through extended phenotyping of different tissues, is highly labor-intensive as the pathogenic mtDNA mutations are commonly heteroplamic and their effects can both be pleiotropic and vary with age (Larsson and Clayton, 1995). In contrast, a purely sequence-driven approach to detect pathogenic mtDNA mutations can be mtDNA

34

mutations can be problematic as generating accurate pathogenicity predictions for mouse merely on human clinical data can be challenging. The additional advantage in our method in comparison with labor-intensive manipulation of ES cells or mouse embryos is the fact that all of the established mutations have already passed through the germline, which increases the changes that they are tolerated and can be stably transmitted in the maternal line. In contrast, this is not the case in all of the cell line or somatic tissue driven mtDNA mutations that have been introduced into mice (Fan et al., 2008; Levy et al., 1999).

As a proof of principle, we presented here the generation of a mouse line that carries a pathogenic C5024T mutation in *tRNA^{ALA}* gene of mtDNA. In high heteroplasmy levels the tRNA^{ALA} mice recapitulate important aspects of human mitochondrial disease e.g. decrease in steady-state level of the mutated tRNA and impaired translation, which leads to respiratory chain dysfunction in different tissues such as colonic crypts and smooth muscle cells

A

B

C
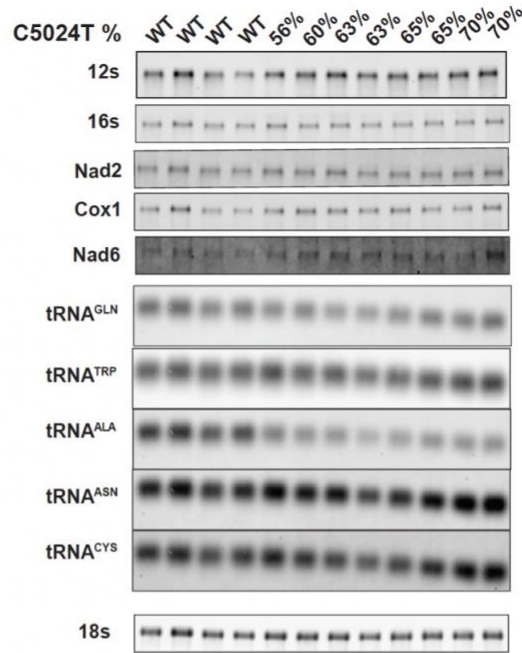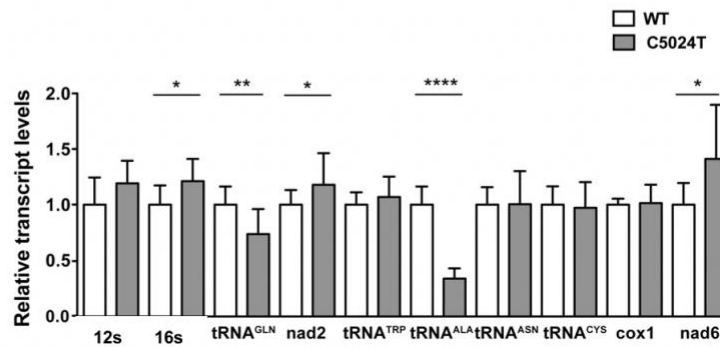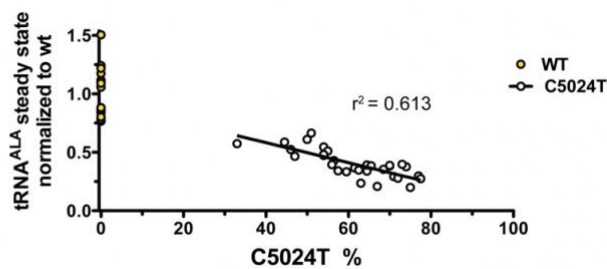
Adapted from Kauppila et al., 2016

Figure 2.7 tRNA^{ALA} steady-state levels decrease with increasing C5024T heteroplasmy level. A. Northern blot analysis of various mitochondrial transcripts from heart tissue. **B.** Quantification of the transcripts levels from three separate northern blot experiments reveals strong depletion of tRNA^{ALA} transcript and mild increase in some other transcripts. The values are normalized to 18S. WT n=12, C5024T n=19. Average age of the mice 65 weeks; C5024T heteroplasmy level 44%–77%. Error bars represent SD. *$p < 0.05$; **$p < 0.01$; ****$p < 0.0001$ (Mann-Whitney U test). **C.** The steady-state level of tRNA^{ALA} transcript is inversely correlated with C5024T relative heteroplasmy level of the mutation in heart tissue. n = 31. *$p < 0.0001$ (linear regression).
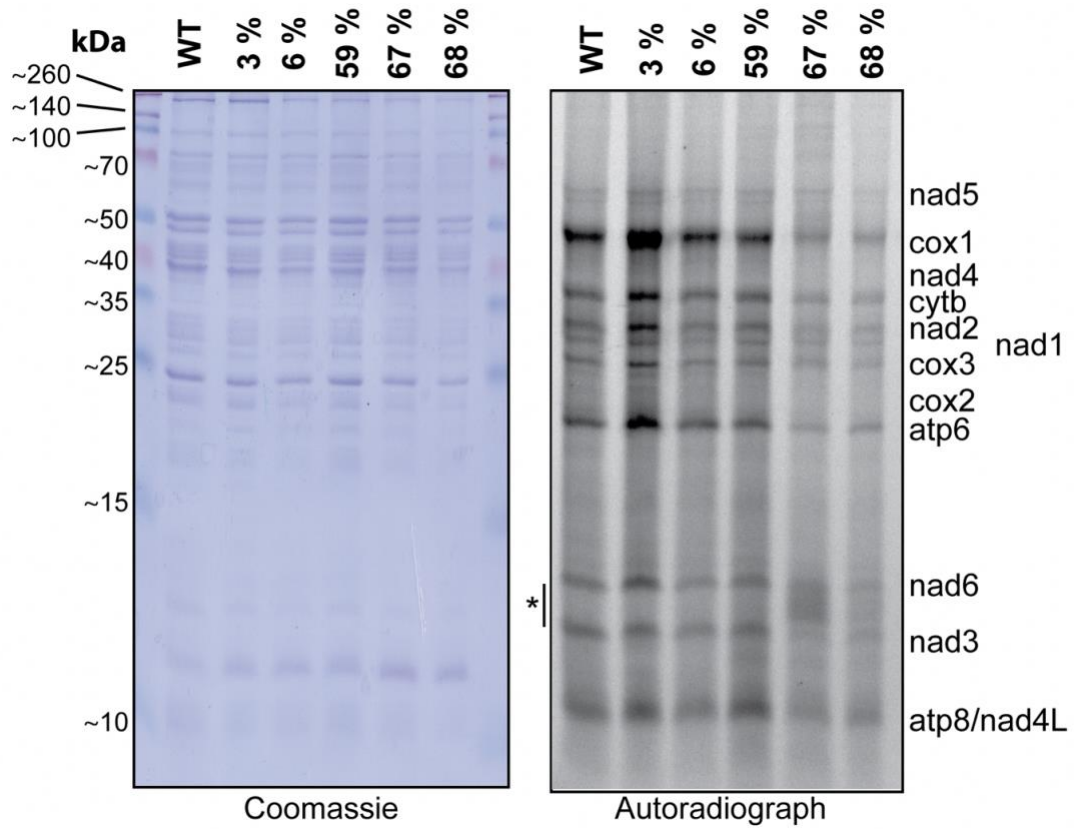
Figure 2.8 TRNA[ALA] mutation impairs translation. *In organello* translation assay from heart tissue of mice carrying C5024T mutation shows decreased translation capacity with rare low- molecular-weight aberrant translation products (*), which are consistent with stalled or prematurely terminated translation. Prior to radiography exposure the gel is stained with Coomassie to control for loading.

GENERATING MTDNA POINT MUTATIONS BY IMPAIRING MITOCHONDRIAL DNA REPAIR

3.1 INTRODUCTION

Pathogenic mutations in mitochondrial tRNA, rRNA and protein-coding genes can cause mitochondrial disease when present at high enough relative level. Mutations in protein-coding genes can be either synonymous or nonsynonymous depending on the mutation type and site. One third of the codons in mammalian mitochondria are four-fold degenerate and the rest are two-fold degenerate (Jia and Higgs, 2008). In four-fold degenerate codons, all mutations in the third codon position are synonymous, whereas, in two-fold degenerative codons only transitions are synonymous. Therefore, transversion mutations can be considered to be more harmful as they lead to nonsynonymous changes more frequently. These nonsynonymous mutations are, however, desirable when generating pathogenic mtDNA mutations to establish mouse models with mitochondrial disease. Transition mutations are induced mainly by spontaneous deamination of bases and replication errors, whereas, transversion mutations are usually caused by DNA oxidation, namely Hoogsteen pairing of oxidized guanosine (8-oxo-dG) with adenosine during DNA replication, which leads to G:C>T:A mutations.

To induce these G:C>T:A transversion mutations into mtDNA, we generated mouse models that lack the mitochondrial repair of 8-oxo-dG lesion. In late 2010, when this project was initiated, the literature was still predominantly consistent with the idea that oxidative DNA damage was a considerable mutation source in mitochondria and that DNA repair deficiency would lead to accumulation of transversion mutations. Mice that lack 8-oxoguanine DNA glycosylase 1 (OGG1) were reported to accumulate more 8-oxo-dG in mtDNA (de Souza-Pinto et al., 2001) and nuclear DNA (Klungland et al., 1999; Minowa et al., 2000). Additionally, these OGG1 knockout mice showed an increase in nuclear mutation load and large fraction of these mutations were transversions (Klungland et al., 1999; Minowa et al., 2000; Xie et al., 2004). In contrast, there was already a study, which reported that Fpg-sensitive modifications do not accumulate into intact mtDNA in repair deficient mice (Trapp et al., 2007).

3.2 RESULTS

3.2.1 Base-excision repair glycosylases OGG1 and MUTYH are predicted to localize to mitochondria in mice

Both OGG1 and MUTYH base-excision repair (BER) glycosylases are dually targeted to mitochondria and nucleus in humans (Ichinoe et al., 2004; Rosenquist et al., 1997; Takao et al., 1998; 1999) and their absence is reported to cause cancer in mice (Xie et al., 2004). To introduce transversion mutations selectively to mtDNA without nuclear effects, a genetic disruption of mitochondrial OGG1 and MUTYH is required. One way to accomplish this is to block the import of these enzymes to mitochondria. Vast majority of mitochondrial matrix proteins require a N-terminal mitochondrial targeting sequence (MTS) for import to mitochondria and thus selective removal of gene sequence which encodes the MTS, would allow selective ablation of mitochondrial MUTYH and OGG1 proteins.

To identify the predicted mitochondrial targeting sequence in mouse OGG1 and MUTYH proteins, we analyzed their peptide sequence using prediction tools. Subcellular localization prediction tools Mitoprot II (Claros and Vincens, 1996) and Target P1.1 (Emanuelsson et al., 2000; Nielsen et al., 1997) identified N-terminal MTS (M1-W23) from mouse OGG1 peptide sequence (AAB94512.1) and gave high probabilities for mitochondrial localization 0.9005 and 0.909, respectively. Similarly, the analysis of mouse MUTYH peptide sequence, (NP_001153053.1) gave high probabilities for mitochondrial localization 0.9184 and 0.871 and identified a predicted N-terminal MTS raging from M1 to P33.

We carried out western blot analyses from total and subcellular fractions of liver and heart tissues to verify the predicted mitochondrial localization of endogenous OGG1 and MUTYH proteins. Unfortunately, neither antibodies that were generated in our laboratory nor commercially available ones recognized the endogenous mouse OGG1 or MUTYH proteins on a western blot (data not shown). A subset of these antibodies, however, recognized the recombinant OGG1 and MUTYH proteins but with endogenous lysates they generated several bands on western blots. This pattern of bands was very similar to that of liver tissue extract from *Mutyh* x *Ogg1* null mice (generous gift from Prof Lars Eide). We thus conclude that the observed band pattern of endogenous tissue extracts was due to unspecific cross reactivity and that the low endogenous steady-state level of OGG1 and MUTYH proteins could hinder their detection.

3.2.2 Removal of the predicted MTS excludes OGG1 protein from mitochondria in HeLa cells

To verify the subcellular localization of OGG1, we generated reporter constructs that express mouse OGG1 protein with a C-terminal FLAG-tag with and without the predicted N-terminal MTS sequence. Next, we transiently transfected HeLa cells with these constructs and studied the localization of the OGG1-FLAG proteins with immunofluorescence microscopy. The wild-type OGG1-FLAG signal clearly co-localized with the signal of mitochondrial TOM20 protein as well as with the nuclear DAPI staining, thus demonstrating the dual localization of mouse OGG1 (Figure 3.1 A). In contrast, the OGG1-dMTS-FLAG protein displayed a dispersed signal that did not co-localize with TOM-20. In ~70% of the analyzed cells the signal was found in both cytosol and nucleus and in the rest ~30% the signal was mostly nuclear (Figure 3.1 A). In light of these results, we conclude that OGG1 in mice contains a N-terminal import signal and the removal of this sequence excludes OGG1 from mitochondria without affecting its nuclear localization. Thus, we engineered a mouse mutant, which expresses OGG1 without the N-terminal mitochondrial import signal to exclude it from mitochondria.

To verify the dual localization of mouse MUTYH protein, we transiently transfected HeLa cells with constructs that express a C-terminally FLAG tagged mouse MUTYH with and without the predicted mitochondrial import signal (MTS). Surprisingly, the wild-type and delta MTS constructs both displayed a dispersed signal that did not co-localize with nuclear DAPI staining or mitochondrial TOM20 signal (Figure 3.1 B). In humans, the mitochondrial variant

has an additional N-terminal extension (transcript variant alpha, (Ohtsubo et al., 2000; Takao et al., 1999) (Figure 3.1 B), whereas, the human nuclear MUTYH variant (transcript variant gamma) lacks this extension and is more similar with the mouse MUTYH (Ohtsubo et al., 2000; Takao et al., 1999). To study the role of this N-terminal extension we engineered a chimeric construct combining the N-terminal extension with the mouse MUTYH but the expressed protein displayed again a dispersed signal that did not co-localize with DAPI staining or mitochondrial TOM20 protein. Similarly, to the mouse MUTYH, the human nuclear variant with and without the MTS did not show a clear co-localization with either nucleus or mitochondria (Figure 3.1 B).

In summary, we were not able to verify the dual localization of mouse MUTYH, as the results from transient transfections with the reporter constructs were inconclusive, and detection of the endogenous MUTYH protein with western blotting was unsuccessful. However, as mouse MUTYH was bioinformatically strongly predicted to be mitochondrial and human MUTYH has a mitochondrial isoform, we decided to generate a mutant mouse expressing MUTYH without the predicted MTS.

3.2.3 Excluding MUTYH and OGG1 proteins from mitochondria does not lead to obvious phenotype in mice

To introduce transversion mutations to mtDNA and study the importance of BER in mitochondria, we generated *Ogg1* dMTS and *Mutyh* dMTS knockout mice that express the endogenous OGG1 and MUTYH glycosylases without the predicted MTS (Figure 3.2 A, B). The removal of nucleotide sequence encoding the MTS was verified by PCR amplification from cDNA of *Mutyh* dMTS and *Ogg1* dMTS mice. As anticipated, the transcripts were shorter in the dMTS mice in comparison with wild-type control (Figure 3.2 C, D). Furthermore, alternative splicing of the Mutyh transcripts was not affected by the removal of the sequence encoding for MTS, as all the published splice variants were still visible in the PCR analysis (Ichinoe et al., 2004).

OGG1 is a bifunctional DNA glycosylase and thus its 8-oxoguanine glycosylase activity can be measured with a simple oligonucleotide digestion assay. To verify the absence of 8-oxoguanine glycosylase/AP lyase activity from *Ogg1* dMTS mice, we incubated total and Percoll-purified mitochondrial lysates with an 8-oxo-dG containing oligonucleotide and resolved the reaction product on a denaturing acrylamide gel. As anticipated, the control lysates harbored 8-oxoguanine glycosylase/lyase activity and produced a nicked oligonucleotide, while with *Ogg1* dMTS mitochondrial lysates the oligonucleotide remained intact, demonstrating that indeed *Ogg1* dMTS mitochondria lack 8-oxoguanine glycosylase/lyase activity (Figure 3.2 E). Surprisingly, we did not detect 8-oxoguanine glycosylase/lyase activity either from total lysates from *Ogg1* dMTS mice, suggesting that the removal of MTS disrupted the activity of OGG1. As we are only evaluating the mitochondrial effects of OGG1 absence, this does not affect our analysis.
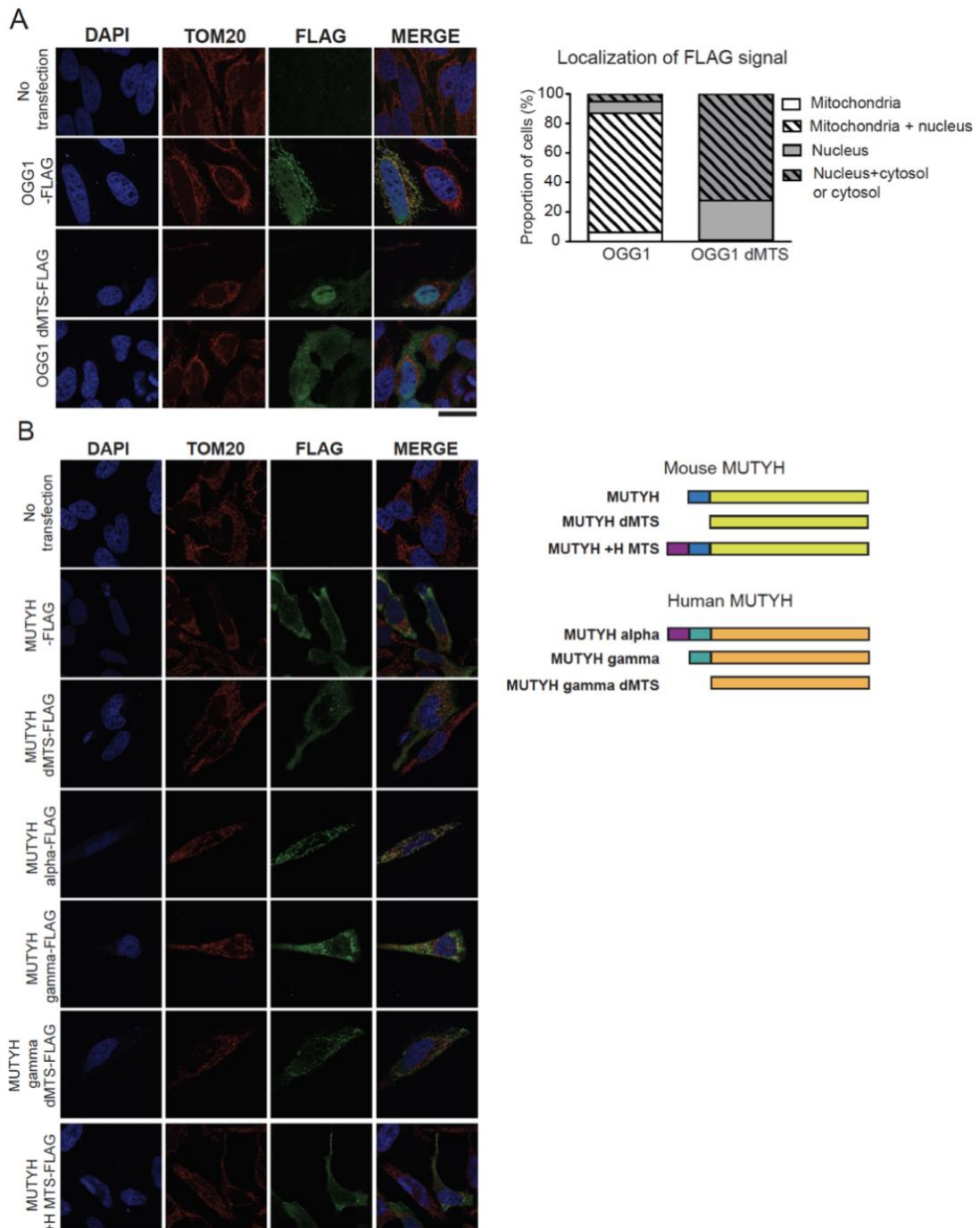
Figure 3.1 Mitochondrial targeting of OGG1 and MUTYH DNA glycosylases. HeLa cells were transiently transfected with the indicated constructs and target proteins were visualized with immunocytochemistry. Nuclear staining (DAPI, blue), mitochondrial signal (TOM20, red), OGG1/MUTYH (green, FLAG). **A.** Subcellular localization of FLAGged OGG1 with and without the predicted sequence encoding for the mitochondrial targeting sequence (dMTS). (NM_010957.4, OGG1-FLAG, OGG1 dMTS-FLAG, ΔL2-W23). Quantification of subcellular localization from 100 cells. **B.** Subcellular localization trials of human and mouse MUTYH with and without the predicted sequence encoding for the mitochondrial targeting sequence (dMTS). Mouse MUTYH variant b/2 (NM_133250.2). Human MUTYH alpha3 variant (NM_001048171.1) and gamma3 variant (NM_001048173.1). Scale bar represents 25 μm.
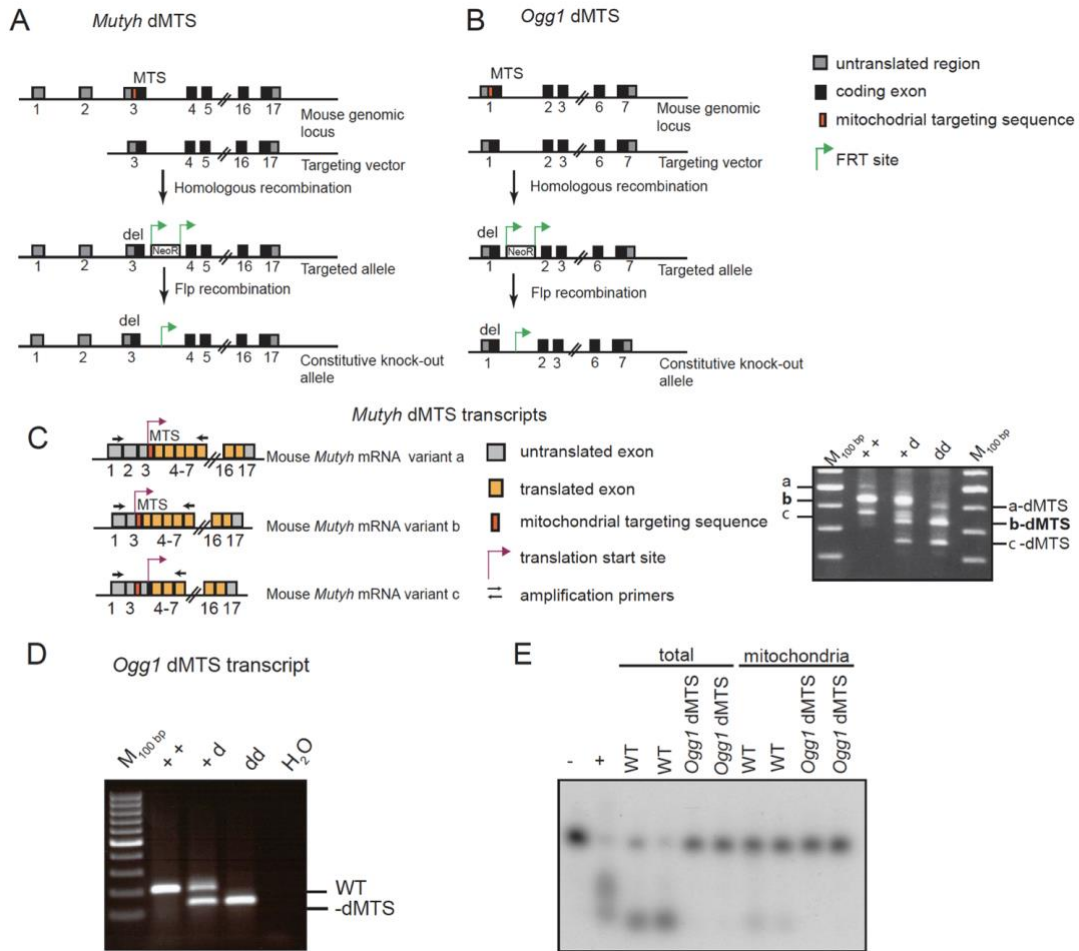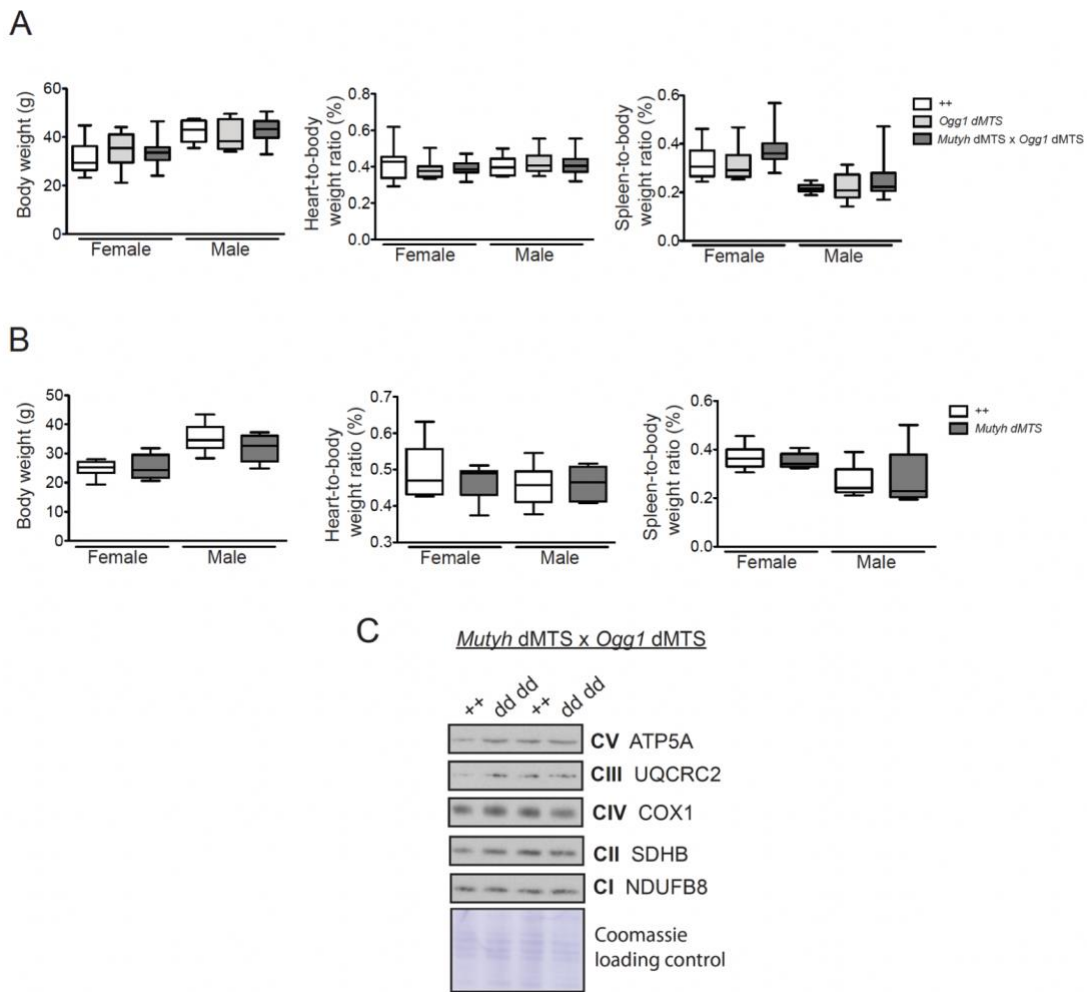
Adapted from Kauppila et al., submitted

Figure 3.2 Generation of OGG1 dMTS and MUTYH dMTS mice. Targeting strategies to generate mice lacking predicted mitochondrial targeting sequence (dMTS) of endogenous *Ogg1* and *Mutyh* genes and thus exclude these proteins from mitochondria. **A.** MUTYH (ΔK2-P33) **B.** OGG1 (ΔL2-W23). **C.** cDNA amplification of Mutyh transcript variants to very that MTS removal did not affect the mRNA splicing of Mutyh transcript. Transcript variants a, b and c are also called variants 1, 2 and 3, respectively. **D.** Correct length of *Ogg1* dMTS transcript was verified with PCR amplification from cDNA of *Ogg1* dMTS mouse. **E.** 8-oxoguanine glycosylase/AP lyase activity was assayed to verify the lack of the activity in mitochondria from *Ogg1* dMTS mice. Total and mitochondrial extracts from liver were incubated with 8-oxo-dG containing double-stranded oligonucleotide and the resulting reaction products were resolved on denaturing acrylamide gel. WT n=4, *Ogg1* dMTS n=5. No protein lysate was added to negative control (-) and recombinant OGG1 was used as positive control (+).

Next, we evaluated the overall phenotype of the *Ogg1* dMTS and *Mutyh* dMTS knockout mice. We observed no changes in body weight, spleen-to-body weight or heart-to-body weight ratios in single (*Ogg1* dMTS, *Mutyh* dMTS) or double knockout (*Mutyh* dMTS x *Ogg1* dMTS) mice (Figure 3.3 A, B). In accordance with the previous reports from *Ogg1* or *Mutyh x Ogg1* null mice (Halsne et al., 2012; Stuart et al., 2005), we observed no alterations in the steady-state level of OXPHOS proteins in liver mitochondria in the double knockout *Mutyh* dMTS x *Ogg1* dMTS mice (Figure 3.3 C). As a conclusion, excluding OGG1 or MUTYH from mitochondria does not induce any immediate negative impact on mitochondrial function or mouse physiology. This is in contrast to other known mtDNA maintenance proteins as their removal is embryonic lethal (Kühl et al., 2014; Larsson et al., 1998; Milenkovic et al., 2013).

Pol γ is demonstrated to have decreased *in vitro* efficiency in incorporating nucleotides opposite to 8-oxo-dG (Graziewicz et al., 2007; Hanes et al., 2006; Stojkovič et al., 2016). Unexpectedly, the absence of 8-oxoguanine glycosylase activity did not, however, lead to decreased mtDNA levels in *Mutyh* dMTS x *Ogg1* dMTS or *Ogg1* dMTS mice (Figure 3.4 A, C). Actually, a slight increase in mtDNA copy number was detected in fraction of the *Ogg1* dMTS and *Mutyh* dMTS x *Ogg1* dMTS mice, which was not associated with mtDNA deletions (Figure 3.4 B,D).

Figure 3.3 Physiological changes in repair deficient mice A. No change in body, heart or spleen weight was detected from *Ogg1* dMTS or *Mutyh* dMTS x *Ogg1* dMTS mice (39-41-week-old). Controls, female n=14, male n=8, homozygous *Ogg1* dMTS mice female n=10, male n=6-7 and homozygous *Mutyh* dMTS x *Ogg1* dMTS mice female n=19-21, male n=27. **B.** Body, heart or spleen weight was not altered in *Mutyh* dMTS mice. (19-21 week old). Controls, female n=10-11, male n=13, homozygous *Mutyh* dMTS mice female n=7, male n=5. Whiskers indicate min and max values, horizontal lines medians. C. Steady-state level analysis of OXPHOS proteins from homozygous *Mutyh* dMTS x *Ogg1* dMTS mice using purified liver mitochondria (40-42 week old).
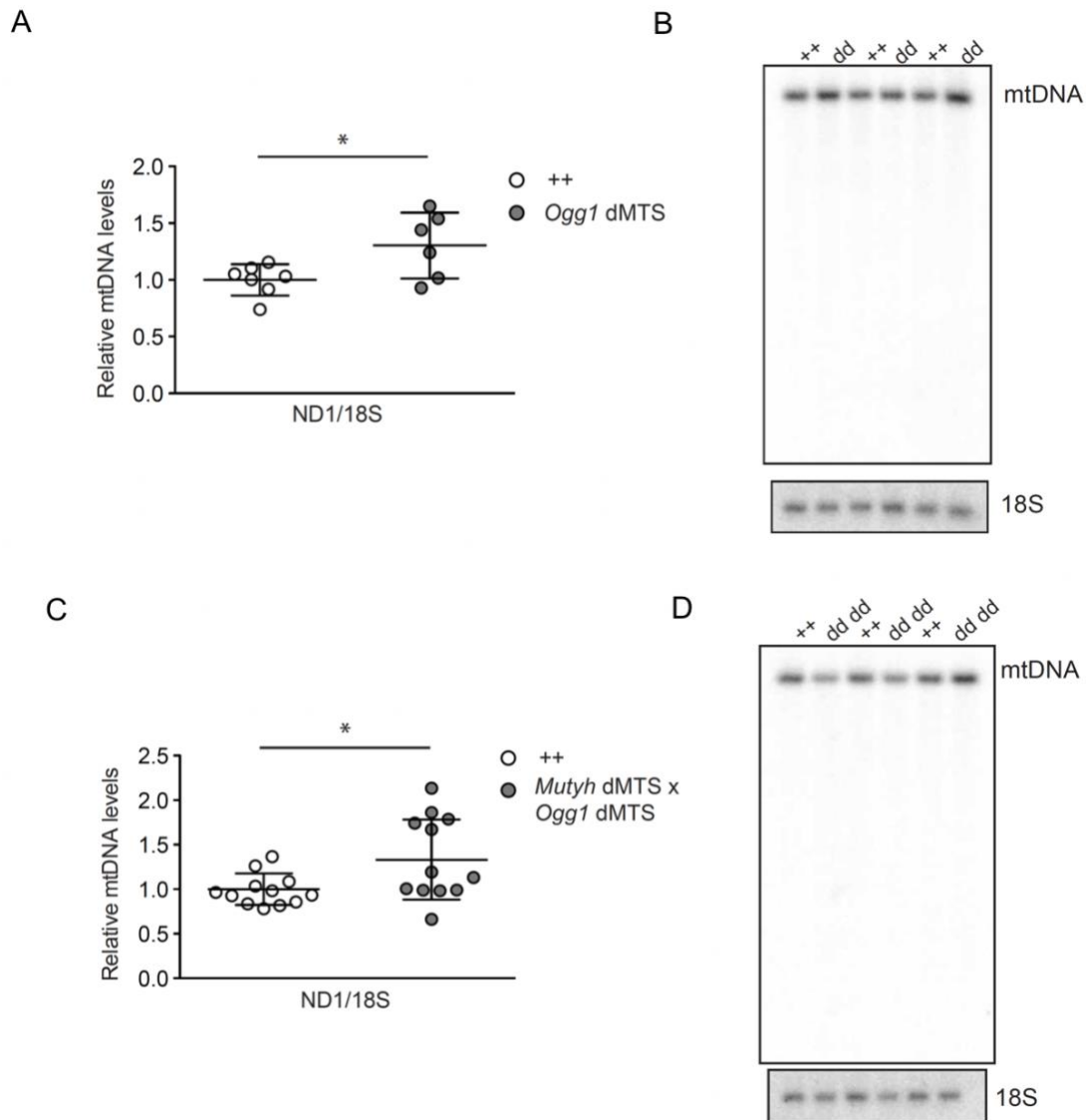
Figure 3.4 mtDNA copy number is not decreased in the repair deficient mice. Relative copy number was assessed from liver with qPCR (A, C) and Southern blotting to verify the absence of mtDNA deletions (C, D). The mtDNA copy number was evaluated with Taqman/radioactive probes against mtDNA and 18S. **A.** ++, n=7, 95-109 week old, homozygous *Ogg1* dMTS mice n=6, 88-107 week old. **C.** ++, n=7, 40-51 week old and from homozygous Mutyh dMTS x Ogg1 dMTS mice n=6, 39-50 week old. Horizontal lines represent means, error bars represent SD, *P < 0.05, Student's t-test, (C) Welch-corrected.

3.2.4 The impaired mitochondrial base-excision repair does not lead to increase in maternally transmitted or somatic mtDNA mutations

We set out to analyze mtDNA mutation load of the BER deficient mouse models by Sanger sequencing the WANCY-COX1 genomic region from cloned PCR products (post-PCR cloning). As some polymerases have been reported to have decreased efficiency in replicating 8-oxo-dG containing DNA, we first analyzed that our approach can detect 8-oxo-dG modifications and/or G>T mutations. To this end, we isolated total DNA from flies using oxidized phenol to induce oxidative damage to the DNA. This damaging *in vitro* procedure induced five-fold increase in G>T mutation load (2.42×10^{-4} versus control 4.72×10^{-5} mutations per G:C pair).

Surprisingly, when we analyzed the mutation load of BER deficient mice, we did not detect an increase in mtDNA mutation load from liver of *Ogg1* dMTS mice (1.82 x10^{-5} mutations/bp) in comparison with control mice (1.62 x10^{-5} mutations/bp) at 100 weeks of age (Table 3.1). Liver tissue was used in the analysis because the *Ogg1* null mice have been reported to show an increase in nuclear DNA mutation load in liver (Klungland et al., 1999). Although the lack of increase in mtDNA mutation load was unexpected, it is consistent with mtDNA mutation load analysis from *Mutyh* x *Ogg1* null mice with random mutation capture assay (RMC) (Halsne et al., 2012).

Table 3.1. Somatic or maternally transmitted mtDNA mutations do not increase in the absence of mitochondrial BER. Post-PCR cloning and Sanger sequencing mutation load analysis from *Ogg1* dMTS mice and *Mutyh* dMTS x *Ogg1* dMTS mice after five generations of consecutive breeding. On average 92 kb were sequenced per sample. The mutation load was analyzed from liver tissue of the WANCY-COX1 tRNA-cluster region.

Mouse line	Genotype	Age (w)	# of mutations	Mutation load	Mutations found
Ogg1 dMTS	++	109	2	2.16 x 10^{-5}	G>A, C>G
Ogg1 dMTS	++	95	0	<1.08 x 10^{-5}	
Ogg1 dMTS	dd	107	2	2.18 x 10^{-5}	A>C, A>C
Ogg1 dMTS	dd	88	0	<1.10 x 10^{-5}	
Ogg1 dMTS	dd	107	2	2.17 x 10^{-5}	G>A, T>A
Mutyh dMTS x *Ogg1* dMTS	dd dd	22	0	<1.07 x 10^{-5}	
Mutyh dMTS x *Ogg1* dMTS	dd dd	22	1	1.12 x 10^{-5}	T>C
Mutyh dMTS x *Ogg1* dMTS	dd dd	23	0	<1.09 x 10^{-5}	

Adapted from Kauppila et al., submitted

It is possible that mtDNA mutations are present in such a low level that their detection with post-PCR cloning is difficult. Therefore, we decided to increase the prevalence of mtDNA mutations by breeding double homozygous *Mutyh* dMTS x *Ogg1* dMTS mice as maternal lineages for five consecutive generations. This approach could increase mtDNA mutation load in two ways. Firstly, the well-known bottleneck phenomenon may cause mutations to clonally expand in the maternal germ line (Stewart et al., 2008a) which in turn would ease their detection. Secondly, DNA repair has been hypothesized to be more stringent in germ line and thus absence of repair could have larger effects in germ cells (Kirkwood, 1977). The mtDNA mutation load of the 5th generation homozygous *Mutyh* dMTS x *Ogg1* dMTS mice was analyzed with post-PCR cloning. However, we still did not observe an increase in mtDNA mutation load (1.09 x10^{-5} mutations/bp) (Figure 3.5 A, Table 3.1). Surprised by this result we decided to

measure the mtDNA mutation load from purified mtDNA with Illumina sequencing. This approach allows us to increase the depth of the mutational analysis and extend it to the entire mtDNA. From previous analysis we know that mtDNA mutations will clonally expand between generations to reach relative heteroplasmy levels above 1% in the offspring (Ross et al., 2013), and thus we applied a minimum variant allele frequency threshold of 0.5% to the variant called and quality filtered Illumina sequencing data. Consistently with post-PCR cloning, Illumina sequencing did not reveal increase in unique or total mtDNA mutation load even after five generations of consecutive breeding with homozygous *Mutyh* dMTS x *Ogg1* dMTS repair deficient mice (Figure 3.5 B). To verify that 0.5 % threshold for mutational frequency was not too stringent, we re-analyzed the mutation load from only quality filtered Illumina sequencing data, but again, no change in the mtDNA mutation load was detected (Figure 3.6 A). Furthermore, there was no difference in mutational spectrum between the control and repair deficient mice even without applying the 0.5% cut-off limit for mutation detection (Figure 3.5 C, Figure 3.6 B). However, the G:C>T:A mutations were highly prevalent in both repair-deficient and control samples in only quality filtered data, suggesting that these mutations were induced during library preparation step, as previously described (Chen et al., 2017; Schmitt et al., 2012) (Figure 3.6 B).

Taking all of our results together, we can conclude that impairing mitochondrial BER does not lead to increase in somatic or maternally transmitted mutations or problems with mtDNA integrity. Thus, exclusion of MUTYH and OGG1 from mitochondria cannot be used to induce transversion mutations to mtDNA in the hopes to generate mitochondrial disease models in mice.

A

B

Unique mutation load

Total mutation load

C

Unique mutations

Total mutations
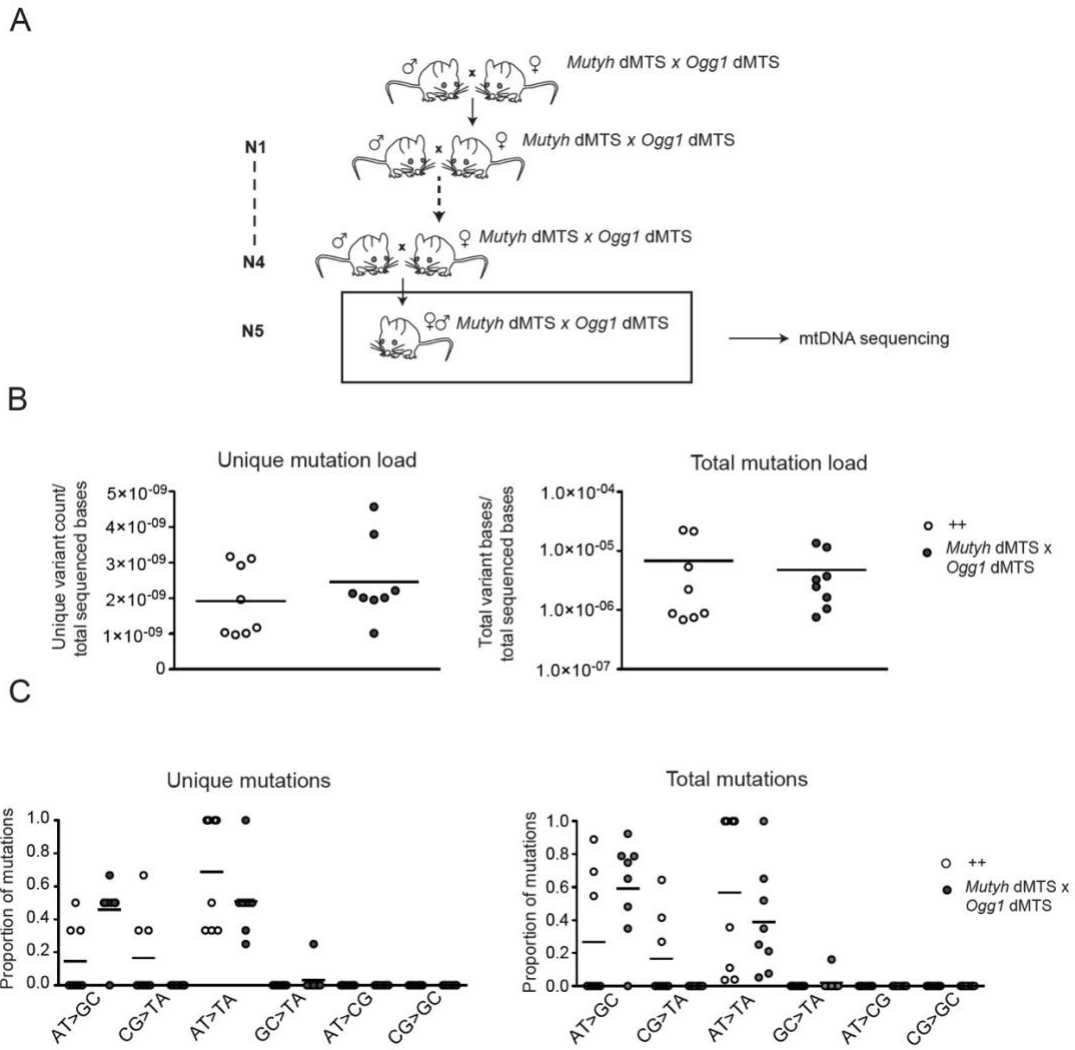
Figure 3.5 No increase in somatic or maternally transmitted mtDNA mutations were detected after five generations of consecutive breeding of repair deficient mice. Illumina sequencing, minimum variant allele frequency is set to 0.5%. A. Breeding scheme to generate repair deficient maternal lineage. To minimize nuclear effects, heterozygote male mice were occasionally used in the breeding. **B.** mtDNA mutation load after five generations of consecutive breeding from purified liver mtDNA. The sequencing data was quality filtered and minimum variant allele frequency is set to 0.5%. Unique mutation load: mutation is only counted once. Total mutation load: each mutation is counted as many times as it is observed. **C.** Mutation profile of the observed mtDNA mutations (same as in B.). Control samples, ++ n=6, pp n=2, 10-13 week old and homozygous *Mutyh* dMTS x *Ogg1* dMTS mice n=8, 10-15 week old. Horizontal line represent mean.

A

B
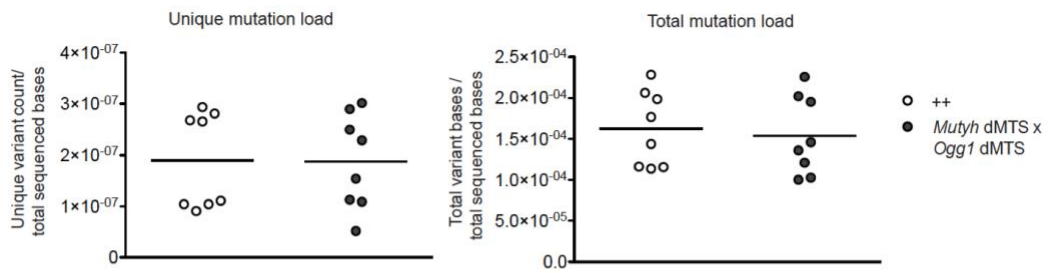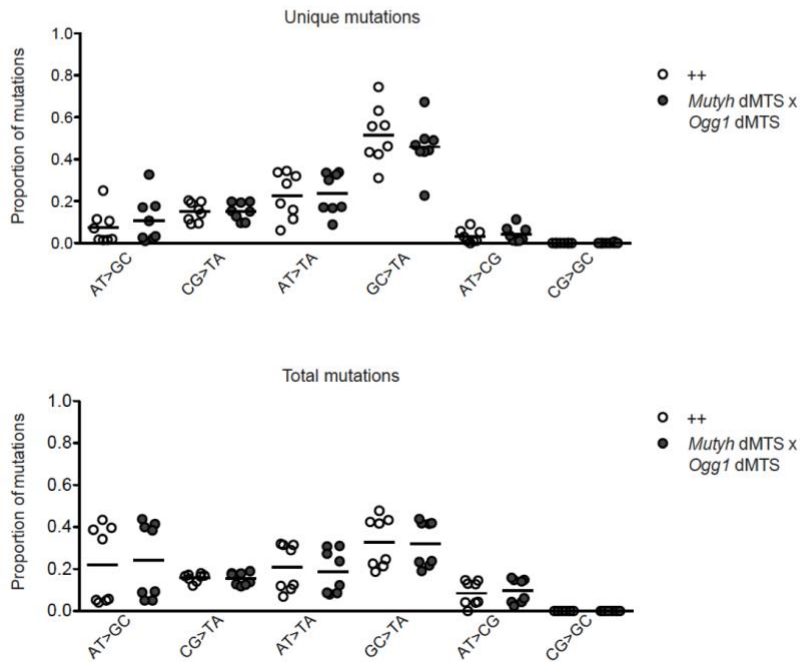
Figure 3.6 No increase in somatic or maternally transmitted mtDNA mutations were detected after five generations of consecutive breeding of repair deficient mice. Illumina sequencing, only quality filtered data. A. mtDNA mutation load after five generations of consecutive breeding from purified liver mtDNA. The sequencing data was only quality filtered. Unique mutation load: mutation is only counted once. Total mutation load: each mutation is counted as many times as it is observed. **B.** Mutation profile of the observed mtDNA mutations (same as in A.). Control samples, ++ n=6, pp n=2, 10-13 week old and homozygous *Mutyh* dMTS x *Ogg1* dMTS mice n=8, 10-15 week old. Horizontal line represent mean.

3.2.5 The absence of SOD2 induces strong increase in oxidative stress and impairs the function of [4Fe-4S] cluster containing proteins

Puzzled by the lack of increase in mtDNA mutation load in the repair-deficient mice, we decided to increase the oxidative stress in mitochondria to enhance the generation of oxidative stress driven mutations. To this end, we used mice that were deficient in mitochondrial matrix superoxide dismutase SOD2. SOD2 is the first line of defense against ROS, because it converts superoxide into hydrogen peroxide (Murphy, 2009; Murphy et al., 2011). It is the sole superoxide dismutase that resides in the mitochondrial matrix and thus it is extensively used in studies that evaluate the consequences of increased oxidative stress on cellular and mitochondrial function (Li et al., 1995; Lustgarten et al., 2009; Nojiri et al., 2006; Strassburger et al., 2005; Van Remmen et al., 2003; Williams et al., 1998). In our study, we utilized a previously published conditional knockout allele (Strassburger et al., 2005) that disrupts the *Sod2* in heart and in certain fiber types in skeletal muscle (*Ckmm cre*, Figure 3.7 A). We refer to these mice from now on as heart *Sod2* knockout mice. Consistently with previous analysis (Nojiri et al., 2006), these mice develop a severe dilated cardiomyopathy (Figure 3.7 B-D) and their medium lifespan is reported to be only 15 ± 4 weeks (Nojiri et al., 2006). However, in our hands, they were severely afflicted already at the age of 11-12 weeks and thus we mainly analyzed them at 10-11 weeks of age. At this age, male mice show weight reduction, whereas, the heterozygote knockout mice are comparable to control mice in both body weight and heart size (Figure 3.7 C, D).
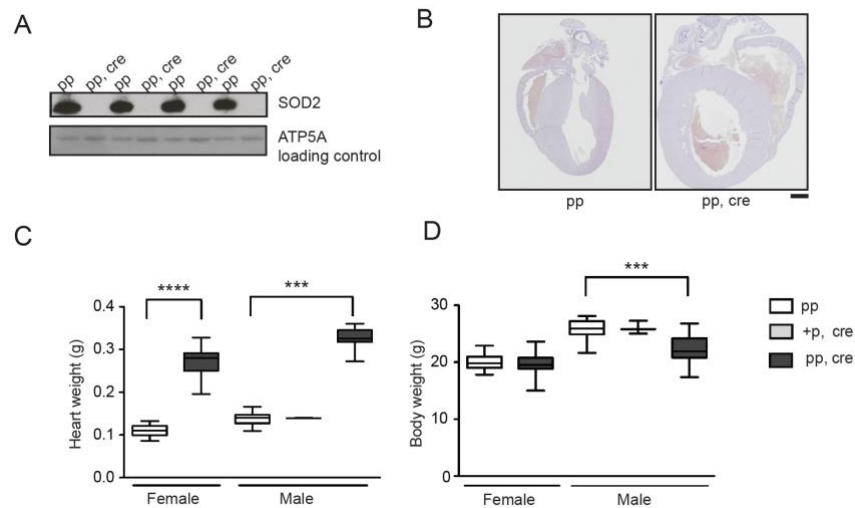
Adapted from Kauppila et al., submitted

Figure 3.7 The absence of SOD2 in heart leads to severe cardiomyopathy. A. SOD2 protein is absent in heart mitochondria in the cre positive heart *Sod2* knockout mice (*Sod2 loxP* x *Ckmm cre* mice, pp, cre). 9-11 week old. ATP5A was used as a loading control. **B**. H&E staining from vertical section of paraffin embedded heart tissue show enlarged heart in the heart *Sod2* knockout mice (pp, cre) in comparison with control. Age of the pp cre mice: 10 weeks, controls: 11 weeks. Scale bar represents 1 mm. **C.** Heart weight of *Sod2 loxP* x *Ckmm cre* mice is increased, which is an indicative of cardiomyopathy. pp female n=22, male n=35, 9-11 week old, heterozygous male +p, cre, n=2, 9-week old, *Sod2 loxP* x *Ckmm cre* mice pp, cre, female n=28, male n=15, 9-10 week old. **D.** At late stage, the body weight of heart *Sod2* knockout male mice (pp, cre) decreases. Control pp female n=26, male n=36, 9-11 week old, heterozygous male +p, cre, n=3, 9-week old, *Sod2 loxP* x *Ckmm cre* mice pp, cre, female n=30, male n=19, 9-10 week old. Whiskers represent min and max values, horizontal lines medians; ****$P< 0.0001$, females Student's t-test, Welch corrected. ***$P< 0.001$, males 1way ANOVA, Dunnett's multiple comparison test.

[4Fe-4S] clusters are highly susceptible to superoxide-induced damage and the loss of SOD2 enzyme activity induced a biochemical dysfunction in [4Fe-4S] cluster-containing proteins (Li et al., 1995; Nojiri et al., 2006), including a strong decrease in aconitase enzyme activity (Figure 3.8 A, B). In aconitase the [4Fe-4S] cluster is solvent accessible and required for its enzyme activity and thus it has been used as a surrogate marker for superoxide levels (Gardner et al., 1995; Tarpey et al., 2004). In addition to decrease in enzyme activity, the steady-state level of aconitase was also decreased in heart *Sod2* mice on a western blot (Figure 3.8 B) and in mass spec analysis (Figure 3.9), together indicating a strong increase in superoxide levels in these mice. In addition to aconitase, OXPHOS complexes I and II, contain [4Fe-4S] clusters, whereas they are absent in other respiratory chain complexes (Gao et al., 2003; Sun et al., 2005; Tsukihara et al., 1996; Wirth et al., 2016). This disposition can be utilized to verify the increase in superoxide levels and study its effects to OXPHOS. To this end, we evaluated respiration of the heart *Sod2* knockout mice on freshly purified intact heart mitochondria with polarographic methods. The measurement was carried out with substrates that result in entry of electrons to complex I (pyruvate, glutamate, malate, PGM) or complex II (succinate, SUCC). The oxygen consumption was measured in phosphorylating (state 3: ADP and Pi, PGM3, SUCC3), non-phosphorylating (state 4: oligomycin to inhibit ATP synthase PMG4, SUCC4) and uncoupled state (with CCCP PMGc, SUCCc). Both complex I and complex II driven respirations were profoundly decreased in heart *Sod2* knockout mitochondria analyzed under phosphorylating and uncoupled conditions (Figure 3.8 C). This dysfunction was accompanied with consistent decrease in isolated enzyme activities of CI, CII and CII-CIII (Figure 3.8 D). In turn, the activity of complex IV, which does not contain [4Fe-4S] clusters, remained unaffected (Figure 3.8 D), as previously demonstrated with COX-SDH enzyme histochemistry from these mice (Li et al., 1995; Nojiri et al., 2006). Correspondingly, we observed no effect in the steady-state levels of protein subunits of complex III, IV and V subunits on a western blot (Figure 3.8 E, (Nojiri et al., 2006)). On the contrary, the steady-state level of subunits of complex I and complex II were strongly decreased on a western blot (Figure 3.8 E) (Nojiri et al., 2006). In summary, heart *Sod2* knockout mice show a specific defect in proteins carrying [4Fe-4S] clusters, indicating an expected increase in superoxide level in these mice.

3.2.6 Label-free quantitative proteomic analysis from enriched mitochondria reveals signs of general mitochondrial stress in heart *Sod2* knockout mice

Next, we analyzed the mitochondrial proteome from Percoll purified mitochondria of heart *Sod2* knockout mice (Figure 3.9). The analysis revealed that, in addition to respiratory dysfunction, multiple subunits of complex I and II were strongly decreased in heart Sod2 knockout mice. The decrease was accompanied with an increase of several assembly factors for complex I, II and IV, suggesting a compensatory response in assembly of OXPHOS complexes (Figure 3.9). Additionally, we observed indications of general mitochondrial stress as the steady-state levels of defense proteins (SOD1, PRDX5, MSRA), mitochondrial proteases (CLPX, LONP1,

YME1L1), proteins involved in mitochondrial translation and mitochondrial import machinery components (TIMM, TOM) were increased (Figure 3.9).
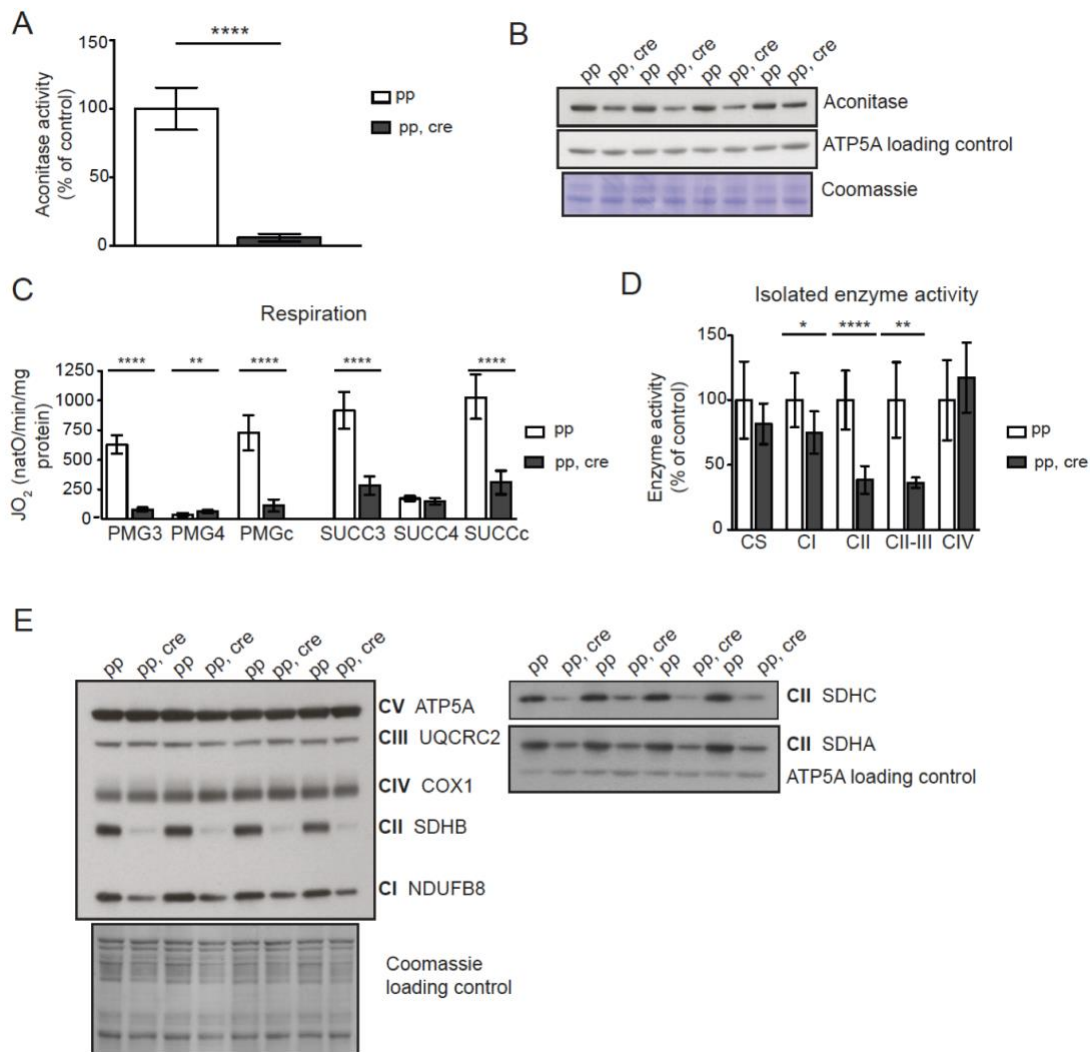
Figure 3.8 The severe impairment of mitochondrial [4Fe-4S] cluster proteins indicates an increase in superoxide levels in heart *Sod2* knockout mice. A. Aconitase activity is severely decreased in heart mitochondria of heart *Sod2* knockout mice. Activity is normalized to control. Control samples (n=6), 9-10 week old, *Sod2 loxP* x *Ckmm cre* samples (n=6), 9-12 week old. **B.** Aconitase steady-state levels assessed from purified heart mitochondria on a western blot. Mice were 9-10 week old. ATP5A and coomassie stained membrane are used as a loading control. **C.** Absence of SOD2 impairs respiration. Oxygen consumption rate was measured from isolated heart mitochondria in the presence of pyruvate glutamate malate (PMG) and succinate (SUCC) complex I and II substrates, respectively. In the presence of the substrate ADP and oligomycin were added successively to measure phosphorylating (PMG3, SUCC3), and non-phosphorylating respiration (PMG4, SUCC4). Lastly CCCP was added to measure uncoupled respiration (PMGc, SUCCc). Control samples (n= 9), 9-11 week old, *Sod2 loxP* x *Ckmm cre* samples (pp, cre, n=9), 9-12 week old. **D.** Isolated enzyme activity of respiratory complexes from heart mitochondria. Citrate synthase activity (CS) was used as a control. Control (pp, n= 3), 11-week old and *Sod2 loxP* x *Ckmm cre* mice (pp, cre, n=3), 11-12 week old. **E.** Steady-state levels of OXPHOS complexes in heart mitochondria. ATP5A and coomassie stained membrane were used as a loading control. Error bars represent SD. *$P< 0.05$, **$P< 0.005$, ****$P< 0.0001$, Student's t-test, Welch corrected.
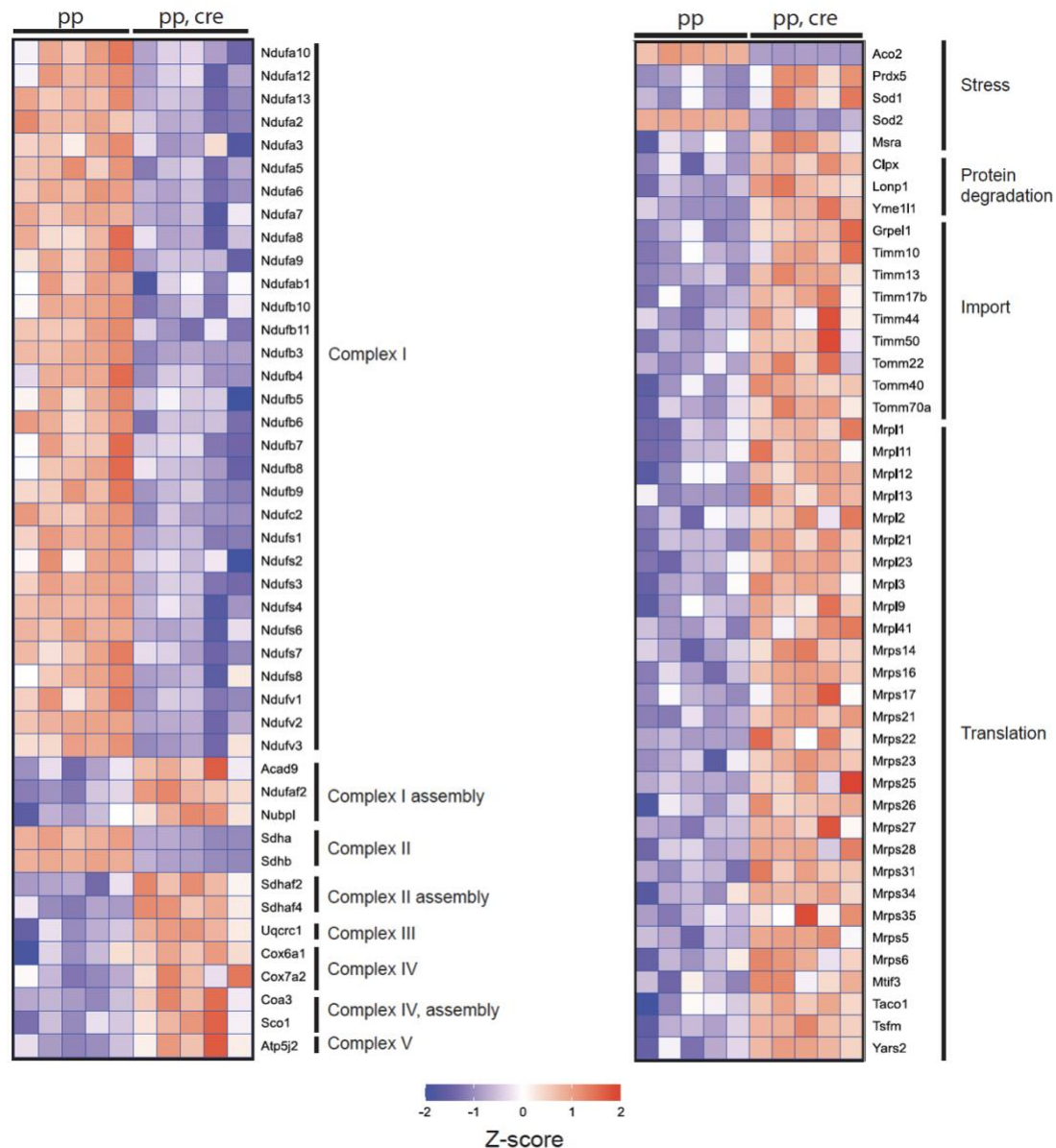
Figure 3.9 A global decrease in complex I proteins is detected in the heart *Sod2* knockout mice. A label-free quantitative proteomics analysis from Percoll purified heart mitochondria. A selected set of proteins with significantly altered steady-state level are depicted in a heat map. Controls pp, 8-9 week old and *Sod2 loxP x Ckmm cre* mice pp, cre, 9-10 week old. Blue color indicates decreased and red increased steady-state level over the mean across all samples. Change in steady-state level was considered significant when Benjamini–Hochberg adjusted p-value was less than 0.05

3.2.7 No increase in mtDNA mutation load is detected in heart *Sod2* knockout mice in the absence of mitochondrial BER

To generate a mouse model with increased oxidative stress and deficiency in BER, we combined the *Ogg1* dMTS mice with heart *Sod2* knockout mice. Surprisingly, the clear increase in oxidative stress in combination with OGG1 deficiency did not lead to increase in mtDNA mutation load in 10-week-old mice in comparison with controls (1.30×10^{-5} vs. 1.10×10^{-5} mutations/bp) in post-PCR cloning and Sanger sequencing analysis (Table 3.2). However, it

should be mentioned that these observed mutation loads are close to the minimum mutation load ($\sim 1.1 \times 10^{-5}$) which can be still detected with the depth of our post-PCR cloning approach. Therefore, they represent the upper limit of the mutation load that is present in these mice. In line with our observations, no increase in mtDNA mutation load was either detected in flies with decreased SOD2 activity combined with a loss-of-function mutation in Ogg1 when the mutation load was measured by RMC (Itsara et al., 2014). To expand the mutation analysis to the whole mtDNA and increase the depth of the analysis, we carried out Illumina sequencing on purified mtDNA from heart *Sod2* knockout x *Ogg1* dMTS mice. However, we observed no increase in mtDNA mutation load from these double mutant mice using the 0.5% minimum variant allele frequency threshold (Figure 3.10) or only quality-filtered data (Figure 3.11). We detected neither an increase in G:C>T:A transversion mutations.

Table 3.2 No increase in mtDNA mutation load was observed in the absence of SOD2 and OGG1 proteins in heart. Post-PCR cloning and Sanger sequencing mutation load analysis from *Sod2* loxP x *Ckmm cre* x *Ogg1* dMTS mice. On average 92 kb were sequenced per sample. The mutation load was analyzed from heart tissue of the WANCY-COX1 tRNA-cluster region.

Mouse line	Genotype	Age (w)	# of mutations	Mutation load	Mutations found
Sod2 loxp	pp	10	1	1.09×10^{-5}	T>C
Sod2 loxp x *Ckmm cre*	pp	10	0	$<1.10 \times 10^{-5}$	
Sod2 loxp x *Ckmm cre* x *Ogg1* dMTS	pp, cre dd	10	2	2.14×10^{-5}	G>T, G>T
Sod2 loxp x *Ckmm cre* x *Ogg1* dMTS	pp, cre dd	9	0	$<1.14 \times 10^{-5}$	
Sod2 loxp x *Ckmm cre* x *Ogg1* dMTS	pp, cre dd	10	1	1.09×10^{-5}	G>A
Sod2 loxp x *Ckmm cre* x *Ogg1* dMTS	pp, cre dd	10	1	1.08×10^{-5}	C>T
Sod2 loxp x *Ckmm cre* x *Ogg1* dMTS	pp, cre dd	10	1	1.07×10^{-5}	A>T
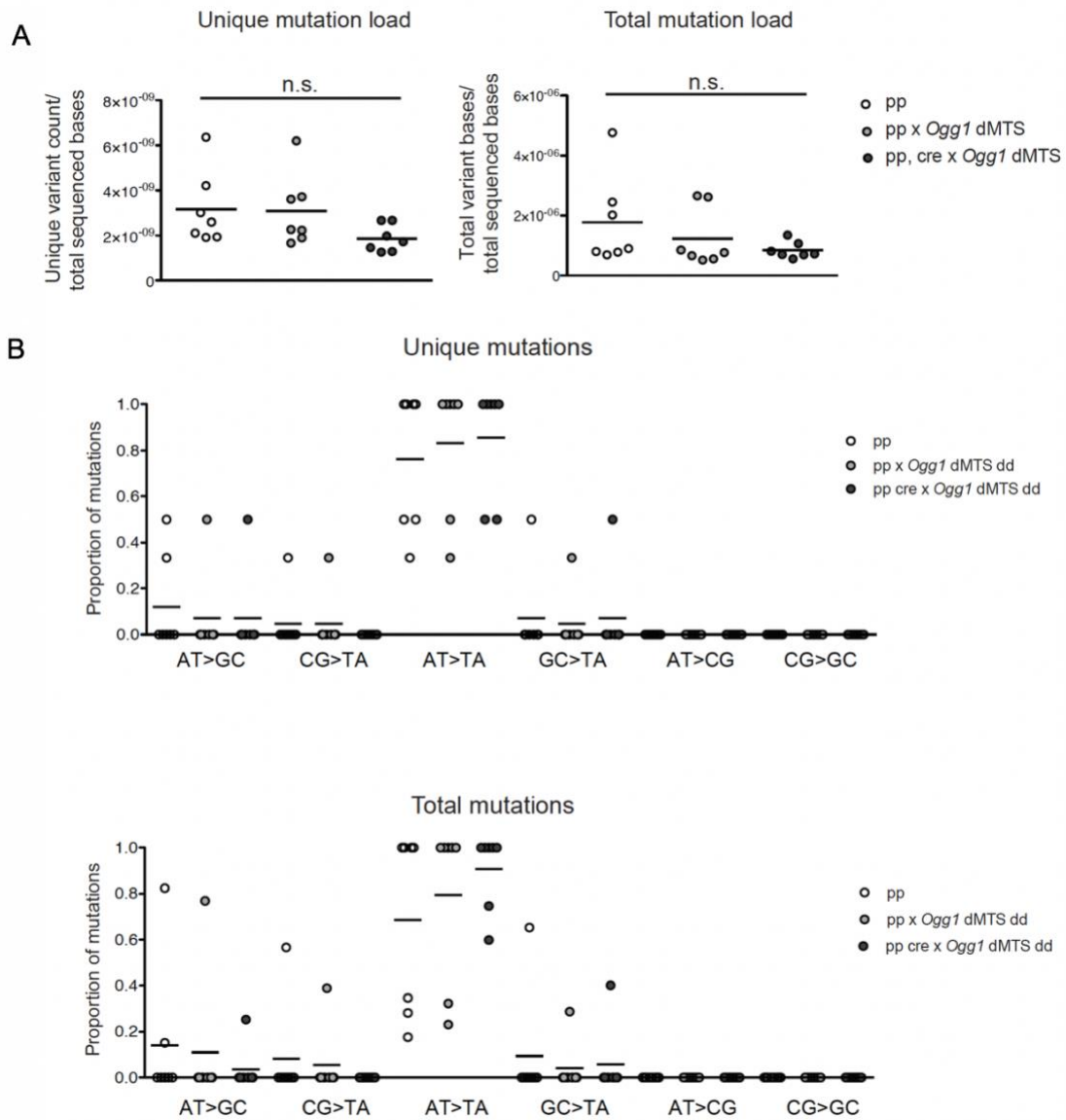
Adapted from Kauppila et al., submitted

Figure 3.10 MtDNA mutation load does not increase in mitochondrial BER deficient mice in the presence of increased oxidative stress. Illumina sequencing, minimum variant allele frequency is set to 0.5%. A. mtDNA mutation load in *Sod2 loxP x Ckmm cre* x *Ogg1* dMTS mice heart measured with Illumina sequencing from purified mtDNA. The sequencing data was quality filtered and minimum variant allele frequency is set to 0.5%. Unique mutation load: mutation is only counted once. Total mutation load: each mutation is counted as many times as it is observed. **B.** Mutation profile of the observed mtDNA mutations (same as in B.). Controls (pp n=4 or ++ n=3), 8-12 week old, *Sod2 loxP x Ogg1* dMTS mice (pp dd n=4 or +p dd n=2 or +p cre+ dd n=1) 8-11 week old and *Sod2 loxP x Ckmm cre* x *Ogg1* dMTS mice (pp, cre dd, n=7), 9-10 week old. Horizontal line represent mean. 1way ANOVA, Tukey's multiple comparison test.
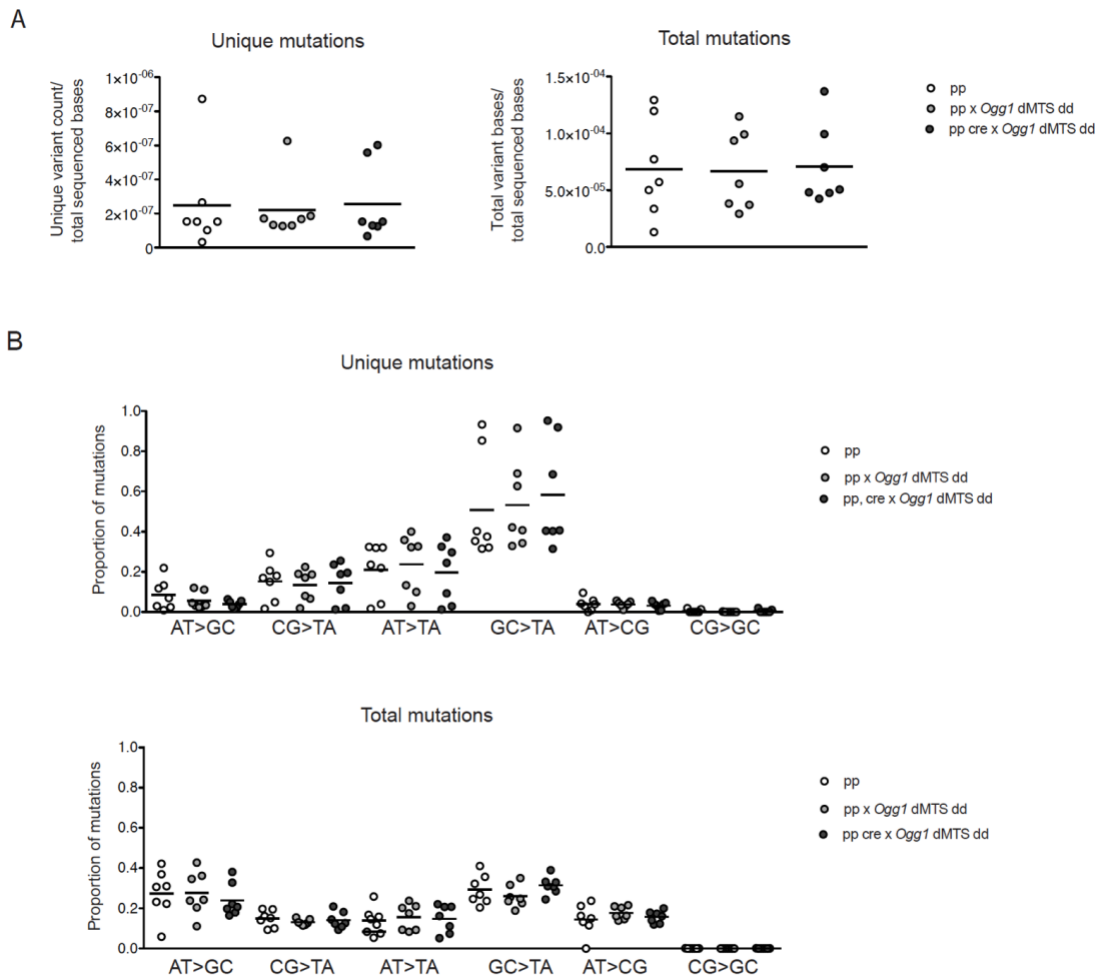
Figure 3.11 MtDNA mutation load does not increase in mitochondrial BER deficient mice in the presence of increased oxidative stress. Illumina sequencing, only quality filtered data. A. mtDNA mutation load in *Sod2 loxP x Ckmm cre* x *Ogg1* dMTS mice heart measured with Illumina sequencing from purified mtDNA. The sequencing data was only quality filtered. Unique mutation load: mutation is only counted once. Total mutation load: each mutation is counted as many times as it is observed. **B.** Mutation profile of the observed mtDNA mutations (same as in B.). Controls (pp n=4 or ++ n=3), 8-12 week old, *Sod2 loxP x Ogg1* dMTS mice (pp dd n=4 or +p dd n=2 or +p cre+ dd n=1) 8-11 week old and *Sod2 loxP x Ckmm cre* x *Ogg1* dMTS mice (pp, cre dd, n=7), 9-10 week old. Horizontal line represent mean.

3.2.8 Mitochondrial RNA mutation load is not increased in SOD2 and BER deficient mice

Based on the mtDNA mutation analysis from our animal models, it seems that oxidative stress has only limited effects to mtDNA mutagenesis. It has been reported, however, that the mitochondrial RNA polymerase, POLRMT, *in vitro* preferentially incorporates adenosine opposite to 8-oxo-dG during transcription (Nakanishi et al., 2013), and thus oxidative modifications in mtDNA could induce G:C>T:A mutations to mitochondrial RNA. To address this question, we carried out total RNA seq from heart *Sod2* knockout mice alone and in combination with mitochondrial OGG1 deficiency. To sequence RNA, it needs to be converted to DNA in reverse transcription reaction, which is known to be highly error-prone process. However, the reverse transcriptase that was used in our library preparation (Moloney murine

56

leukemia virus reverse transcriptase) rarely makes G>T transversion mutations (Ellefson et al., 2016), which justifies our approach to RNA mutation analysis. We observed no increase in RNA mutation load or frequency of G:C>T:A mutations in the heart *Sod2* knockout mice alone and combined with mitochondrial OGG1 deficiency in comparison with control mice with only quality-filtered data (Figure 3.12). Similar results were additionally, obtained with the quality-filtered and 0.5% cut-off data (Figure 3.13). POLRMT has been shown *in vitro* to stall on 8-oxo-dG during transcription (Nakanishi et al., 2013), which might explain the lack of increase in G:C>T:A mutations. However, transcription elongation factor (TEFM) has been shown *in vitro* to stimulate transcription past 8-oxo-dG, suggesting that 8-oxo-dG is not a stalling lesion for POLRMT *in vivo* (Posse et al., 2015).

3.2.9 No topological alterations were detected in mtDNA from heart *Sod2* knockout mice

In addition to mtDNA mutations, oxidative stress can induce various DNA lesions such as single-stranded breaks and abasic sites (Pogozelski and Tullius, 1998; Shokolenko et al., 2009). Because mouse mtDNA is a circular molecule, double and single-stranded breaks will alter the topology of mtDNA. To analyze the changes in mtDNA integrity we extracted total DNA from fresh heart tissue and resolved the different topological stages of mtDNA with low percent agarose gel and visualized them with radioactive mtDNA specific probes. The DNA was resolved in the presence and absence of ethidium bromide (EtBr), which intercalates with DNA and thus, concentrates different stages of supercoiling of the closed-circle mtDNA into a quantifiable band (Figure 3.14 A). We analyzed the proportional distribution of mtDNA molecules in the different topological states (catenanes, nicked circles, linear and closed circles) but we observed no substantial changes in the proportions between knockout *Sod2* mice and controls (Figure 3.14 A, B). If the presence of single-strand breaks would be increased, the number of nicked circles would increase at the expense of closed circles. As this was not the case, it suggests that the heart *Sod2* knockout mice seem not to accumulate extensive number of single-stranded breaks during continuous oxidative stress.

Abasic sites do not induce distortion to mtDNA topology and thus they cannot be visualized on a topology gel without an enzymatic treatment, which converts them to single-stranded nicks. To reveal abasic sites in heart *Sod2* knockout mice, we treated the extracted DNA with EndoIV prior to electrophoresis. However, we did not observe an increase in conversion of closed to nicked circles upon EndoIV treatment, in heart *Sod2* knockout mice (Figure 3.14 C). Together these topological analyses suggest that either mtDNA is quickly repaired after an oxidative insult or that mtDNA is sufficiently shielded from damage in nucleoids. Additional possibility is that the damaged mtDNA is degraded and thus not detected. Previous studies have reported that the proportion of oxidized bases is higher in fragmented than intact mtDNA (Suter and Richter, 1999) and that oxidized mtDNA is degraded (Shokolenko et al., 2009). Furthermore, mitochondrially-targeted restriction enzyme experiments in mice have demonstrated that linear mtDNA fragments are digested rapidly, which causes a decrease in mtDNA copy number. To

address this possibility, we measured the mtDNA copy number with qPCR approach from heart *Sod2* knockout mice but found in turn a slight increase in mtDNA copy number (Figure 3.15 A). Additionally, we verified the absence of mtDNA deletions with Southern blot (Figure 3.15 B).
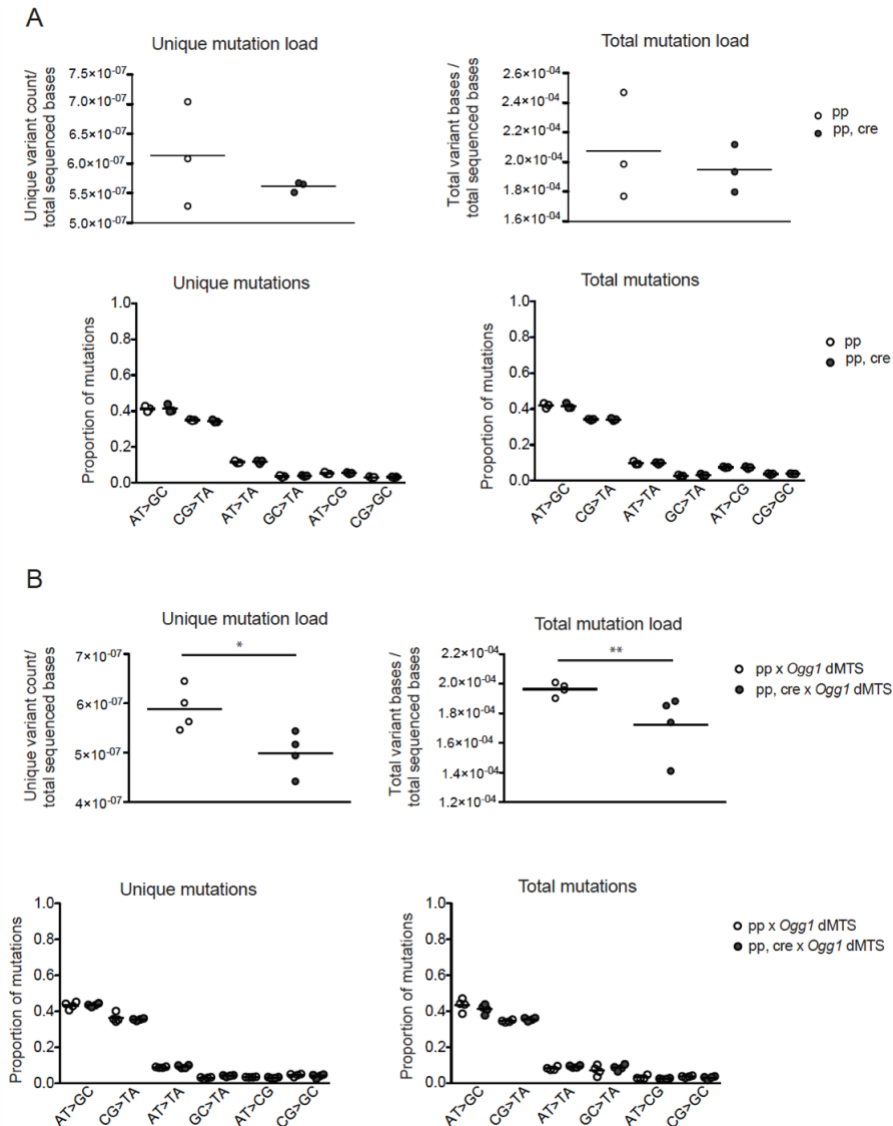
Adapted from Kauppila et al., submitted

Figure 3.12 MtRNA mutation load does not increase in heart *Sod2* knockout mice in the absence and presence of mitochondrial BER. Illumina sequencing, only quality filtered data. A. mtRNA mutation load was evaluated from *Sod2 loxP x Ckmm cre* mice with Illumina sequencing. Variant call was carried out to reads that mapped to mtDNA. The sequencing data was quality filtered. Unique mutation load: mutation is only counted once. Total mutation load: each mutation is counted as many times as it is observed. Profile of the of the mtRNA mutations. Controls (+p n=1 pp n=2), 10-11 week old, *Sod2 loxP x Ckmm cre* mice (pp, cre n=3) 10-11 week old. **B.** mtRNA mutation load was evaluated from *Sod2 loxP x Ckmm cre x Ogg1* dMTS mice with Illumina sequencing. Variant call was carried out to reads that mapped to mtDNA. The sequencing data was quality filtered. Unique mutation load: mutation is only counted once. Total mutation load: each mutation is counted as many times as it is observed. Profile of the of the mtRNA mutations. Controls (pp dd n=4), 9-10 week old, *Sod2 loxP x Ckmm cre x Ogg1* dMTS mice (pp, cre dd, n=4), 9-10 week old. *$P < 0.05$, **$P < 0.005$, Student's t-test.
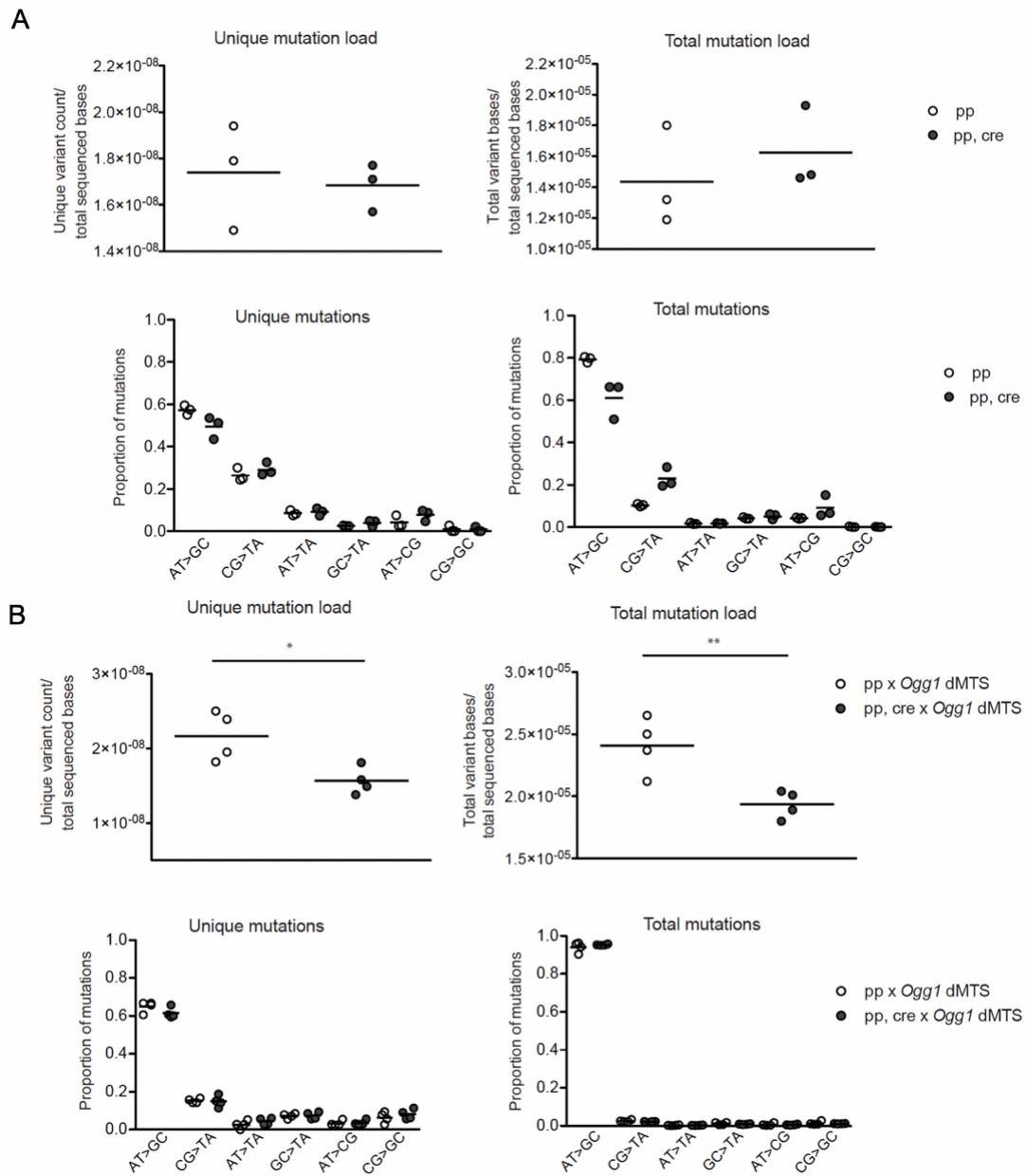
Figure 3.13 MtRNA mutation load does not increase in heart *Sod2* knockout mice in the absence and presence of mitochondrial BER. Illumina sequencing, minimum variant allele frequency is set to 0.5%. A. mtRNA mutation load was evaluated from *Sod2 loxP x Ckmm cre* mice with Illumina sequencing. Variant call was carried out to reads that mapped to mtDNA. The sequencing data was quality filtered and minimum for variant allele frequency was set to 0.5%. Unique mutation load: mutation is only counted once. Total mutation load: each mutation is counted as many times as it is observed. Profile of the of the mtRNA mutations. Controls (+p n=1 pp n=2), 10-11 week old, *Sod2 loxP x Ckmm cre* mice (pp, cre n=3) 10-11 week old. **B.** mtRNA mutation load was evaluated from *Sod2 loxP x Ckmm cre* x *Ogg1* dMTS mice with Illumina sequencing. Variant call was carried out to reads that mapped to mtDNA. The sequencing data was quality filtered and minimum for variant allele frequency was set to 0.5%. Unique mutation load: mutation is only counted once. Total mutation load: each mutation is counted as many times as it is observed. Profile of the of the mtRNA mutations. Controls (pp dd n=4), 9-10 week old, *Sod2 loxP x Ckmm cre* x *Ogg1* dMTS mice (pp, cre dd, n=4), 9-10 week old. $*P< 0.05$, Student's t-test.

A

B

C
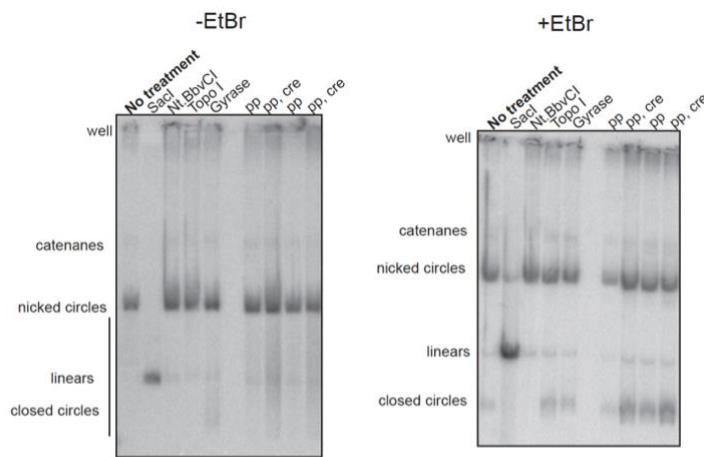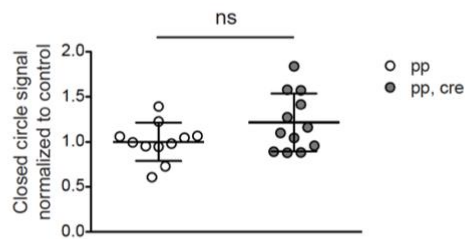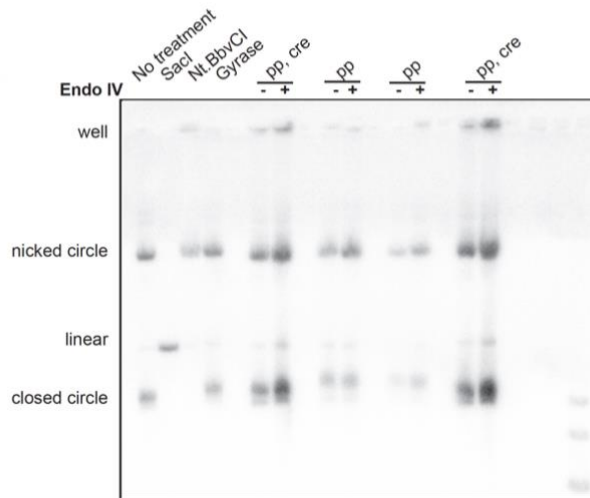
Adapted from Kauppila et al., submitted

Figure 3.14 No change in mtDNA integrity is observed with increased oxidative stress. A. Topological analysis of mtDNA integrity. A representative exposure of a topology gel of *Sod2 loxP x Ckmm cre.* Control samples are treated with various enzymes to reveal different mtDNA topologies. SacI makes double-stranded nick in mtDNA, Nt.BbvCI makes a single-stranded nick. Topo I relaxes and Gyrase induces coiling to closed circle mtDNA. Experimental samples are untreated. Ethidium bromide (EtBr) intercalates with DNA and condenses closed circle DNA to quantifiable band. PhosphorImager images are filtered with averaging to reduce noise. Quantifications were made from the original images **B.** Quantification of proportion of closed circle mtDNA from phosphorImager exposure. Control (pp, n=11), 9-10 week old and *Sod2 loxP x Ckmm cre* mice (pp,cre, n=12), 10-week old. **C.** Abasic site analysis of mtDNA from *Sod2 loxP x Ckmm cre* mice. Abasic sites are converted to single-stranded nicks with EndoIV prior to gel analysis. No proportional increase in the presence of nicked circle was detected after EndoIV treatment in *Sod2 loxP x Ckmm cre* mouse samples.

that the damaged mtDNA is degraded and thus not detected. Previous studies have reported that the proportion of oxidized bases is higher in fragmented than intact mtDNA (Suter and Richter, 1999) and that oxidized mtDNA degraded (Shokolenko et al., 2009). Furthermore, mitochondrially-targeted restriction enzyme experiments in mice have demonstrated that linear mtDNA fragments are digested rapidly, which causes a decrease in mtDNA copy number. To address this possibility, we measured the mtDNA copy number with qPCR approach from heart *Sod2* knockout mice but found in turn a slight increase in mtDNA copy number in some heart *Sod2* knockout individuals (Figure 3.15 A). Additionally, we evaluated the mtDNA copy number with Southern blot to verify the absence of mtDNA deletions (Figure 3.15 B).
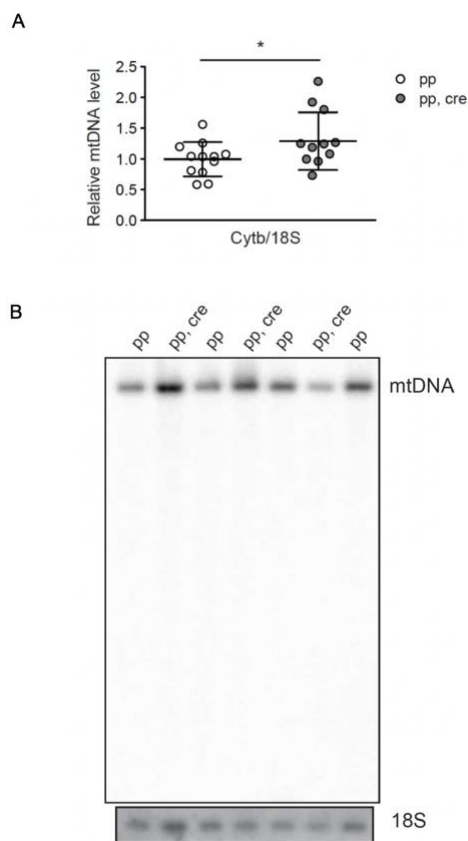
Adapted from Kauppila et al., submitted

Figure 3.15 mtDNA copy number in heart *Sod2* knockout mice. A. QPCR analysis revels slight increase in mtDNA copy number in some heart *Sod2* knockout mice individuals. mtDNA levels were evaluated with Cytb probe and nuclear DNA levels with 18S probe. Controls (pp, n=12), 10-12 week old and *Sod2 loxP x Ckmm cre* mice (pp, cre, n=11), 10-12 week old. Horizontal lines represent means, error bars represent SD, *P< 0.05, Student's t-test. **B.** Southern blot analysis from heart *Sod2* knockout mice.

3.2 .10 *De novo* replication capacity is decreased in heart *Sod2* knockout mice while *de novo* transcription remains unaffected

Topology gels only reveal oxidative damage that induces double or single-stranded nicks to mtDNA. To be able to evaluate the presence of lesions that would stall replication or transcription such as bulky adducts and other modifications (Kasiviswanathan et al., 2013; Nakanishi et al., 2013; Stojkovič et al., 2016), we carried out *in organello* replication and transcription experiments on the heart *Sod2* knockout mice. In these experiments, the

incorporation of radioactive dNTP or NTP in intact mitochondria is used as a marker for the functionality of replication or transcription machinery, respectively. The *de novo* replication and transcription is quantified by resolving the nucleic acids on an agarose gel. In the case of replication assay, large fraction of OriH initiated replication is prematurely terminated, producing abortive replication product called 7S DNA. This DNA fragment anneals in the control region and forms a triple-stranded displacement loop (Gustafsson et al., 2016). In *in organello* replication assay, we observed a severe reduction in both total and 7S DNA *de novo* replication with heart *Sod2* knockout mice (Figure 3.16 A). The impairment was not afflicted further by the absence of BER repair (Figure 3.16 B). Interestingly, the *de novo* transcription (pulse) or RNA turn over (chase) was normal heart *Sod2* knockout mice (Figure 3.17 A,B). The specific decrease in *in organello* replication suggests that either the decrease seen in replication was not driven by mtDNA damage or that the replication and transcription machineries do not have the same sensitivity to mtDNA damage. To decipher this, the steady-state levels of replication and transcription proteins were evaluated from purified mitochondria on a western blot. The experiment revealed an increase in the POLRMT steady-state levels, while in turn, the steady state-level of Pol γ was decrease in heart *Sod2* knockout mice (Figure 3.18), which at least partially explains the discrepancies between *de novo* transcription and replication. Consistently, previous experiments have shown that Pol γ is vulnerable to oxidative stress (Graziewicz et al., 2002). All the other evaluated replication and transcription proteins were not strongly afflicted (mtSSB, TFAM and TFB2M) in heart *Sod2* knockout mice.

A

B
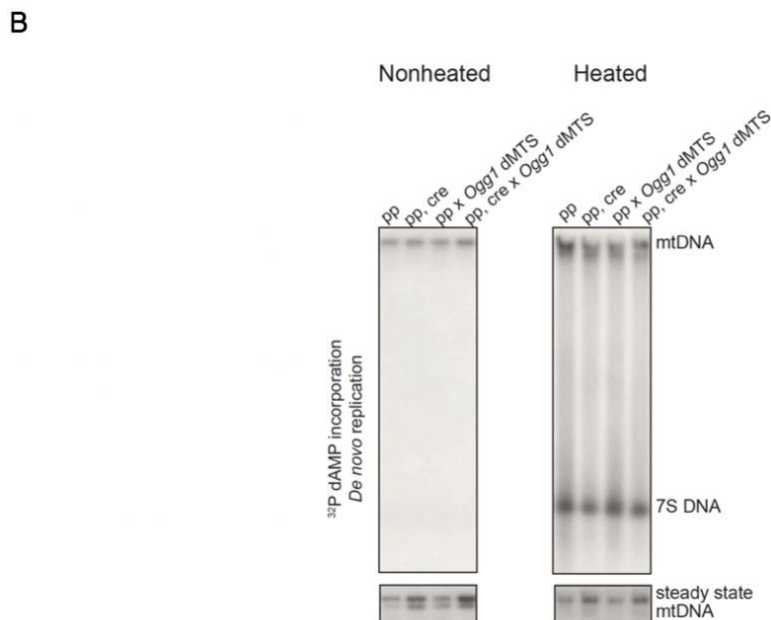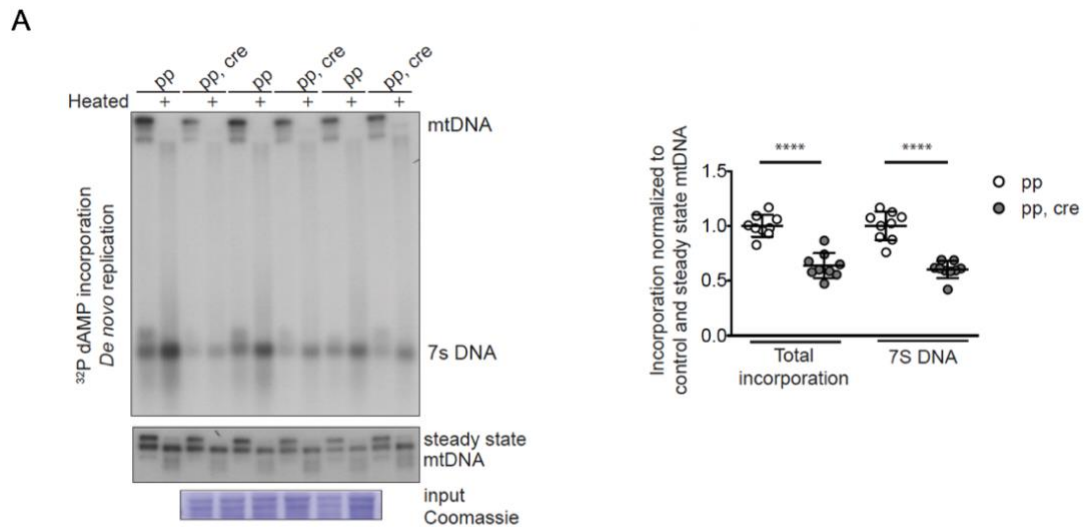
Figure 3.16 De novo replication is decreased in heart *Sod2* knockout mice in the presence and absence of mitochondrial BER. A. *In organello* replication assay from heart *Sod2* knockout mice. Purified mitochondria are incubated with radioactive dATP nucleotide and its incorporation to mtDNA is used as a proxy for *de novo* replication. To evaluate levels of newly synthetized 7S DNA, samples were heated to release the 7S DNA. Loading is normalized to the steady-state level of the mtDNA, which is measured by probing the same membrane with mtDNA recognizing probes when the *de novo* signal was diminished. Additionally, an aliquot representing the input was analyzed with Coomassie staining after the labeling to normalize the loading for mitochondrial protein per sample. To quantify *de novo* replication, it was normalized by steady-state level of mtDNA. Controls (pp, n=9,), 10-11 week old and *Sod2 loxP x Ckmm cre* mice (pp, cre, n=9), 9-10 week old. Combined from three separate experiments. Horizontal lines represent means, error bars represent SD, ****P< 0.0001, Student's t-test. **B.** *In organello* replication assay from heart *Sod2 loxP x Ckmm cre* x *Ogg1* dMTS mice.
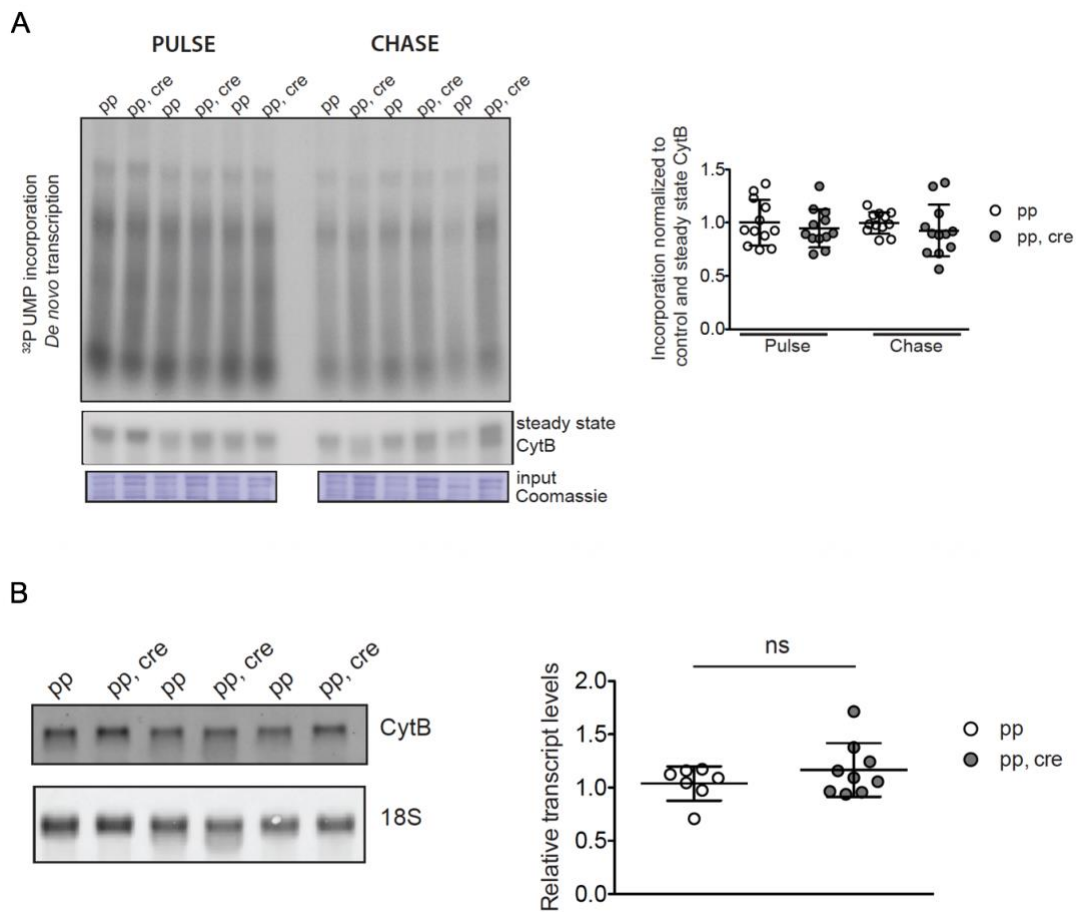
Figure 3.17 *De novo* transcription is not afflicted in the heart *Sod2* knockout mice. A. *In organello* transcription analysis from heart *Sod2* knockout mice. Radioactive UMP incorporation is used as a proxy for *de novo* transcription. RNA turnover is evaluated by 2hr-chase. Loading is normalized to the steady-state level of CytB transcript, which is measured by probing the same membrane with a CytB probe after *de novo* signal is diminished. Additionally, an aliquot representing the input was analyzed with Coomassie staining after the labeling to normalize the loading for mitochondrial protein per sample. To quantify *de novo* transcription, it was normalized by steady-state level of CytB. Controls (pp, n=9,), 10-11 week old and *Sod2 loxP x Ckmm cre* mice (pp, cre, n=9), 9-10 week old. Combined from three separate experiments. Controls (pp, n=12), 10-11 week old and *Sod2 loxP x Ckmm cre* mice (pp, cre, n=12), 9-10 week old. Horizontal lines represent means, error bars represent SD. **B.** A representative northern blot analysis of steady-state levels of CytB transcript. Quantification is made from combined experiments. Controls (pp, n=7), 10-11 week old and Sod2 loxP x Ckmm cre mice (pp, cre, n=9),10-11 week old. Horizontal lines represent means, error bars represent SD, ns= not significant, Student's t-test.
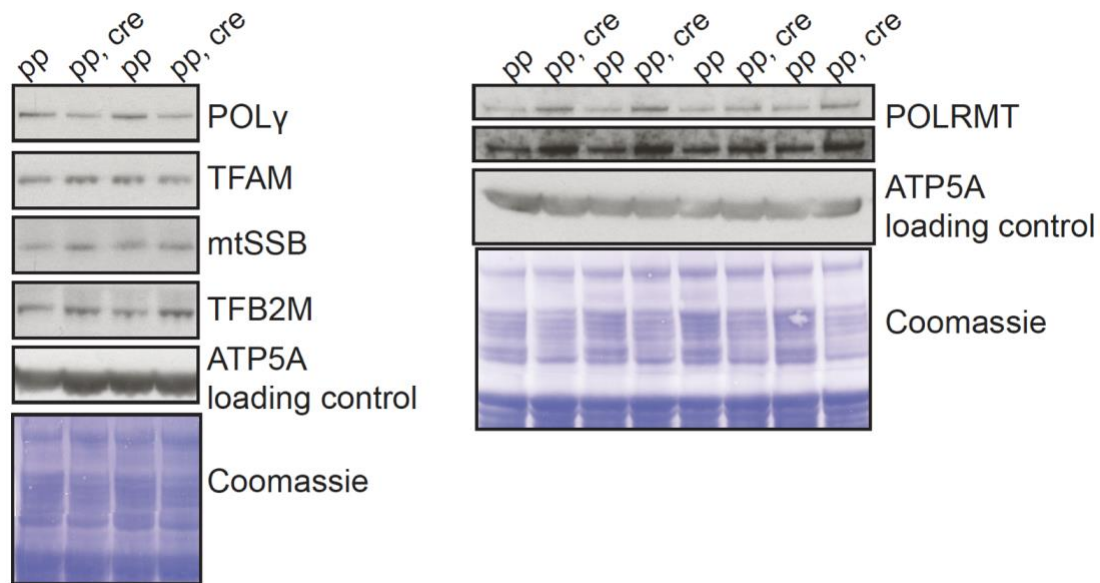
Figure 3.18 The steady-state level of Pol γ is decreased in heart *Sod2* knockout mice. Western blot analysis of steady-state levels of mitochondrial maintenance and expression proteins from purified heart mitochondria of controls (pp) and *Sod2 loxP x Ckmm cre* (pp, cre) mice (9-10 week old). Coomassie-stained membrane and ATP5A protein steady-state levels were used as loading controls.

3.3 DISCUSSION

For decades, mitochondria have been postulated to contribute to the aging process. With age the prevalence of focal OXPHOS dysfunction increases in certain tissues such as brain, skeletal muscle and colonic crypts. Accordingly, at these focal sites, individual cells contain mtDNA point mutations and/or deletions (Brierley et al., 1998; Bua et al., 2006; Cortopassi and Arnheim, 1990; Greaves et al., 2014b; Müller-Höcker, 1989; Taylor et al., 2003). The origin of mtDNA mutations is still under debate, while two, not mutually exclusive, sources have been proposed, namely replication errors and oxidative damage to mtDNA.

Similarly, the origin of mutations in nuclear DNA is widely discussed, especially in the cancer field. Recent studies have reported that cancers, which lack strong environmental component to their development, show a clear correlation between lifetime number of stem cell divisions and life time risk of cancer (Tomasetti et al., 2017). This risk is additionally not dependent on geographical regions. Thus, it suggests that in certain cancers, the source of mutations is replication errors rather than exogenous DNA damage (Tomasetti et al., 2017). Despite the high fidelity of DNA replication, somatic mutations have been suggested to slowly accumulate to DNA especially in highly proliferative cells. Newborns have been estimated to harbor 50-100 new mutations while at 60 years of age the mutation load in e.g. epidermis could be 4 000-40 000 per cell (Lynch, 2010). Similarly, mtDNA replication is highly accurate process (Lynch, 2010; Zheng et al., 2006) but somatic point mutations have been observed to be more prevalent with age (Greaves et al., 2014b; Itsara et al., 2014; Kennedy et al., 2013). Throughout life mtDNA is replicated extensively. During primordial germ cell development, the mtDNA copy number decreases down to few hundreds of copies per cell (Cree et al., 2008). These copies

are not only replicated to account for all of the mtDNA copies in an individual, but they are also turned over and replicated through life without cell cycle control. The high number of mtDNA replication cycles explains why replication errors still may occur despite high replication fidelity.

In addition to somatic mtDNA mutations, oxidative damage to macromolecules is also more prevalent with age (Bokov et al., 2004; Stadtman, 2006). Accordingly, the concentration of H_2O_2 is observed to increase with age in flies (Cochemé et al., 2011), while, no increase was detected between young and old mice (Logan et al., 2014). Interestingly, cells that were exposed to rotenone or H_2O_2 showed indications of mtDNA damage, but no increase in mtDNA mutation load was detected (Shokolenko et al., 2009). In line with this, in the heart *Sod2* knockout mice we observed clear increase in oxidative stress, however we detected no increase in mtDNA mutation load. Furthermore, mtDNA is observed to be less sensitive to exogenous mutagens than nuclear DNA, while concentrations that cause increase in nuclear mutation load are not mutagenic in mitochondria in cells (Marcelino et al., 1998), even if the mutational adducts can be detected in mtDNA and the mutagen has been given systemically to mice (Valente et al., 2016). These observations suggest that direct causality cannot be draw between increase in oxidative stress or exogenous mutagenic substances and increase in mtDNA mutation load. Nucleus has 14 different DNA polymerases, which include also translesion polymerases that allow replication machinery to by-pass various lesions, albeit it occurs commonly with lower fidelity (Pata, 2010). Mitochondria, in turn, have only one DNA polymerase to replicate and repair mtDNA. However, the multicopy nature of mtDNA might decrease the pressure of lesion by-pass in comparison to nucleus. It could be thus imagined that increased replication termination and/or mtDNA turnover are important reasons why DNA lesions do not commonly lead to mutations in mtDNA.

In summary, we did not observe any increase in the somatic or maternally transmitted mtDNA mutation load in BER-deficient mice, indicating that disruption of BER is not a successful approach to introduce mtDNA mutations to generate mouse models for mtDNA diseases. Furthermore, we did not to detect an increase in mtDNA damage or mitochondrial DNA or RNA mutation load even when we combined deficiency in BER with profound increase in oxidative stress. This stress was induced by absence of SOD2 and exemplified by the loss of aconitase activity. Even though, the increased ROS levels caused a plethora of changes in mitochondrial function, we cannot exclude that different types of oxidative stress is present during ageing, which might induce mtDNA damage and lead to an increase in mtDNA mutation load. This is, however, unlikely when we consider that in old individuals, the mitochondrial mutational profile includes mostly transitions and demonstrates a clear strand-specific bias (Greaves et al., 2010; 2012; Itsara et al., 2014; Kennedy et al., 2013; Taylor et al., 2003; Williams et al., 2013). This is a mutational signature, which is more consistent with replication errors (Zheng et al., 2006) or spontaneous deaminations (Lindahl, 1993), rather than by random oxidative damage. Furthermore, the *de novo* mutations that occurs with old age induced by increased oxidative stress would not have enough time to clonally expand to high levels that would impair OXPHOS and are thus most likely not relevant for ageing. Consistently, the

66

clonally expanded mutations that induce the focal OXPHOS deficiency associated with ageing (Larsson, 2010), are inconsistent with being induced by oxidative damage (Greaves et al., 2010; 2014b; Taylor et al., 2003). With our experimental observations and the correlative data from sequencing studies, we can conclude that the oxidative stress driven hypothesis of mtDNA point mutations requires a re-evaluation. Additionally, BER repair deficiency is not a feasible approach to introduce mutations to mtDNA. Instead in both ageing research and mitochondrial disease models we should focus on mtDNA replication errors as a source of somatic mtDNA mutations.

DISCUSSION AND FUTURE PERSPECTIVES

The first disease-linked mtDNA mutations were identified nearly 30 year ago (Holt et al., 1988; Wallace et al., 1988). Since the first discoveries, mitochondrial research has advanced in leaps. Our knowledge has not only increased in the field of mitochondrial disease biology but also in the functional aspects of mitochondrial biology such as DNA expression, replication and translation. However, many questions still remain unanswered, e.g. the enigmatic phenotype-genotype correlation and the tissue specificity of these disorders. The comprehensive understanding of mitochondrial diseases has been partially hindered by the absence of suitable animal models. One of the greatest obstacles in establishing mtDNA mutant animal models is the inability to modify mtDNA with the molecular biology techniques commonly used to manipulate nuclear DNA. In this thesis the role of replication errors as the main source for mtDNA point mutations was strengthen and a new phenotype-driven approach to generate mouse models that carry pathogenic mtDNA point mutations was described. The presented approach allows not only technically simple generation of new disease models but also described a new way to screen for the presence of low-level pathogenic mtDNA mutations from rapidly clonally expanding colonic crypts. This improvement is highly important, while the identification of low-level pathogenic mutation from postmitotic tissues of a potential disease model, can be like looking for a needle in the hay stack. Firstly, only cells with high enough heteroplasmy level show respiratory chain dysfunction and secondly, this dysfunction can also be present in low levels in postmitotic tissues especially with mildly-pathogenic mutations. For example, the mice harboring C5024T mutation in mitochondrial *tRNA*^{ALA} gene, show distinct decrease in translation and clear correlation between C5024T heteroplasmy levels and OXPHOS dysfunction in colonic crypts and smooth muscle cells. However, only occasional complex IV dysfunctional cardiomyocytes can be detected in these mice.

An interesting contrast with the relatively mild phenotype of the tRNA^{ALA} mice, is that at high relative heteroplasmy levels the transmission of the C5024T allele deviated from neutral drift model and no progeny was observed with higher than 80 % relative levels of the C5024T allele, suggesting that higher heteroplasmy levels than 80 % were not compatible with life. However, studies addressing mtDNA deletions have demonstrated that heteroplasmy analyses conducted from tissue homogenates often represent lower heteroplasmy levels that what can be detected from single-cell studies of the same tissue (Brierley et al., 1998). Accordingly, when the heteroplasmy levels of the C5024T allele were measured from single cells in the colonic smooth muscle, the relative levels of C5024T allele reached more than 90% in COX dysfunctional cells, although the homogenate levels of the analyzed mice were close to 70%.

Pathogenic mtDNA mutations can lead to mitochondrial disorders with onset in neonatal period or in adulthood. Even though pathogenic *de novo* mutations require time to clonally expand to reach high enough levels to disrupt the oxidative phosphorylation system. Commonly, this is, however, not the cause for the late onset of mitochondrial diseases because

high to medium heteroplasmy levels of the mutation are generally present already in the germ cells generating the affected individual. Accordingly, the most common mutations associated with Leber's hereditary optic neuropathy (LHON) are frequently homoplasmic and still induce only late onset loss of vision (Howell et al., 1991). With certain mutations, the level of heteroplasmy can, however, be associated with the clinical presentation of the disease. For example, a correlation with heteroplasmy level and symptoms of the disease was found with A3243G MELAS mutation. Individuals with low heteroplasmy level presented more frequently with CPEO and myopathy than individuals with high heteroplasmy level, who, in turn, presented more frequently with recurrent strokes and epilepsy (Chinnery et al., 1997).

Still most human pathogenic mtDNA mutations are heteroplasmic and cause a disease only when the relative heteroplasmy level of a mutation exceeds the biochemical threshold level. Therefore, decreasing the relative levels of the pathogenic mutation could be a successful strategy to restore the respiratory chain function and relieve the symptoms of the mitochondrial disease. The mitochondrially-targeted restriction enzyme has demonstrated that one can selectively target the mtDNAs with heteroplamic mutations and decrease their relative heteroplasmy levels (Bayona-Bafaluy et al., 2005). However, most pathogenic mutations do not alter common restriction sites; thus, the restriction enzymes need to be engineered to specifically target the mutant mtDNA to decrease its relative heteroplasmy levels. Recently, experiments with mitochondrially-targeted TALENs and Zn-finger nucleases have successfully sifted the rations of mutant to wild-type mtDNA in oocytes and human cell lines (Bacman et al., 2013; Gammage et al., 2016; 2014; Minczuk et al., 2006; Reddy et al., 2015). tRNA^{ALA} mice could be a perfect tool set up and test these mitochondrially-targeted nucleases *in vivo.* In these tests, the readout for rescue could be the improved molecular phenotype of the tRNA^{ALA} mice, namely a decrease in heteroplasmy level of the mutation and/or increased steady-state levels of *tRNA^{ALA}* transcript.

Another treatment approach that could be tested *in vivo* with the tRNA^{ALA} mice is an approach that utilizes overexpression of cognate aminoacyl synthetases to suppress the molecular defects of a pathogenic tRNA mutation. It has been shown that overexpression of cognate tRNA aminoacyl synthetase could suppress a pathogenic mutation induced phenotype in yeast and mammalian cells (Montanari et al., 2010; Rorbach et al., 2008). Additionally, full length and a truncated version of yeast leucyl-tRNA synthetase and its human orthologue has been observed to partially rescue molecular phenotype of a non-cognate pathogenic mitochondrial tRNA mutation (Hornig-Do et al., 2014; Montanari et al., 2010; Perli et al., 2014). However, it is possible that the molecular phenotype of tRNA^{ALA} mice can be only rescued with overexpression of alanyl-tRNA synthetase as it is a Class II aminoacyl synthetase and leucyl-tRNA synthetase is a Class I amino acyl synthetase.

One of the challenges in mitochondrial disease modeling and rescue studies in mice is that they live only ~ 2 years. It is, for example, difficult to anticipate what would have been the phenotype of tRNA^{ALA} mice if they had lived until 20-30 years of age. How to then induce the adult onset like symptoms or histological changes in a lifetime of a mouse model? Based on

the examples from LHON and MELAS patients and the already reached transmission threshold of C5024T mutation, it is clear that only increasing the heteroplasmy level of the pathogenic mutation is not a feasible solution. Another way could be to induce mild translational impairment in the tRNA^{ALA} mice and thus increase the sensitivity of the mice to the decrease in *tRNA^{ALA}* transcript levels. This could be potentially established with a genetic approach, by crossing the tRNA^{ALA} mice with mice that are heterozygote for mutated ribosomal subunit MRPS34 allele (Richman et al., 2015). Alternatively, tRNA^{ALA} mice could be treated with low concentrations of translation inhibitors such as chloramphenicol or actinonin (Richter et al., 2013). However, neither of these approaches are free from pitfalls and in-built biases, and thus the observations that they provide should be evaluated critically to verify that they are not caused by the off-target effects of chemical treatment or the tissue-specific sensitivity of MRPS34 mutation. If these approaches are successful, they could be a highly valuable tool to establish stronger histological changes in mouse tissues in tRNA^{ALA} mice that are relevant for human mitochondrial disease. These changes, would enable demonstration of phenotypical rescue with different mitochondrial treatments such as the mitochondrially-targeted nucleases.

In general, with or without further translation impairment, additional analysis of the tissue specificity of tRNA^{ALA} mice could provide insights in the puzzling tissue specificity of mitochondrial disorders. For example, it is not currently understood how the LHON mutation, that causes isolated visual impairment, can in some patients also induce devastatingly severe dystonia, which no obvious eye involvement (Lightowlers et al., 2015; McFarland et al., 2007).

Indeed, with the current knowledge in mitochondrial biology, animal models and new molecular tools, the future of mitochondrial disease biology seems brighter than before. Now, it seems likely that in the future treatment options for mitochondrial diseases could be advanced beyond palliative care.

METHODS

4.1 MOUSE WORK

4.1.1 Mouse husbandry

The mouse strain C57Bl/6NCrl (Charles River, Germany strain code 027) was used in all experiments. The mice were housed at 21°C in a 12-hr light/dark cycle and fed *ad libitum* on a standard diet (ssniff M-H Low-Phytoestrogen). An enhanced diet was used with newly weaned mice or during breeding (ssniff M-Z Low-Phytoestrogen) by Ssniff Spezialdiaeten GmbH. All experiments were approved and permitted by the Landesamt für Natur, Umwelt und Verbraucherschutz Nordrhein-Westfalen (LANUV) in accordance with German and European Union regulations. All animal work was performed in accordance to recommendations and guidelines of the Federation of European Laboratory Animal Science Associations (FELASA).

4.1.2 Mouse models

All mice were backcrossed and maintained on the inbred C57BL/6NCrl background (Charles River, Germany strain code 027).

Mouse line	Details	From
Sod2 loxP	Floxed superoxide dismutase 2	Dr. Karin Scharffetter-Kochanek University of Ulm (Strassburger et al 2005)
MutYh delta-MTS	MutY homolog (E.coli) delta-mitochondrial targeting sequence	Taconic Artemis
Ogg1 delta-MTS	8-oxoguanine DNA-glycosylase 1 delta-MTS	Taconic Artemis
PolgA (D257A) loxP	Proofreading-deficient DNA polymerase gamma	Generated in-house (Trifunovic 2004)

4.1.2.1 MtDNA mutator mouse

The mutator mouse line with the D257A mutation in the catalytic subunit of DNA polymerase γ ($Pol\gamma A^{D257A}$, $Pol\gamma A^{MUT/MUT}$) was generated previously, (Trifunovic et al., 2004). To avoid accumulation of mtDNA mutations, the line was maintained by backcrossing the heterozygous male mice to wild-type C57Bl/6N females.

4.1.2.2 Generation of mice with mtDNA mutations

Heterozygous *PolγA+/MUT* females are bred with wild-type C57Bl/6N males. The wild-type female pups from this cross are then used to generate the lineages carrying mtDNA mutations by continuously backcrossing them with wild-type C57Bl/6N males.

4.1.2.3 Generation of Ogg1 dMTS mice

To exclude OGG1 protein from mitochondria, the endogenous *Ogg1* gene was modified to lack the genomic region encoding the predicted mitochondrial targeting sequence (MTS). First, the location of the OGG1 MTS was predicted from AAB94512.1 protein sequence with Mitoprot II (Claros and Vincens, 1996) and Target P1.1 (Emanuelsson et al., 2000; Nielsen et al., 1997) to extend from L2 to W23. Then, a targeting vector (BAC C57BL/6J RPCIB-731) was transfected into the TaconicArtemis C57BL/6N Tac ES cell line. This vector lacked the predicted MTS encoding region and carried a positive selection marker (Neomycin resistance) flanked by FRT sites. After a successful homologous recombination, the neomycin cassette was removed by Flp recombination to obtain the constitutive knockout allele of *Ogg1* lacking the genomic region encoding the MTS (*Ogg1* dMTS). The mice were generated at TaconicArtemis and they were maintained on the C57Bl/6NCrl background (Charles River Laboratories, Germany strain code 027). To minimize accumulation of mutations to mtDNA, heterozygous mice were continuously generated by crossing homozygous males for *Ogg1* allele with wild-type C57Bl/6N females.

4.1.2.4 Generation of Mutyh dMTS mice

The endogenous *Mutyh* gene was modified to lack the genomic region encoding the predicted MTS to exclude MUTYH protein from mitochondria. First, the location of the MTS in MUTYH protein was predicted with Mitoprot II (Claros and Vincens, 1996) and Target P1.1 (Emanuelsson et al., 2000; Nielsen et al., 1997) prediction tools using NP_001153053.1 protein sequence. The prediction tools suggested that the MTS extends from K2 to P33. Then, a targeting vector (BAC C57BL/6J RPCIB-731) was transfected into the TaconicArtemis C57BL/6N Tac ES cell line. This vector lacked the predicted MTS encoding region and it contained a positive selection marker (Neomycin resistance) flanked by FRT sites After a successful homologous recombination, the neomycin cassette was removed by Flp recombination to obtain the constitutive knockout allele of *Mutyh* lacking the genomic region encoding the MTS (*Mutyh* dMTS). The mice were generated at TaconicArtemis and they were maintained on the C57Bl/6NCrl background (Charles River Laboratories, Germany strain code 027). To minimize accumulation of mutations to mtDNA, heterozygous mice were continuously generated by crossing homozygous males for *Mutyh* allele with wild-type C57Bl/6N females.

4.1.2.5 Heart Sod2 knockout mice

Superoxide dismutase 2 loxP mice (Strassburger et al., 2005) were received from Prof. Dr. Karin Scharffetter-Kochanek from Universitätklinikum Ulm. To generate tissue specific knockout of the SOD2 protein in heart and skeletal muscle, the *Sod2* loxP mice were crossed with a *Ckmm cre* transgenic line (Wang et al., 1999). The *Sod2 loxP* x *Ckmm cre* mice were maintained on C57Bl/6NCrl background (Charles River Laboratories, Germany strain code 027).

4.1.3 Body composition measurements

Lean mass content and body fat were measured by nuclear magnetic resonance with minispec LF50H (Bruker) at the Phenotyping Core Facility of MPI for Biology of Ageing.

4.2 HISTOLOGICAL ANALYSES

4.2.1 Tissue preparation for histological analysis

To collect tissues, mice were sacrificed with CO_2 and cervical dislocation. Then the target tissues such as heart or colon were removed and washed with PBS. Tissues, that were intended for histological staining, were frozen in liquid nitrogen cooled (-160 °C) isopentane (15 s) and thin sections (7 µm heart, 10 µm colon) were cut from the frozen tissues with an OFT 5000 cryostat (Bright). Sections that were meant for laser-capture dissection (15 µm) were cut on to polyethylenenaphthalate (PEN) slides (Leica Microsystems) and the sections for histological staining were cut on to glass colorcoat adhesion slides (CellPath). Prior to further analysis both sections were stored in -80°C.

4.2.2 Laser-capture Microdissection

The sections for laser-capture microdissection were cut to 15 µm thickness, mounted on polyethylenenaphthalate (PEN) slides (Leica Microsystems) and air-dried at room temperature for 1hr. Thereafter, slides were stored in sealed slide mailers at -80°C until use. Microdissection was carried out on a Leica LMD7000 Lasermicrodissection Microscope. Single colonic crypt section or 5 smooth muscle fibers were sorted into single tubes for analysis and settled to the bottom of the tube by centrifugation at 7000 rcf for 10 min.

4.2.3 Dual cytochrome c oxidase (COX)/ succinate dehydrogenase (SDH) enzyme histochemistry

First, sections were incubated at 37 °C in 50 µl of COX staining medium (100 µM cytochrome *c*, 4 mM diaminobenzidine tetrahydrochloride, 20 µg/ml catalase, 0.2 M phosphate buffer pH 7.0) 60 min for heart and 25 min for colon sections. Then, the sections were washed 3 x 5 min with PBS. Next, the sections were incubated at room temperature with 50 µl of SDH solution

(130 mM sodium succinate, 200 µM phenazinemethosulphate, 1 mM sodium azide, 1.5 mM nitroblue tetrazolium, 0.2 M phosphate buffer pH 7.0), for 30 min for heart and for 35 min for colon. Then, the sections were washed 3 x 5 min with PBS, dehydrated through graded ethanol series (70%, 95% and 2x 100%), cleared in Histoclear™ (National Diagnostics, Atlanta, Georgia, USA), and mounted in DPX. The sections that were meant for laser-capture microdissection, were only air-dried for 90 min after dehydration.

4.2.4 Complex I immunohistochemistry

To asses steady-state levels of complex I subunits, the colons were fixed in 4% PFA overnight at room temperature. Next, the tissue was washed in 70% ethanol and paraffin embedded. The paraffin embedded tissue was cut to 4µm sections and the sections were incubated on slides overnight at 37 °C to verify adherence to the slides. Next, the sections were de-paraffinised with two rounds of Histoclear and rehydrated in a graded ethanol series. Then, antigens were retrieved by pressure cooking the sections in 1mM EDTA pH 8.0 for 20 minutes. To block the endogenous peroxidase activity, 0.3% H_2O_2 was added to the 95% ethanol in the rehydration step. Then, the sections were blocked with 10% Normal Goat Serium for 1 hour at room temperature and endogenous biotin was blocked using an avidin/biotin blocking kit (Vector Laboratories). Next, the sections were incubated overnight with anti-NDUFB8 antibody (Abcam) diluted 1:100 in 10% normal goat serum in TBS. Then they were washed with TBS-Tween 20, and incubated in goat anti-IgG1-biotin (Jackson Immuno Research) for 2 hours at 4ºC, followed by incubation with the VECTASTAIN® Elite ABC (Vector Laboratories) following manufacturer's recommendations. NDUFB8 steady-state level was measured from 4 sections that were taken at 100µm intervals.

4.2.5 Hematoxylin and eosine staining from paraffin embedded heart sections

Hearts were fixed with PFA and embedded in paraffin (ThermoFisher). The paraffin embedded tissue was cut to 5µm sections with a microtome (HM340E, Thermo) and the sections were deparaffinized in xylene (AppliChem), rehydrated with an alcohol series (100-70% ethanol, AppliChem) and stained with Haematoxylin (AppliChem) and Eosin Y (Carl Roth) following standard protocols. Then, the sections were dehydrated through an alcohol series (70-100% ethanol, AppliChem), mounted (Cytoseal, ThermoFisher) and imaged with a brightfield microscope (Nikon Eclipse Ci).

4.3 CELL CULTURE ANALYSES

4.3.1 Constructs encoding OGG1 and MUTYH for immunocytochemistry

To generate a construct expressing the wild-type form of OGG1, a cDNA encoding mouse OGG1 (NM_010957.4) was inserted into the multiple cloning site of pCMV-tag4 (Agilent). Next,

the region encoding for the predicted MTS (4T-69G) was removed by adding a new start codon and restriction site after the predicted MTS sequence by PCR. The resulting oligonucleotide was then inserted to pCMV-tag4a vector. To study the subcellular localization of MUTYH protein a construct that encodes mouse Myc-DDK-tagged MUTYH (pCMV6-Entry) was purchased (Origene, MR208268, NM_133250.1) and the predicted MTS encoding sequence (A4-T99) was removed and N-terminal extension of human alpha variant (A1-C42) was added. Additionally, a construct encoding human Myc-DDK-tagged MUTYH alpha variant (pCMV6-Entry, Origene) (NM_001048171.1) was modified to lack the N-terminal extension of alpha3 variant (A1-C42) and the MTS encoding sequence (A4-G162).

4.3.2 Immunocytochemistry

To evaluate the subcellular localization of the target proteins, HeLa cells were grown on coverslips at 37°C, 5% CO_2 and transfected with plasmids encoding OGG1 or MUTYH proteins using Lipofectamine2000 (ThermoFisher). First, the cells were fixed with 4% paraformaldehyde (EMS) and incubated with antibodies that recognize the FLAG peptide (Sigma-Aldrich, F1804) and TOM20 protein (Santa Cruz, sc-11415). Next, the primary antibodies were recognized with secondary antibodies (goat anti-mouse Alexa Fluor 488, A11001 and goat anti-rabbit Alexa Fluor 594 A11012 (ThermoFisher) and stained with 1 µg/ml DAPI (AppliChem) and mounted with Prolong Gold (ThermoFisher). Finally, the images were acquired with a Leica TCS SP8-X inverted confocal microscope (Leica Microsystems) using a 100x/1.4 oil objective.

4.4 PROTEIN ANALYSIS

4.4.1 Mitochondria purification

Mitochondria were purified from fresh tissue with differential centrifugation. First, the target tissue was collected (heart ~100 mg, liver ~200 mg), minced into small pieces and rinsed with PBS. The tissue was then combined with 10 ml of mitobuffer (320 mM sucrose, 20 ml Tris-HCl, 1 mM EGTA, 0.2% BSA, pH 7.2) in a glass homogenizer. For softer disruption, heart tissue was first homogenized with loose Teflon pestle in hand with 10 strokes. Then, both liver and heart were homogenized with a tight Teflon pestle with 5 (liver) or 10 strokes (heart) at 200 rpm. To pellet cell debris, the homogenates were then spun for 10 min at 1000 g, followed by a 10 min spin at 10 000 g to pellet the mitochondria. The mitochondria-enriched pellets were thereafter resuspended into mitobuffer without BSA. The centrifugations were performed at +4°C and the samples were kept on ice throughout the procedure. For label-free quantitative proteomics, mitochondria were prepared in the presence of protease inhibitor cocktail (cOmplete, EDTA-free, Roche), and purified further with Percoll gradient to exclude the mitochondria-associated membranes in the following way. 8 ml of Percoll gradient solution (20% Percoll solution in mitobuffer with BSA) was poured into Ultraclear ultracentrifugation tubes (14 x 89 mm) and the resuspended mitochondria were layered on top of the gradient.

The gradient was then spun in SW41 swing-out rotor (Beckman) at 40 000 g at +4°C for 30 min. The brown mitochondrial layer was collected and diluted 10 x with mitobuffer lacking BSA to remove the residual Percoll. Finally, the diluted mitochondria were re-collected with centrifugation at 6 300 g for 10 min at +4°C. The Percoll protocol was a modified from previously published protocol (Wieckowski et al., 2009).

4.4.2 Western blot analysis

Western blot analysis was carried out to evaluate the steady-state levels of proteins of interest. First the differential-centrifugation purified mitochondria were lyzed and reduced with NuPAGE LDS sample buffer (Invitrogen) and 50 µM DTT. Then they were resolved on a NuPAGE SDS-PAGE gel system (Invitrogen) and transferred with wet-transfer onto a PVDF membrane (Immobion FL, Millipore or Amesham Hybond, GE Healthcare). Next, the membrane was blocked with 5% milk TBS, 0.05% TWEEN-20 and proteins of interest were detected with primary antibody (see table below) and visualized with horseradish peroxidase-linked secondary antibody (Goat anti-Rabbit IgG (H+L) Cross-Adsorbed Secondary Antibody, HRP, Invitrogen; Amersham ECL Mouse IgG, HRP-linked, GE Healthcare) with enhanced chemiluminescence (Amersham ECL Western Blotting Detection Reagent, GE Healtcare) on to a film (Amersham hyperfilm MP, GE Healthcare). After detection, the membrane was stained with staining solution (Coomassie Blue-R, 10% acetic acid, 20% EtOH), destained and scanned either with the Odyssey infrared imaging system (LI-COR Biosciences) or a normal scanner to control for loading.

Target	Company	Catalog number
ACO2	Abcam	ab110321
ATP5A	Abcam	ab14748
MitoProfile Total OXPHOS Rodent WB Antibody Cocktail	Mitoscience	MS604
mtSSB	Sigma	HPA002866
NDUFV2	Sigma	HPA003404
POLRMT	self-made	
POLγ	Abcam	ab128899
SDHA	Invitrogen	459200
SDHC	Proteintech	14575-1-AP
SOD2	Millipore	06-984
TFAM	Abcam	ab131607
TFB2M	self-made	

4.4.3 Blue Native PAGE Electrophoresis

Isolation of mitochondria from mouse hearts was performed by differential centrifugation and 75-100 µg of purified mitochondria were lyzed in 50 µl of ice-cold digitonin buffer (1% digitonin, 20 mM Tris pH 7.4, 0.1 mM EDTA, 50 mM NaCl, 10% glycerol, 1 mM PMSF). The lysis was continued for 15 min on ice and then the unsolubilized material was removed by centrifugation at 4°C. Next, the collected supernatant was then combined with 5 µl of 10x loading dye (5% (w/v) Coomassie Brilliant Blue G-250, 100 mM Tris pH 7, 500 mM 6-aminocaproic acid) and loaded on a 4-10% gradient blue native PAGE gel (Wittig et al., 2007). Once the proteins were resolved onto the gel, they were transferred to a PVDF membrane with semi-dry transfer. The mitochondrial proteins were then detected on the membrane following the western blot practices described above.

4.4.3.1 In gel activity assay

To assess the activity of Complex I, Blue Native PAGE gels were incubated in 2mM Tris-HCl pH 7.4, 0.1 mg/ml NADH (Roche) and 2.5 mg/ml iodonitrozolium (Sigma) for ~30 min at the room temperature. The reaction was stopped by changing the incubation solution to 2mM Tris-HCl pH 7.4.

4.4.4 Mitochondrial respiration analysis

Mitochondrial oxygen consumption was measured with Oxygraph-2k (OROBOROS INSTRUMENTS, Innsbruck, Austria). The measurement was done at 37°C using 65-125 µg of fresh differential-centrifugation purified mitochondria, which were diluted in 2.1 ml of mitochondrial respiration buffer (120 mM sucrose, 50 mM KCl, 20 mM Tris-HCl, 4 mM KH_2PO_4, 2 mM $MgCl_2$, 1 mM EGTA, pH 7.2). The oxygen consumption rate was analyzed with 10 mM pyruvate, 10 mM glutamate and 5 mM malate (PGM, complex I) or 10 mM succinate and 10 nM rotenone (complex II). First, the phosphorylating state respiration (state 3) was measured in the presence of 1 mM ADP. Subsequently, the non-phosphorylating state was measured with of 2.5 µg/ml oligomycin (pseudo state 4). The mitochondrial quality was verified by measuring respiration control rate (RCR) with 1 mM ADP (state 3) or 1 mM ADP and 2.5 µg/ml oligomycin (pseudo state 4). The RCR values were 10 with PGM and 6 with succinate and rotenone. Finally, the uncoupled respiration was measured by adding carbon cyanide m-chloriphenyl hydrazone (CCCP) up to 3 µM to reach the maximal respiration. The oxygen consumption was normalized to mitochondrial protein content, which was measured with protein DC kit (Bio-Rad Laboratories).

4.4.5 Measurement of isolated respiratory chain enzyme activities

The isolated respiratory chain enzyme activities were measured from differential-centrifugation purified mitochondria stored at -80°C. The measurements were performed with a Hitachi UV-

3600 spectrophotometer at 37°C. Mitochondria, 15-50 µg, were diluted in phosphate buffer (50 mM KH_2PO_4, pH 7.4). Citric synthase activity (CS) was measured at 412 nm (E=13,600 M^{-1} cm^{-1}) in the presence of 0.1 mM acetyl-CoA, 0.5 mM oxaloacetate and 0.1 mM 5,5'-dithiobis-2-nitrobenzoic acid (DTNB). NADH dehydrogenase (Complex I) activity was measured at 340 nm (E=6,220 M^{-1} cm^{-1}) in the presence of 0.25 mM NADH, 0.25 mM decylubiquinone and 1 mM KCN, controlling for rotenone sensitivity. Succinate dehydrogenase (Complex II) activity was measured at 600 nm (E=21,000 M^{-1} cm^{-1}) in the presence of 40 mM succinate, 35 µM dichlorophenolindophenol (DCPIP) and 1 mM KCN. The cytochrome c oxidase (Complex IV, CIV) activity was measured using the classical TMPD/ascorbate assay, explained in detail elsewhere (Mourier et al., 2015). The complex II to complex III (II-III) activity was measured after reduction of cytochrome c at 540 nm (E=18,000 M^{-1} cm^{-1}) in the presence of 1 µg/ml decylubiquinol, 1 mM sodium azide, 80 µg/ml cytochrome c, 1 µM antimycin A and 40 mM succinate. The difference in flux before and after addition of antimycin A reflects the complex II to III activity. All chemicals used in the measurements were from Sigma-Aldrich.

4.4.6 Mitochondrial aconitase activity

The aconitase activity was measured from purified mitochondria with an aconitase activity kit following manufacturer's recommendations (ab109712, Abcam). Briefly, conversion of isocitrate to cis-aconitate with aconitase activity is measured at 240 nm in the presence of isocitrate and manganese. The increase in absorbance indicates the activity of mitochondrial aconitase.

4.4.7 8-oxo-dG glycosylase/AP lyase activity

The 8-oxo-guanine incision activity was evaluated following previously published protocol with small alterations (de Souza-Pinto et al., 2001). Mitochondria were purified from fresh liver tissue (~200 mg) with differential centrifugation and Percoll gradients as described above. When the tissue was homogenized an aliquot for 'total' fraction was collected. 300 µg of total and mitochondrial fractions were first lyzed in lysis buffer (10µl, 20 mM HEPES-KOH (pH 7.6), 1 mM EDTA, 2 mM DTT, 300 mM KCl, 5% Glycerol, 0.05 % Triton X-100) and then resuspended in dilution buffer (20 µl, 20 mM HEPES-KOH (pH 7.6), 1 mM EDTA, 2 mM DTT, 5% Glycerol) to bring the final protein concentration to 10 µg/µl and the KCl concentration back to 100 mM. Next, the 8-oxoguanine incision activity was measured by incubating 100 µg of protein with 100 fmol of [α-^{32}P]-5' labelled 8-oxo-dG dsDNA in reaction buffer (60 mM HEPES-KOH pH 7.6, 10 mM EDTA, 2 mM DTT, 50 mM KCl, 15 % Glycerol, final volume 20µl) for 16 hrs at 32°C.

The incision reaction (20μl)	
100 μg of protein	10 μl
Reaction buffer	10 μl
100 fmol of 8-oxoG dsDNA	
ddH₂O to 21 μl	

Thereafter, the reaction was stopped with stop solution (final concentration 0.4 % SDS, 0.2 mg/ml Protease K), and incubation at 55°C for 15 min. Finally, DNA was ethanol precipitated and resolved on a 15% Novex TBE-Urea Polyacrylamide gel (7M Urea, ThermoFisher Scientific).

Incision substrate (Page and Stuart, 2009)	
8-oxo-dG oligo	5'-GAACGACTGT[8-oxo-dG]ACTTGACTGCTACTGA -3'
Complementary oligo	5'-ATCAGTAGCAGTCAAGTCACAGTCGTTC -3'

4.4.8 In organello assays

4.4.8.1 In organello replication

Mitochondria were purified from ~100 mg of fresh heart tissue with differential centrifugation as described above. Freshly purified mitochondria, 800 μg, were resuspended to cold incubation buffer (25 mM sucrose, 75 mM sorbitol, 10 mM Tris HCl, 10 mM K_2HPO_4, 100 mM KCl, 0.05 mM EDTA, 1 mM ADP, 5 mM $MgCl_2$, 10 mM glutamate, 2.5 mM malate, 1 mg/ml BSA, pH 7.4) and pelleted at 9000 rpm, 2 min at 4°C. The mitochondria were then washed twice with cold incubation buffer and finally resuspended in 500 μl of warm (37°C) incubation buffer with 50 μM of dCPT, dGTP, dTTP and 20 μCi of [α-^{32}P]dATP, followed by 1 hr rotation at 37°C to incorporate the radioactivity into mtDNA. Thereafter, mitochondria were pelleted at 9000 rpm for 2 min at 4°C and washed twice with cold wash buffer (10% glycerol, 0.15 mM $MgCl_2$, 10 mM Tris HCl pH 6.8). To evaluate loading, an aliquot of the washed mitochondrial was collect prior to DNA extraction. The DNA was extracted with Gentra Puregene Tissue Kit (QIAGEN) following the manufacturer's recommendations with following adjustments. Mitochondrial were lyzed with 30 min incubation at 55°C and isopropanol precipitation of DNA was performed overnight in the presence of 30 μg of glycogen (Ambion). Next, the DNA was collected with centrifugation and resuspended in 20 μl of TE. An aliquot of the labeled DNA (5 μl) was resolved on a 0.9% agarose gel with EtBr (0.5 mg/ml) at 30V for 14 hrs. To release 7S DNA an aliquot (5μl) of the purified DNA was heated for 5 min at 95°C prior to loading. After the run, the gel was transferred to a membrane (Hybond-N+, GE Healthcare) by Southern blotting and used to expose to a phosphorImager screen or an autoradiography film (Amersham hyperfilm MP, GE Healthcare). The assay quantifications were made from exposures to phosphorImager screen.

Later, the membrane was reprobed with mtDNA-specific probe (pAM1) to normalize the *de novo* incorporation signal to steady-state mtDNA levels. The method was modified form a previously described protocol (Gensler et al., 2001).

4.4.8.2 In organello transcription

The mitochondria were prepared and purified similarly to the *in organello* replication protocol. In the *in organello* transcription assay, the washed mitochondria were resuspended to 800 µl of warm incubation buffer with 50 µCi of [α-^{32}P]UTP and incubated for 1 hr with rotation at 37°C to incorporate the radioactive UTP to mtRNA. Next, the mitochondria were collected with centrifugation at 9000 rpm for 2 min at 4°C and resuspended into incubation buffer with 80 nM of UTP. Thereafter, the samples were divided in two and one part of the sample was incubated for an additional period of 2 hrs at 37°C to study RNA turnover (chase) and the other half was washed twice by pelleting and resuspending it in cold wash buffer (10% glycerol, 0.15 mM MgCl$_2$, 10 mM Tris HCl pH 6.8) (pulse). An aliquot of the mitochondria was collected for loading control. Next, the RNA from pulse sample was extracted with 1 ml of TRIzol (Ambion) following manufacturer's recommendations including an overnight isopropanol precipitation at -20°C. The purified RNA was loaded onto a formaldehyde-agarose gel and treated as in northern blotting as described later in the methods section. Then, the northern blot membrane (Hybond-N+, GE Healthcare) was exposed to a phosphorImager screen or an autoradiography film (Amersham hyperfilm MP, GE Healthcare). The quantifications were made from exposures to phosphorImager screen. To normalize the loading, the membrane was later reprobed with an [α-^{32}P]dCTP-labeled CytB probe to assess the steady-state of CytB transcripts. The method was modified form a previously described protocol (Enríquez et al., 1996).

4.4.8.3 In organello translation

Mitochondria were extracted from freshly isolated hearts by differential centrifugation and 500µg mitochondria were washed twice in translation buffer (100 mM mannitol, 10 mM sodium succinate, 80 mM KCl, 5 mM MgCl2, 1 mM KH2PO4, 25 mM HEPES, 5 mM ATP, 20 µM GTP, 6 mM Creatine phosphate, 60 µg/ml Creatine kinase, 200ug/ml emetine, 100ug/ml cycloxemide with 60 µg/ml of every amino acid except methionine) as previously described for other in organello assays. Next the purified mitochondria were resuspended to 750 µl of warm translation buffer with 115 µCi/ml of ^{35}S- labeled methionine and incubated at 37°C and for 60 minutes to incorporate the radioactivity to translated proteins. Next, the mitochondria were collected by centrifugation and washed in translation buffer twice followed by resuspension into 2X Lämmli buffer (125 mM Tris pH 6.8, 4% SDS, 20% glycerol, 1.4 M 2-mercapto-ethanol, 0.025% bromophenol blue). To visualize the incorporated ^{35}S- labeled methionine the mitochondrial proteins were resolved on a 17 % SDS-PAGE gel (5% stacking gel, ran overnight at 80V). The the gel was stained with Coomassie and scanned to control for loading followed by signal amplification in amplifier solution (GE Healthcare) for 30 min at room temperature and

gel drying. Finally, the gel was used to expose to a film (Amersham hyperfilm MP, GE) or phosphorImager screen. The protocol is originally described in *(Côté et al., 1989)*.

4.4.9 Label-free quantitative proteomics

Percoll purified heart mitochondria were prepared for LC MS/MS with guanidinium chloride preparation in the following way. First, the mitochondrial pellets were resuspended in lysis buffer (6 M guanidium chloride, 10 mM TCEP, 40 mM CAA, 100 mM Tris-HCl, 100 µl per 100 mg of heart tissue) and a 20 µl aliquot of the resuspended mitochondria were lyzed with two cycles of heating (95°C, 10 min) and sonication (Bioruptor, 30 s sonication, 30 s break, 10 cycles). Next, the formed cellular debris was removed by pelleting at 20 000 g for 20 min. A small aliquot of the lyzed sample (supernatant) was diluted 10 x with 20 mM Tris-HCl pH 8.3 to dilute the guanidium chloride and 50 µg of the sample was digested with trypsin (1:30 ratio enzyme:protein, Promega Mass spec grade) overnight at 37°C. After digestion, the peptides were cleaned with home-made StageTip (Empore Octadecyl C18; 3M) (Rappsilber et al., 2003) and eluted to 60% ACN/0.1% formic acid. The eluate was dried with speed-vac and resuspended to 0.1% formic acid.

The peptides were analyzed using an Orbitrap Q Exactive HF mass spectrometer (ThermoFisher Scientific) with a Nano-electrospray ion source, coupled with an EASY-nLC 1000 (ThermoFisher Scientific) UHPLC. A 25 cm long reversed-phase C18 column with 75 µm inner diameter (PicoFrit, LC Packings) was used for separating peptides. The LC runs lasted 130 min with a concentration of 2% solvent B (0.1% formic acid in acetonitrile) increasing to 25% over 120 min and further to 40% over 10 min. The column was subsequently washed and re-equilibrated. The flow rate was 200 nl/min. MS spectra were acquired in a data-dependent manner with a top 10 method. For MS, the mass range was set to 300−1500 m/z and resolution to 60 K at 200 m/z. The AGC target of MS was set to 3e6, and the maximum injection time was 100 ms. Peptides were fragmented with HCD with collision energy of 25. For MS/MS, the resolution was set to 30 K. The AGC target was 2e5 and the maximum injection time was 80 ms.

MaxQuant version 1.5.3.8 (Cox and Mann, 2008) with integrated Andromeda search engine (Cox et al., 2011) was used for analyzing the LC/MS/MS raw data. The raw data were searched against the mouse proteome from UniProt (knowledgebase 2016_04). The following parameters were used for data analysis: for ''fixed modification'': cysteine carbamidomethylation, methionine oxidation; for ''variable modification'': methionine oxidation and protein N-terminal acetylation; for ''digestion'' specific with Trypsin/P, Max. missed cleavages 2; for label-free quantification, match between runs was selected. Other parameters were set as default. Protein quantification significant analysis was performed with the Perseus statistical framework (Cox et al., 2014) (http://www.perseus-framework.org/) version 1.5.2.4. After removing the contaminants and reverse identifications, the intensities were transformed to log2. The replicates of each genotype were grouped and filtered with at least 3 validate values in at least one group. The missing values were replaced from normal distribution with

width of 0.3 and down shift of 1.8. Two-sample test was performed to identify the significantly different proteins between knockout and wild-type groups. Proteins with an adjusted p-value ("BH" correction) of less than 0.05 were designated as differentially expressed.

4.5 NUCLEIC ACID ANALYSIS

4.5.1 Nucleic acid extraction

4.5.1.1 Total DNA extraction from tissue
Total DNA was extracted from snap-frozen heart or liver tissue with Gentra Puregene Tissue Kit (QIAGEN) following the manufacturer's recommendations.

4.5.1.2 Total DNA extraction from laser-capture microdissected tissue pieces
The total DNA was extracted from microdissected single colonic crypt section or 5 smooth muscle fibers by adding 10 µl of lysis buffer (50 mM Tris-HCl pH 8.5, 1% Tween-20, 20 mg/ml proteinase K) onto the collected pieces and incubating them for at least two hours at 55 °C followed by a heat-inactivation step at 95 °C for 10 min (Taylor et al., 2003). The DNA extract was then directly used in PCR reactions for mutation level quantification or diluted in 30 µl water for PCR and sequencing.

4.5.1.3 Total DNA extraction from coagulated blood
After cervical dislocation, total blood was quickly removed from the thoracic cavity of the mouse and allowed to coagulate at room temperature for 2 hrs. Thereafter, the serum was separated from the blood by centrifugation at 2000 g for 20 min at room temperature. The coagulated blood was then stored at -80 °C and the DNA was extracted from the clot with Nucleospin 96 well blood quick pure kit (MN) following manufacturer's recommendations.

4.5.1.4 Total DNA extraction from tail piece or ear clip for genotyping
Around 30 µl of lysis buffer (25mM NaOH, 0.2mM EDTA) was added to a tail piece or an ear clip and incubated at 96°C for 45 min. The lysate was then neutralized by adding 30 µl of 40mM Tris pH 7.5 -8. The lysated was stored at 4°C until further use.

4.5.1.5 mtDNA purification for Illumina sequencing
First, fresh tissue (~100 mg heart, 400-500 mg liver) was minced into small pieces, washed in PBS and mitochondria were purified with differential centrifugation, as described in the mitochondria purification section with following modifications. To pellet cellular debris, the homogenate was spun at 800 g for 10 min at 4°C and to collect the mitochondria, the

supernatant of which was spun at 8500g for 10 min at 4°C. The resulting mitochondrial pellet was then resuspended in 600 µl of Mito-DNase buffer (300 mM sucrose, 10 mM MgCl$_2$, 20 mM Tris HCl, pH 7.5, 0.15% BSA, 0.03 mg/ml DNase I type IV, 170 ng/µl RNase A). Heart mitochondria were kept as one 600 µl aliquot but the liver mitochondria were further divided into multiple 600 µl aliquots each containing ~100 mg of starting material. Next the samples were incubated at 37°C for 1 hr to digest the nuclear DNA and RNA. Mitochondria were repelleted at 13 000 g, for 15 min at 4°C and washed twice with 500 µl of mitobuffer (320 mM sucrose, 20 ml Tris-HCl, 1 mM EGTA, 0.2% BSA, pH 7.2) and the samples were frozen in N$_2$(l) and stored in -80°C until further use. Later the same day, the frozen mitochondrial pellets were resuspended into 400 µl lysis buffer (20 mM Tris HCl, 150 mM NaCl, 20 mM EDTA, 1% SDS, pH 8.75, 0.2 mg/ml Proteinase K, 0.2 mg/ml RNase A) and incubated at 56°C overnight. The samples were cooled down to room temperature and DNA was extracted with chloroform (100 µl of 6M K-acetate, 500 µl chloroform:isoamylalcohol (24:1, Amresco)). RNase A 100-200 µg of was added to each of the aqueous phase fractions (heart and liver, respectively) and samples were incubated for 45 min at 37°C to digest the remaining RNA. Thereafter, the samples were ethanol precipitated with 15 µg of glycogen (Ambion) and the purified DNA pellet was resuspended into 20-30 µl of 5 mM Tris buffer pH 8.5 (Macherey-Nagel). The protocol was modified from a previously described protocol (Kennedy et al., 2013). For details see (dx.doi.org/10.17504/protocols.io.mycc7sw)

4.5.1.6 Total RNA extraction

Total RNA was isolated from snap frozen heart or liver tissue with Trizol (Ambion) following the manufacturer's standard protocol with an overnight isopropanol precipitation at -20°C.

4.5.2 PRC based methods

4.5.2.1 Genotyping PCRs

Genotyping PCRs were carried out from the DNA lysate of an ear clip or a tail piece following common laboratory practices with the following primers.

Mouse line	Genotyping primers (5'-3')
PolgA (D257A) loxP	CTTCGGAAGAGCAGTCGGGTG
	GGGCTGCAAAGACTCCGAAGG
Ogg1 delta-MTS	AATTACACCGGACCCATAAGCTAGG
	GCACTGAGAAGTCAACATCCTAGG
MutYh delta-MTS	GTCTCTGAGGGTCGCACATGG
	GCTCCTTACCATCCAGGCTGG
Sod2 loxP	CGAGGGGCATCTAGTGGAGAAG
	AGCTTGGCTGGACGTAA
	CCCCAGATCTGCAATTTCCA
Ckmm cre	CAC GAC CAA GTG ACA GCA AT
	AGA GAC GGA AAT CCA TCG CT

4.5.2.2 cDNA synthesis and PCR amplification to verify the expression of Ogg1 dMTS and Mutyh dMTS transcripts

Total RNA (2 µg) of was converted to cDNA with High Capacity cDNA reverse transcription kit (Applied Biosystems) following the manufacturer's recommendations. To verify the correct length of the produced Ogg1 transcript from the *Ogg1* dMTS mice, cDNA was amplified with primers binding to exon 1 and exon 3 (5'CGTAATGGGCTGGGGCTG3', 5'CAGCACGCCACTCCAGTGAG3'). Similarly, cDNA from *Mutyh* dMTS mice was amplified with primers binding to exon 1 and exon 7 (5'TCGGAGACTGCGCAGGAG3', 5'GGGAAGCGCTGGCCAGGT3') (Ichinoe et al., 2004). The resulting PCR products were resolved on an agarose gel.

4.5.2.3 qPRC

To analyze mtDNA copy number total DNA was extracted as described above with Gentra Puregene Tissue Kit (QIAGEN) with included RNase treatment. First the quality of DNA was verified with NanoDrop (2000C) and then it was quantified with a fluorometric method (Qubit, ThermoFisher). The qPCR analysis of the mtDNA to the nuclear DNA ratio was performed in 7900HT qPCR machine (Applied Biosystems) with the Taqman method using the Taqman Universal PCR Master Mix (Applied Biosystems). All reactions were made in triplicates with 5 ng of total DNA per reaction (final volume 10 µl). Taqman probes were used to detect the target genes (see table below). Each mtDNA copy number analysis was carried out with two mitochondrial probes and the results were always consistent between the used probes. The amplification data was analyzed with standard-curve method using an artificial standard curve, which was produced by mixing a small aliquot of all analyzed samples into one standard sample (SDS 2.4). MtDNA copy number (mtDNA/nDNA) was normalized to control samples.

Taqman probes (Applied Biosystems)	
Gene	Probe
ATP6	Mm03649417-g1
Cytb	AIS062S
ND1	Mm04225274_s1
18S	Hs99999901_s1, detects also mouse 18S

4.5.3 Sequencing methods

4.5.3.1 mtDNA sequence analysis with Sanger sequencing

mtDNA was amplified with PCR using 30 overlapping M13-tagged primer pairs. The amplified fragments were sequenced using the M13 primers tags with Dye 3.1-based sequencing chemistry followed by purification using the BigDye Xterminator cleanup kit. Next, the sequences were resolved on an ABI 3730 DNA Analyzer with 50 cm capillary arrays and long sequencing run protocols. The generated mtDNA sequences were then assembled with SeqScape Version 2.7. Mixed-base calls used a >20% threshold to detect heteroplasmic mtDNA mutations, each of which was confirmed manually. The alignment issues induced by the circularity of mtDNA were overcome by duplicating the first 212bp of the mtDNA to the 3' end of the reference genome.

4.5.3.2 Quantification of C5024T heteroplasmy level

The heteroplasmy level of C5024T mutation was quantified with two methods during the course of this study. The first method was a modified RFLP analysis, similar to (Freyer et al., 2012) and later one was a Allelic Quantification analysis using a PyroMark Q24 pyrosequencer.

RFLP analysis:

A restriction fragment length polymorphism (RFLP) -PCR analysis method, similar to (Freyer et al., 2012) was developed to quantify the levels of C5024T mutation. This mutation disrupts a HpyCH4III restriction site, which can be used to distinguish the wild-type (270bp) digested fragment from the longer non-digested mutant fragment (360bp). The region surrounding the C5024T mutation was PCR amplified for 35 cycles with following primers: shorter 5' CACTCATAGCAATAATAGCTC 3' primer and a longer 5' CAGGAAACAGCTATG ACCACAGTTTCGTAGGTTTAATTCCTGCC 3' primer which contains a control restriction site, which allows testing for incomplete digestion by the presence of a 380bp band in the assay. First, the amplification was controlled by running a small aliquot of the PCR on an agarose gel. Then, the PCR was run for an additional cycle in the presence of 6HEX labeled version of the shorter primer. The resulting PCR product was then purified with Agencourt AMPure XP and eluted from the beads with restriction enzyme buffer (15 µl) and the DNA was digested with

HpyCH4III restriction enzyme (New England Biolabs). An 2 µl aliquot of the digestion product was mixed with 0.1 µl of ROX 500 sizing ladder (ABI) and 7.9 µl of HiDi formamide, heated to 96 °C for 5 min and cooled on ice followed by separation on an ABI 3730 DNA analyzer using Fragment Analysis protocols (for 50 cm capillary array with POP7 polymer). The RFLP analysis was used to quantify the early generations of the mother-offspring data.

Pyrosequencing:

An allele quantification assay was designed with PyroMark assay design software v2.0 (Qiagen). A 178 bp region surrounding the C5024T mutation was PCR amplified with 5'-Biotin-TTCCACCCTAGCTATCATAAGC, and non-biotinylated reverse primer: GTAGGTTTAATTCCTGCCAATCT. Next, the biotinylated strand was denatured and purified on a Pyromark Q24 vacuum workstation, following manufacturer's recommendations. The strand was then sequenced with PyroMark Gold Q24 Reagents on a PyroMark Q24 pyrosequencer according to manufacturer's directions, using the sequencing primer (TGTAGGATGAAGTCTTACA). The pyrosequencing approach was used to quantify all dissected tissue sample data, microdissection quantification and later-generations of mom-pup data.

4.5.3.3 Post-PCR cloning and Sanger sequencing

MtDNA mutation load was measured on WANCY-COX1 tRNA-cluster region with post-PCR cloning and Sanger sequencing, similarly as in (Wanrooij et al., 2012). This ~1kb region is expected to allow higher mutation accumulation than protein encoding regions because of the known sequence flexibility of tRNA sequences (Stewart et al., 2008a). The region has been used extensively in mutation load analysis (Ross et al., 2013; Wanrooij et al., 2012). Total DNA was extracted and quantified as described in the previous sections. Then, the WANCY-COX1 region of mtDNA was amplified from the purified DNA with Phusion DNA polymerase (New England Biolabs) with following primers (F 5'CCTACCCCTAGCCCCCC3' R 5'AGTATAGTAATGCCTGCG3'). Next, the PCR amplification was verified on an agarose gel and aliquot of the PCR products were cloned into a plasmid with Zero Blunt TOPO PCR Cloning Kit (Invitrogen) and transformed to TOP10 chemically competent *E. coli*. The bacteria were then grown overnight on selective plates and the resulting colonies were then picked and sent out for sequencing (Plateseq service, Eurofins). The obtained sequences were analyzed with SeqScape software, version 2.7 (Applied Biosystems). From previous analysis it is known that 0 to 3 mutations are usually found in wild-type mice when ~ 93 000 bp were sequenced, which means that the mutation load in wild-type sample is $<1.07 \times 10^{-5}$ to 3.21×10^{-5} mutations/base pair (Ross et al., 2013). Previously, the background error rate of the method was evaluated to be 3.48×10^{-6} mutations/bp by clone of a clone experiment (Wanrooij et al., 2012).

4.5.3.4 Illumina sequencing

MtDNA was purified from liver (*Mutyh* dMTS x *Ogg1* dMTS) and heart (*Sod2 loxP* x *Ckmm cre* x *Ogg1* dMTS) tissue as described above. Prior to DNA library preparation the DNA quality was analyzed with Genomic DNA analysis ScreenTape (Agilent). First, the purified DNA was fragmented with Covaris to 400 bp (50 ng, 50 µl, 5% duty cycle, intensity 5, 200 cycles per burst, treatment time 55 s). *Sod2 loxP* x *Ckmm cre* x *Ogg1* dMTS set was fragmented with Covaris to 350 bp with 53 s treatment time. Then the fragmented DNA was used to prepare DNA library with NEBNext Ultra II DNA library prep kit for Illumina (New England Biolabs). Then the libraries were single-end sequenced with HiSeq3000, with HiSeq3000/4000 SR Cluster Kit and the corresponding SBS Kit (Illumina) until 1 Gbase of sequence was achieved. The first *Mutyh* dMTS x *Ogg1* dMTS preparation was pre-purified with AMPureBeads (Beckman Coulter) before the library preparation to remove contaminating small DNA/RNA fragments. The mutation load was measured from two separate sets of samples in both *Mutyh* dMTS x *Ogg1* dMTS and *Sod2* loxP x *Ckmm cre* x *Ogg1* dMTS mtDNA mutation analysis.

To carry out RNA seq, total RNA was extracted from snap-frozen heart tissue with TRIzol (Ambion) as described above. Prior to library preparation the quality of the RNA was first verified with northern blotting as described below. After the quality was verified, the rRNAs were depleted from ~1 µg total RNA with RiboZero rRNA Removal Kit (Human/Mouse/Rat) (Epicentre) following manufacturer's recommendations. Thereafter, the RNA library was prepared with NEBNext Ultra Directional RNA Kit (New England Biolabs) following manufacturer's recommendations. Finally, the prepared library was sequenced with HiSeq3000 by using the HiSeq3000/4000 SR Cluster Kit and the corresponding SBS Kit (Illumina) until 5 Gbases of sequence was achieved.

MtDNA and RNA Illumina sequencing experiments, library preparation and sequencing were performed by the Max Planck Genome Center Cologne, Germany (http://mpgc.mpipz.mpg.de/home/).

Data analysis and variant calling of Illumina sequencing of mitochondrial RNA and DNA:
Demultiplexed sequencing reads were first trimmed with Flexbar version 2.5 (Dodt et al., 2012) for quality and TruSeq adapters (default parameters except -q 28 -m 50 -ae ANY -ao 10). Then, RNA reads were aligned to mouse mitochondrial reference genome (GRCm38, release 81) with STAR aligner version 2.4.1d (Dobin et al., 2013) (default parameters except for genome indexing --genomeSAindexNbases 6). In turn a "dual alignment" approach was used for DNA read alignment with BWA version 0.7.12-r1039 (Li and Durbin, 2009) invoking mem (default parameters except -T 19 -B 3 -L 5,4). DNA reads were first aligned to the mouse mitochondrial reference genome and then separately to a split reference genome in which the first 8150 bases were transferred to the end of the genome. Such dual alignment approach was applied in order to enable complete alignment and variant detection at the junction region of the circular mitochondrial genome. With this approach ~50% and ~90% of the reads aligned to mtDNA from heart and liver samples, respectively.

With samtools (Li et al., 2009), the aligned reads were converted to bam format and only uniquely aligned reads (parameter -q 1) were kept for downstream analysis. Then the reads were further sorted and indexed. Per base coverage was determined with bedtools version 2.22.1 (Quinlan and Hall, 2010) genomecov (parameters -split -d). Variants were detected with Lofreq* version 2.1.2 (Wilm et al., 2012) using the following command and parameters: lofreq call-parallel --pp-threads 20 -N -B -q 30 -Q 30 --no-default-filter (referred as "only quality-filtered data"). Both RNA and DNA variants were further filtered for quality and strand bias using LoFreq*: lofreq filter --no-defaults --snvqual-thresh 70 -B 60, for minimum number of variant supporting reads using snpSift filter (Cingolani et al., 2012a) with the expression DP*AF >= 15. DNA variants were additionally filtered for minimum of three variant supporting reads on each strand (expression DP4[2] >= 3 & DP4[3] >= 3). Finally, variant lists were filtered for minimum variant allele frequency (AF value) of 0.5% (quality-filtered and 0.5% minimum variant allele frequency filtered data). Furthermore, known variants in our mouse strain (positions 4891, 9027 and 9461) were removed from all results. In addition, two maternally occurring variants (positions 9993 and 15403) were removed from four Sod2 loxP control siblings (pp). Heavily strand-biased variants (SB Phred score > 100 or 1000 for RNA and DNA variants, respectively) passing the earlier filters were also removed from the minimum allele frequency filtered data. DNA coverage and variant result files originating from the dual alignment approach were combined: results obtained by the alignment to the normal reference genome were kept for genome positions 200 to 16099. Results for the rest of the genome positions, i.e. genome junction region, were obtained by the alignment to the split reference genome and the genome positions were corrected to represent the original position numbers.

Final vcf-files were converted to tab-delimited format with SnpEff version 4.2 (Cingolani et al., 2012b) and mutation loads were calculated as follows: Over the whole mitochondrial genome, a "unique" mutation load was calculated by dividing number of detected variants by coverage (total base pairs aligned to mitochondrial genome), whereas total mutation load was calculated by dividing the sum of variant supporting bases (obtained from DP4 values) by coverage. To obtain the corresponding mutation loads per mutation type (e.g. G>T), the variant or total variant read counts were divided by the total coverage on the reference base in question. The variant calls for each mouse are available in the supplement section.

4.5.4 Southern blotting

To analyze mtDNA copy number and presence of mtDNA deletions total DNA was extracted Gentra Puregene Tissue Kit (QIAGEN), as described above, and digested overnight with Sac-HF restriction enzyme (New England Biolabs). The digested DNA was the purified with ethanol precipitation. Then, ~700-800 ng of the digested DNA was resolved on an agarose gel. The gel was treated with HCl, denatured, neutralized and set up for a capillary transfer on to a Hybond-N+ (GE Healthcare) membrane following common molecular biology techniques. Following transfer, the membrane was cross-linked and blocked with hybridization buffer (Perfect Hyb Plus, Sigma-Aldrich). Then mtDNA and nuclear DNA were detected by incubating the membrane with [α-^{32}P]dCTP labeled mtDNA (pAM1) and nuclear DNA (18S) probes. The

probed membrane was exposed to a phosphorImager screen or to a film (Amersham Hyperfilm MP, GE Healthcare).

4.5.5 Northern blotting

Total RNA was extracted from snap-frozen tissue as described above and quantified with a fluorometric method (Qubit, ThermoFisher). First, 2 µg of total RNA was treated with NorthernMax-Gly sample loading dye (Ambion) and then resolved on a 1.2 % formaldehyde-agarose gel. Afterwards the gel was incubated in 0.05 M NaOH, DEPC-water and 20X SSC. The treated gel was then set up for a capillary transfer with 20 x SSC. Following transfer, the membrane (Hybond-NX, GE Healthcare) was cross-linked and incubated with hybridization solution (5 x SSC, 20 mM Na_2HPO_4, 7% SDS, 0.5 x RNA secure (Ambion), 100 µg/ml heparin). Next, the transcripts were visualized with an overnight incubation with biotin labeled oligonucleotide probe (100 pmol) at 50°C in hybridization solution followed by washing and signal detection with IRDye 800CW dye-labeled streptavidin (LI-COR Biosciences) (in TBS, 0.05% TWEEN-20, dilution 1:5000) in the Odyssey infrared imaging system (LI-COR Biosciences). This method has previously been described (Davies et al., 2012).

4.5.6 Topology gel

50 mg of mouse heart tissue was collected for gentle total DNA extraction. The tissue was first rinsed in PBS, minced and then lyzed in 600 µl of lysis buffer (100 mM Tris-HCl pH 7.5, 100 mM EDTA, 100 mM NaCl, 0.5% SDS, 0.8 mg/ml Proteinase K) with 3hrs long incubation at 55°C. Next the sample was incubated on ice for 2 hrs in the presense of premixed LiCl and K-acetate (final concentration 250 mM K-acetate, 760 mM LiCl) to precipitate contaminants. To collect the precipitate, samples were spun for 15 min at 15 000 rpm at 18°C. The supernatant was then combined with isopropanol and incubated on ice for 30 min and the precipated DNA was collection by centrifugation for 30 min at 16 000 g at 18°C. Next the DNA was washed and resuspended to 10 mM Tris-HCl, 1 mM EDTA pH 8.0 by flicking the tube. To accurately quantify the DNA with a fluorometric method (Qubit, ThermoFisher), a small aliquot of the sample was digested with SacI-HF (New England Biolabs) at 37°C for 30 min prior to quantification. Then, 400 ng of total DNA was then resolved on 0.4% agarose gel (15 x 15 cm) (Seakem Gold agarose, Lonza) with 40 V for 16-20 hrs with and without EtBr (0.5 mg/ml). EtBr was used to condense the different supercoiling states of the closed circle molecule. Following electrophoresis, the gel was pretreated and transferred similar to a Southern blot gel (described above). Next, the mtDNA was visualized from the membrane with a [α-^{32}P]dCTP-labeled probe (pAM1) and used to expose a phosphorImager screen or autoradiography film (Amersham hyperfilm MP, GE Healthcare). The quantifications were made from the phosphorImager screen. The control samples (400 ng each) were treated (37°C 30 min) with various DNA modifying enzymes prior to electrophoresis to reveal the different topological isomers of mtDNA, namely only buffer (no treatment), SacI (linear) (New England Biolabs; 20 U), Nt.BbvCI

(nicked circles) (New England Biolabs; 10 U), Topo I (relaxes the closed circles) (New England Biolabs; 5 U), DNA gyrase (compacts the closed circles) (New England Biolabs; 5 U). The method was modified form a previously described protocol (Kolesar et al., 2013).

4.5.7 Abasic-site analysis

To reveal the abasic site in mtDNA, the extracted DNA was treated with EndoIV (New England Biolabs, 10U) to convert the abasic sites to single-stranded nicks prior to analysis on a topology gel. Briefly, total DNA was extracted as described in the topology gel method. Before loading to the topology gel, each sample was split in half and one half was treated only with buffer and the other with EndoIV (New England Biolobs; 10 U). The presence of abasic sites was quantified by measuring the decrease in closed circle form of mtDNA between the treated and untreated sample from a phosphorImager screen.

4.6 STATISTICAL ANALYSIS

All values are expressed as means ± standard deviation, unless differently indicated. Statistical analyses were performed and graphs were drawn with the Prism software version 5.0f. Mass spectrometry data were analyzed with the Perseus statistical framework version 1.5.2.4 with two-sample test with Benjamini–Hochberg adjusted p-values. Statistical significance was considered at $P < 0.05$. (*$P < 0.05$, **$P < 0.005$, ***$P > 0.001$ ****$P < 0.0001$). Details of statistical analysis applied to each experiment can be found in the figure legends.

4.6.1 Test of neutral segregation in the female germline

The segregation of the C5024T allele in the mom-offspring pairs was tested against a neutral model with Kimura distribution (Wonnapinij et al., 2008). First, the Kimura003.c code was downloaded and then the variables (initial population mutation proportion in the mothers, sample size, variance) were modified in the code before compiling, for each run. Multiple females with ±4% of the C5024T mutation and their offspring were grouped together for each analysis to gain large enough sample numbers for a robust analysis. The *p* was defined from the weighted mean of the C5024T mutation levels in the 3-week-old tail or earclip biopsies from the mothers. The population of pup 3-week-old tail or earclip biopsy measurements was used to calculate the *Var.* The result of the statistical test for conforming to the neutral distribution was retrieved from the monte_carlo1000.txt file output from each analysis. All tests for neutral segregation are included in Supplement section.

REFERENCES

Adams, K.L., and Palmer, J.D. (2003). Evolution of mitochondrial gene content: gene loss and transfer to the nucleus. Mol. Phylogenet. Evol. *29*, 380–395.

Agaronyan, K., Morozov, Y.I., Anikin, M., and Temiakov, D. (2015). Mitochondrial biology. Replication-transcription switch in human mitochondria. Science *347*, 548–551.

Akbari, M., Visnes, T., Krokan, H.E., and Otterlei, M. (2008). Mitochondrial base excision repair of uracil and AP sites takes place by single-nucleotide insertion and long-patch DNA synthesis. DNA Repair *7*, 605–616.

Alcázar-Fabra, M., Navas, P., and Brea-Calvo, G. (2016). Coenzyme Q biosynthesis and its role in the respiratory chain structure. Biochim. Biophys. Acta *1857*, 1073–1078.

Alexeyev, M.F. (2009). Is there more to aging than mitochondrial DNA and reactive oxygen species? Febs J. *276*, 5768–5787.

Alexeyev, M., Shokolenko, I., Wilson, G., and LeDoux, S. (2013). The Maintenance of Mitochondrial DNA Integrity—Critical Analysis and Update. Cold Spring Harb Perspect Biol *5*, a012641–a012641.

Allen, J.F. (2015). Why chloroplasts and mitochondria retain their own genomes and genetic systems: Colocation for redox regulation of gene expression. Proc. Natl. Acad. Sci. U.S.a. *112*, 10231–10238.

Aller, P., Rould, M.A., Hogg, M., Wallace, S.S., and Doublie, S. (2007). A structural rationale for stalling of a replicative DNA polymerase at the most common oxidative thymine lesion, thymine glycol. Proc. Natl. Acad. Sci. U.S.a. *104*, 814–818.

Andreyev, A.I., Kushnareva, Y.E., and Starkov, A.A. (2005). Mitochondrial metabolism of reactive oxygen species. Biochemistry Mosc. *70*, 200–214.

Anson, R.M., Hudson, E., and Bohr, V.A. (2000). Mitochondrial endogenous oxidative damage has been overestimated. Faseb J. *14*, 355–360.

Bacman, S.R., Williams, S.O.N.L., Pinto, M., Peralta, S., and Moraes, C.T. (2013). Specific elimination of mutant mitochondrial genomes in patient-derived cells by mitoTALENs. Nat. Med. *19*, 1111–1113.

Bai, Y., and Attardi, G. (1998). The mtDNA-encoded ND6 subunit of mitochondrial NADH dehydrogenase is essential for the assembly of the membrane arm and the respiratory function of the enzyme. Embo J. *17*, 4848–4858.

Baines, H.L., Stewart, J.B., Stamp, C., Zupanic, A., Kirkwood, T.B.L., Larsson, N.-G., Turnbull, D.M., and Greaves, L.C. (2014). Similar patterns of clonally expanded somatic mtDNA mutations in the colon of heterozygous mtDNA mutator mice and ageing humans. Mech. Ageing Dev. *139*, 22–30.

Bandaru, V., Sunkara, S., Wallace, S.S., and Bond, J.P. (2002). A novel human DNA glycosylase that removes oxidative DNA damage and is homologous to Escherichia coli endonuclease VIII. DNA Repair *1*, 517–529.

Barja, G., and Herrero, A. (2000). Oxidative damage to mitochondrial DNA is inversely related to maximum life span in the heart and brain of mammals. Faseb J. *14*, 312–318.

Bayona-Bafaluy, M.P., Blits, B., Battersby, B.J., Shoubridge, E.A., and Moraes, C.T. (2005). Rapid directional shift of mitochondrial DNA heteroplasmy in animal tissues by a mitochondrially targeted restriction endonuclease. Proc. Natl. Acad. Sci. U.S.a. *102*, 14392–14397.

Berk, A.J., and Clayton, D.A. (1974). Mechanism of mitochondrial DNA replication in mouse L-cells: asynchronous replication of strands, segregation of circular daughter molecules, aspects of topology and turnover of an initiation sequence. J. Mol. Biol. *86*, 801–824.

Blanchard, J.L., and Lynch, M. (2000). Organellar genes: why do they end up in the nucleus? Trends Genet. *16*, 315–320.

Bogenhagen, D., and Clayton, D.A. (1977). Mouse L cell mitochondrial DNA molecules are selected randomly for replication throughout the cell cycle. Cell *11*, 719–727.

Bogenhagen, D.F., and Clayton, D.A. (2003). The mitochondrial DNA replication bubble has not burst. Trends Biochem. Sci. *28*, 357–360.

Bokov, A., Chaudhuri, A., and Richardson, A. (2004). The role of oxidative damage and stress in aging. Mech. Ageing Dev. *125*, 811–826.

Boulet, L., Karpati, G., and Shoubridge, E.A. (1992). Distribution and threshold expression of the tRNA(Lys) mutation in skeletal muscle of patients with myoclonic epilepsy and ragged-red fibers (MERRF). Am. J. Hum. Genet. *51*, 1187–1200.

Boveris, A., Oshino, N., and Chance, B. (1972). The cellular production of hydrogen peroxide. Biochem. J. *128*, 617–630.

Bowmaker, M., Yang, M.Y., Yasukawa, T., Reyes, A., Jacobs, H.T., Huberman, J.A., and Holt, I.J. (2003). Mammalian mitochondrial DNA replicates bidirectionally from an initiation zone. J. Biol. Chem. *278*, 50961–50969.

Bratic, A., Kauppila, T.E.S., Macao, B., Grönke, S., Siibak, T., Stewart, J.B., Baggio, F., Dols, J., Partridge, L., Falkenberg, M., et al. (2015). Complementation between polymerase- and exonuclease-deficient mitochondrial DNA polymerase mutants in genomically engineered flies. Nat Commun *6*, 8808.

Brieba, L.G., Eichman, B.F., Kokoska, R.J., Doublie, S., Kunkel, T.A., and Ellenberger, T. (2004). Structural basis for the dual coding potential of 8-oxoguanosine by a high-fidelity DNA polymerase. Embo J. *23*, 3452–3461.

Brierley, E.J., Johnson, M.A., Lightowlers, R.N., James, O.F., and Turnbull, D.M. (1998). Role of mitochondrial DNA mutations in human aging: implications for the central nervous system and muscle. Ann. Neurol. *43*, 217–223.

Brown, T.A., Cecconi, C., Tkachuk, A.N., Bustamante, C., and Clayton, D.A. (2005). Replication of mitochondrial DNA occurs by strand displacement with alternative light-strand origins, not via a strand-coupled mechanism. Genes Dev. *19*, 2466–2476.

Bua, E., Johnson, J., Herbst, A., Delong, B., McKenzie, D., Salamat, S., and Aiken, J.M. (2006). Mitochondrial DNA-deletion mutations accumulate intracellularly to detrimental levels in aged human skeletal muscle fibers. Am. J. Hum. Genet. *79*, 469–480.

Cadet, J., Delatour, T., Douki, T., Gasparutto, D., Pouget, J.P., Ravanat, J.L., and Sauvaigo, S. (1999). Hydroxyl radicals and DNA base damage. Mutat. Res. *424*, 9–21.

Calvo, S.E., Julien, O., Clauser, K.R., Shen, H., Kamer, K.J., Wells, J.A., and Mootha, V.K. (2017). Comparative Analysis of Mitochondrial N-Termini from Mouse, Human, and Yeast. Mol. Cell Proteomics *16*, 512–523.

Cerritelli, S.M., and Crouch, R.J. (2009). Ribonuclease H: the enzymes in eukaryotes. FEBS Journal *276*, 1494–1505.

Chae, H.Z., Kim, H.J., Kang, S.W., and Rhee, S.G. (1999). Characterization of three isoforms of mammalian peroxiredoxin that reduce peroxides in the presence of thioredoxin. Diabetes Res. Clin. Pract. *45*, 101–112.

Chan, D.C. (2012). Fusion and fission: interlinked processes critical for mitochondrial health. Annu. Rev. Genet. *46*, 265–287.

Chang, D.D., and Clayton, D.A. (1985). Priming of human mitochondrial DNA replication occurs at the light-strand promoter. Proc Natl Acad Sci USA *82*, 351–355.

Chattopadhyay, R., Wiederhold, L., Szczesny, B., Boldogh, I., Hazra, T.K., Izumi, T., and Mitra, S. (2006). Identification and characterization of mitochondrial abasic (AP)-endonuclease in mammalian cells. Nucleic Acids Res. *34*, 2067–2076.

Chen, L., Liu, P., Evans, T.C., and Ettwiller, L.M. (2017). DNA damage is a pervasive cause of sequencing errors, directly confounding variant identification. Science *355*, 752–756.

Chinnery, P.F., Howell, N., Lightowlers, R.N., and Turnbull, D.M. (1997). Molecular pathology of MELAS and MERRF. The relationship between mutation load and clinical phenotypes. Brain *120 (Pt 10)*, 1713–1721.

Ciafaloni, E., Ricci, E., Servidei, S., Shanske, S., Silvestri, G., Manfredi, G., Schon, E.A., and DiMauro, S. (1991). Widespread tissue distribution of a tRNALeu(UUR) mutation in the mitochondrial DNA of a patient with MELAS syndrome. Neurology *41*, 1663–1664.

Cingolani, P., Patel, V.M., Coon, M., Nguyen, T., Land, S.J., Ruden, D.M., and Lu, X. (2012a). Using Drosophila melanogaster as a Model for Genotoxic Chemical Mutational Studies with a New Program, SnpSift. Front Genet *3*, 35.

Cingolani, P., Platts, A., Wang, L.L., Coon, M., Nguyen, T., Wang, L., Land, S.J., Lu, X., and Ruden, D.M. (2012b). A program for annotating and predicting the effects of single nucleotide polymorphisms, SnpEff: SNPs in the genome of Drosophila melanogaster strain w1118; iso-2; iso-3. Fly (Austin) *6*, 80–92.

Claros, M.G., and Vincens, P. (1996). Computational method to predict mitochondrially imported proteins and their targeting sequences. Eur. J. Biochem. *241*, 779–786.

Clayton, D.A. (1991). Replication and transcription of vertebrate mitochondrial DNA. Annu. Rev. Cell Biol. *7*, 453–478.

Clayton, D.A., Doda, J.N., and Friedberg, E.C. (1975). Absence of a pyrimidine dimer repair mechanism for mitochondrial DNA in mouse and human cells. Basic Life Sci. *5B*, 589–591.

Cochemé, H.M., Quin, C., McQuaker, S.J., Cabreiro, F., Logan, A., Prime, T.A., Abakumova, I., Patel, J.V., Fearnley, I.M., James, A.M., et al. (2011). Measurement of H2O2 within living Drosophila during aging using a ratiometric mass spectrometry probe targeted to the mitochondrial matrix. Cell Metab. *13*, 340–350.

Copeland, W.C., and Longley, M.J. (2014). Mitochondrial genome maintenance in health and disease. DNA Repair *19*, 190–198.

Cortopassi, G.A., and Arnheim, N. (1990). Detection of a specific mitochondrial DNA deletion in tissues of older humans. Nucleic Acids Res. *18*, 6927–6933.

Costello, M., Pugh, T.J., Fennell, T.J., Stewart, C., Lichtenstein, L., Meldrim, J.C., Fostel, J.L., Friedrich, D.C., Perrin, D., Dionne, D., et al. (2013). Discovery and characterization of

artifactual mutations in deep coverage targeted capture sequencing data due to oxidative DNA damage during sample preparation. Nucleic Acids Res. *41*, e67–e67.

Cox, J., and Mann, M. (2008). MaxQuant enables high peptide identification rates, individualized p.p.b.-range mass accuracies and proteome-wide protein quantification. Nat. Biotechnol. *26*, 1367–1372.

Cox, J., Hein, M.Y., Luber, C.A., Paron, I., Nagaraj, N., and Mann, M. (2014). Accurate proteome-wide label-free quantification by delayed normalization and maximal peptide ratio extraction, termed MaxLFQ. Mol. Cell Proteomics *13*, 2513–2526.

Cox, J., Neuhauser, N., Michalski, A., Scheltema, R.A., Olsen, J.V., and Mann, M. (2011). Andromeda: a peptide search engine integrated into the MaxQuant environment. J. Proteome Res. *10*, 1794–1805.

Côté, C., Poirier, J., and Boulet, D. (1989). Expression of the mammalian mitochondrial genome. Stability of mitochondrial translation products as a function of membrane potential. J. Biol. Chem. *264*, 8487–8490.

Cree, L.M., Samuels, D.C., de Sousa Lopes, S.C., Rajasimha, H.K., Wonnapinij, P., Mann, J.R., Dahl, H.-H.M., and Chinnery, P.F. (2008). A reduction of mitochondrial DNA molecules during embryogenesis explains the rapid segregation of genotypes. Nature Genet. *40*, 249–254.

Daley, D.O., Clifton, R., and Whelan, J. (2002). Intracellular gene transfer: reduced hydrophobicity facilitates gene transfer for subunit 2 of cytochrome c oxidase. Proc Natl Acad Sci USA *99*, 10510–10515.

Das, K., and Roychoudhury, A. (2014). Reactive oxygen species (ROS) and response of antioxidants as ROS-scavengers during environmental stress in plants. Front. Environ. Sci. *2*, 67–13.

David, S.S., and Wiliams, S.D. (1998). Chemistry of glycosylases and endonucleases involved in base-excision repair. Chem. Rev. *98*, 1221–1261.

Davies, S.M.K., Lopez Sanchez, M.I.G., Narsai, R., Shearwood, A.-M.J., Razif, M.F.M., Small, I.D., Whelan, J., Rackham, O., and Filipovska, A. (2012). MRPS27 is a pentatricopeptide repeat domain protein required for the translation of mitochondrially encoded proteins. FEBS Lett. *586*, 3555–3561.

De Bont, R., and van Larebeke, N. (2004). Endogenous DNA damage in humans: a review of quantitative data. Mutagenesis *19*, 169–185.

de Souza-Pinto, N.C., Eide, L., Hogue, B.A., Thybo, T., Stevnsner, T., Seeberg, E., Klungland, A., and Bohr, V.A. (2001). Repair of 8-oxodeoxyguanosine lesions in mitochondrial dna depends on the oxoguanine dna glycosylase (OGG1) gene and 8-oxoguanine accumulates in the mitochondrial dna of OGG1-defective mice. Cancer Res. *61*, 5378–5381.

de Souza-Pinto, N.C., Mason, P.A., Hashiguchi, K., Weissman, L., Tian, J., Guay, D., Lebel, M., Stevnsner, T.V., Rasmussen, L.J., and Bohr, V.A. (2009). Novel DNA mismatch-repair activity involving YB-1 in human mitochondria. DNA Repair *8*, 704–719.

Dobin, A., Davis, C.A., Schlesinger, F., Drenkow, J., Zaleski, C., Jha, S., Batut, P., Chaisson, M., and Gingeras, T.R. (2013). STAR: ultrafast universal RNA-seq aligner. Bioinformatics *29*, 15–21.

Dodt, M., Roehr, J.T., Ahmed, R., and Dieterich, C. (2012). FLEXBAR-Flexible Barcode and Adapter Processing for Next-Generation Sequencing Platforms. Biology (Basel) *1*, 895–905.

Dou, H., Mitra, S., and Hazra, T.K. (2003). Repair of oxidized bases in DNA bubble structures by human DNA glycosylases NEIL1 and NEIL2. J. Biol. Chem. *278*, 49679–49684.

Dudek, J., Rehling, P., and van der Laan, M. (2013). Mitochondrial protein import: common principles and physiological networks. Biochim. Biophys. Acta *1833*, 274–285.

Duxin, J.P., Dao, B., Martinsson, P., Rajala, N., Guittat, L., Campbell, J.L., Spelbrink, J.N., and Stewart, S.A. (2009). Human Dna2 is a nuclear and mitochondrial DNA maintenance protein. Mol. Cell. Biol. *29*, 4274–4282.

Ellefson, J.W., Gollihar, J., Shroff, R., Shivram, H., Iyer, V.R., and Ellington, A.D. (2016). Synthetic evolutionary origin of a proofreading reverse transcriptase. Science *352*, 1590–1593.

Elliott, H.R., Samuels, D.C., Eden, J.A., Relton, C.L., and Chinnery, P.F. (2008). Pathogenic mitochondrial DNA mutations are common in the general population. Am. J. Hum. Genet. *83*, 254–260.

Elson, J.L., Samuels, D.C., Turnbull, D.M., and Chinnery, P.F. (2001). Random intracellular drift explains the clonal expansion of mitochondrial DNA mutations with age. Am. J. Hum. Genet. *68*, 802–806.

Emanuelsson, O., Nielsen, H., Brunak, S., and Heijne, von, G. (2000). Predicting subcellular localization of proteins based on their N-terminal amino acid sequence. J. Mol. Biol. *300*, 1005–1016.

Emblem, Å., Okkenhaug, S., Weiss, E.S., Denver, D.R., Karlsen, B.O., Moum, T., and Johansen, S.D. (2014). Sea anemones possess dynamic mitogenome structures. Mol. Phylogenet. Evol. *75*, 184–193.

Enríquez, J.A., Pérez-Martos, A., López-Pérez, M.J., and Montoya, J. (1996). In organello RNA synthesis system from mammalian liver and brain. Meth. Enzymol. *264*, 50–57.

Ericson, N.G., Kulawiec, M., Vermulst, M., Sheahan, K., O'Sullivan, J., Salk, J.J., and Bielas, J.H. (2012). Decreased mitochondrial DNA mutagenesis in human colorectal cancer. PLoS Genet *8*, e1002689.

Esworthy, R.S., Ho, Y.S., and Chu, F.F. (1997). The Gpx1 gene encodes mitochondrial glutathione peroxidase in the mouse liver. Arch. Biochem. Biophys. *340*, 59–63.

Faith, J.J., and Pollock, D.D. (2003). Likelihood analysis of asymmetrical mutation bias gradients in vertebrate mitochondrial genomes. Genetics *165*, 735–745.

Fan, L., Kim, S., Farr, C.L., Schaefer, K.T., Randolph, K.M., Tainer, J.A., and Kaguni, L.S. (2006). A novel processive mechanism for DNA synthesis revealed by structure, modeling and mutagenesis of the accessory subunit of human mitochondrial DNA polymerase. J. Mol. Biol. *358*, 1229–1243.

Fan, W., Waymire, K.G., Narula, N., Li, P., Rocher, C., Coskun, P.E., Vannan, M.A., Narula, J., Macgregor, G.R., and Wallace, D.C. (2008). A mouse model of mitochondrial disease reveals germline selection against severe mtDNA mutations. Science *319*, 958–962.

Farge, G., Pham, X.H., Holmlund, T., Khorostov, I., and Falkenberg, M. (2007). The accessory subunit B of DNA polymerase gamma is required for mitochondrial replisome function. Nucleic Acids Res. *35*, 902–911.

Fellous, T.G., Islam, S., Tadrous, P.J., Elia, G., Kocher, H.M., Bhattacharya, S., Mears, L., Turnbull, D.M., Taylor, R.W., Greaves, L.C., et al. (2009). Locating the stem cell niche and tracing hepatocyte lineages in human liver. Hepatology *49*, 1655–1663.

Ferreira, N., Rackham, O., and Filipovska, A. (2017). Regulation of a minimal transcriptome by repeat domain proteins. Semin. Cell Dev. Biol.

Finnila, S., Tuisku, S., Herva, R., and Majamaa, K. (2001). A novel mitochondrial DNA mutation and a mutation in the Notch3 gene in a patient with myopathy and CADASIL. J. Mol. Med. *79*, 641–647.

Flint, D.H., Tuminello, J.F., and Emptage, M.H. (1993). The inactivation of Fe-S cluster containing hydro-lyases by superoxide. J. Biol. Chem. *268*, 22369–22376.

Fonseca, M.M., Harris, D.J., and Posada, D. (2014). The inversion of the Control Region in three mitogenomes provides further evidence for an asymmetric model of vertebrate mtDNA replication. PLoS ONE *9*, e106654.

Foster, L.J., de Hoog, C.L., Zhang, Y., Zhang, Y., Xie, X., Mootha, V.K., and Mann, M. (2006). A mammalian organelle map by protein correlation profiling. Cell *125*, 187–199.

Foury, F., and Vanderstraeten, S. (1992). Yeast mitochondrial DNA mutators with deficient proofreading exonucleolytic activity. Embo J. *11*, 2717–2726.

Fox, E.J., Reid-Bayliss, K.S., Emond, M.J., and Loeb, L.A. (2014). Accuracy of Next Generation Sequencing Platforms. Next Gener Seq Appl *1*.

Freyer, C., Cree, L.M., Mourier, A., Stewart, J.B., Koolmeister, C., Milenkovic, D., Wai, T., Floros, V.I., Hagström, E., Chatzidaki, E.E., et al. (2012). Variation in germline mtDNA heteroplasmy is determined prenatally but modified during subsequent transmission. Nature Genet. *44*, 1282–1285.

Fusté, J.M., Wanrooij, S., Jemt, E., Granycome, C.E., Cluett, T.J., Shi, Y., Atanassova, N., Holt, I.J., Gustafsson, C.M., and Falkenberg, M. (2010). Mitochondrial RNA polymerase is needed for activation of the origin of light-strand DNA replication. Molecular Cell *37*, 67–78.

Gammage, P.A., Gaude, E., Van Haute, L., Rebelo-Guiomar, P., Jackson, C.B., Rorbach, J., Pekalski, M.L., Robinson, A.J., Charpentier, M., Concordet, J.-P., et al. (2016). Near-complete elimination of mutant mtDNA by iterative or dynamic dose-controlled treatment with mtZFNs. Nucleic Acids Res. *44*, 7804–7816.

Gammage, P.A., Rorbach, J., Vincent, A.I., Rebar, E.J., and Minczuk, M. (2014). Mitochondrially targeted ZFNs for selective degradation of pathogenic mitochondrial genomes bearing large-scale deletions or point mutations. EMBO Mol Med *6*, 458–466.

Gao, X., Wen, X., Esser, L., Quinn, B., Yu, L., Yu, C.-A., and Xia, D. (2003). Structural basis for the quinone reduction in the bc1 complex: a comparative analysis of crystal structures of mitochondrial cytochrome bc1 with bound substrate and inhibitors at the Qi site. Biochemistry *42*, 9067–9080.

Gao, Y., Katyal, S., Lee, Y., Zhao, J., Rehg, J.E., Russell, H.R., and McKinnon, P.J. (2011). DNA ligase III is critical for mtDNA integrity but not Xrcc1-mediated nuclear DNA repair. Nature *471*, 240–244.

Gardner, P.R., Raineri, I., Epstein, L.B., and White, C.W. (1995). Superoxide radical and iron modulate aconitase activity in mammalian cells. J. Biol. Chem. *270*, 13399–13405.

Gedik, C.M., Collins, A., ESCODD (European Standards Committee on Oxidative DNA Damage) (2005). Establishing the background level of base oxidation in human lymphocyte DNA: results of an interlaboratory validation study. Faseb J. *19*, 82–84.

Gensler, S., Weber, K., Schmitt, W.E., Pérez-Martos, A., Enríquez, J.A., Montoya, J., and Wiesner, R.J. (2001). Mechanism of mammalian mitochondrial DNA replication: import of

mitochondrial transcription factor A into isolated mitochondria stimulates 7S DNA synthesis. Nucleic Acids Res. *29*, 3657–3663.

Goto, Y., Nonaka, I., and HORAI, S. (1990). A mutation in the tRNA(Leu)(UUR) gene associated with the MELAS subgroup of mitochondrial encephalomyopathies. Nature *348*, 651–653.

Graves, S.W., Johnson, A.A., and Johnson, K.A. (1998). Expression, purification, and initial kinetic characterization of the large subunit of the human mitochondrial DNA polymerase. Biochemistry *37*, 6050–6058.

Gray, M.W. (2012). Mitochondrial evolution. Cold Spring Harb Perspect Biol *4*, a011403.

Graziewicz, M.A., Bienstock, R.J., and Copeland, W.C. (2007). The DNA polymerase gamma Y955C disease variant associated with PEO and parkinsonism mediates the incorporation and translesion synthesis opposite 7,8-dihydro-8-oxo-2'-deoxyguanosine. Hum. Mol. Gen. *16*, 2729–2739.

Graziewicz, M.A., Day, B.J., and Copeland, W.C. (2002). The mitochondrial DNA polymerase as a target of oxidative damage. Nucleic Acids Res. *30*, 2817–2824.

Greaves, L.C., Barron, M.J., Plusa, S., Kirkwood, T.B., Mathers, J.C., Taylor, R.W., and Turnbull, D.M. (2010). Defects in multiple complexes of the respiratory chain are present in ageing human colonic crypts. Exp. Gerontol. *45*, 573–579.

Greaves, L.C., Beadle, N.E., Taylor, G.A., Commane, D., Mathers, J.C., Khrapko, K., and Turnbull, D.M. (2009). Quantification of mitochondrial DNA mutation load. Aging Cell *8*, 566–572.

Greaves, L.C., Elson, J.L., Nooteboom, M., Grady, J.P., Taylor, G.A., Taylor, R.W., Mathers, J.C., Kirkwood, T.B.L., and Turnbull, D.M. (2012). Comparison of mitochondrial mutation spectra in ageing human colonic epithelium and disease: absence of evidence for purifying selection in somatic mitochondrial DNA point mutations. PLoS Genet *8*, e1003082.

Greaves, L.C., Nooteboom, M., Elson, J.L., Tuppen, H.A.L., Taylor, G.A., Commane, D.M., Arasaradnam, R.P., Khrapko, K., Taylor, R.W., Kirkwood, T.B.L., et al. (2014a). Clonal expansion of early to mid-life mitochondrial DNA point mutations drives mitochondrial dysfunction during human ageing. PLoS Genet *10*, e1004620.

Greaves, L.C., Nooteboom, M., Elson, J.L., Tuppen, H.A.L., Taylor, G.A., Commane, D.M., Arasaradnam, R.P., Khrapko, K., Taylor, R.W., Kirkwood, T.B.L., et al. (2014b). Clonal expansion of early to mid-life mitochondrial DNA point mutations drives mitochondrial dysfunction during human ageing. PLoS Genet *10*, e1004620.

Greber, B.J., and Ban, N. (2016). Structure and Function of the Mitochondrial Ribosome. Annu. Rev. Biochem. *85*, 103–132.

Grossman, L.I., Watson, R., and Vinograd, J. (1973). The presence of ribonucleotides in mature closed-circular mitochondrial DNA. Proc Natl Acad Sci USA *70*, 3339–3343.

Gustafsson, C.M., Falkenberg, M., and Larsson, N.-G. (2016). Maintenance and Expression of Mammalian Mitochondrial DNA. Annu. Rev. Biochem. *85*, 133–160.

Hagström, E., Freyer, C., Battersby, B.J., Stewart, J.B., and Larsson, N.-G. (2014). No recombination of mtDNA after heteroplasmy for 50 generations in the mouse maternal germline. Nucleic Acids Res. *42*, 1111–1116.

Halliwell, B., and Aruoma, O.I. (1991). DNA damage by oxygen-derived species. Its mechanism and measurement in mammalian systems. FEBS Lett. *281*, 9–19.

Halliwell, B., and Gutteridge, J.M. (1992). Biologically relevant metal ion-dependent hydroxyl radical generation. An update. FEBS Lett. *307*, 108–112.

Halliwell, B. (2006). Reactive species and antioxidants. Redox biology is a fundamental theme of aerobic life. Plant Physiol. *141*, 312–322.

Halsne, R., Esbensen, Y., Wang, W., Scheffler, K., Suganthan, R., Bjørås, M., and Eide, L. (2012). Lack of the DNA glycosylases MYH and OGG1 in the cancer prone double mutant mouse does not increase mitochondrial DNA mutagenesis. DNA Repair *11*, 278–285.

Hancock, D.K., Tully, L.A., and Levin, B.C. (2005). A Standard Reference Material to determine the sensitivity of techniques for detecting low-frequency mutations, SNPs, and heteroplasmies in mitochondrial DNA. Genomics *86*, 446–461.

Hanes, J.W., Thal, D.M., and Johnson, K.A. (2006). Incorporation and replication of 8-oxo-deoxyguanosine by the human mitochondrial DNA polymerase. J. Biol. Chem. *281*, 36241–36248.

Hansford, R.G., Hogue, B.A., and Mildaziene, V. (1997). Dependence of H2O2 formation by rat heart mitochondria on substrate availability and donor age. J. Bioenerg. Biomembr. *29*, 89–95.

Harman, D. (1956). Aging: a theory based on free radical and radiation chemistry. J Gerontol *11*, 298–300.

Harman, D. (1972). The biologic clock: the mitochondria? J Am Geriatr Soc *20*, 145–147.

Hatefi, Y. (1985). The mitochondrial electron transport and oxidative phosphorylation system. Annu. Rev. Biochem. *54*, 1015–1069.

Hayashi, J.I., Ohta, S., Kikuchi, A., Takemitsu, M., Goto, Y., and Nonaka, I. (1991). Introduction of Disease-Related Mitochondrial-Dna Deletions Into Hela-Cells Lacking Mitochondrial-Dna Results in Mitochondrial Dysfunction. Proc. Natl. Acad. Sci. U.S.a. *88*, 10614–10618.

Hayes, R.C., Petrullo, L.A., Huang, H.M., Wallace, S.S., and LeClerc, J.E. (1988). Oxidative damage in DNA. Lack of mutagenicity by thymine glycol lesions. J. Mol. Biol. *201*, 239–246.

Hazra, T.K., IZUMI, T., Boldogh, I., Imhoff, B., Kow, Y.W., Jaruga, P., Dizdaroglu, M., and Mitra, S. (2002a). Identification and characterization of a human DNA glycosylase for repair of modified bases in oxidatively damaged DNA. Proc. Natl. Acad. Sci. U.S.a. *99*, 3523–3528.

Hazra, T.K., Kow, Y.W., Hatahet, Z., Imhoff, B., Boldogh, I., Mokkapati, S.K., Mitra, S., and Izumi, T. (2002b). Identification and characterization of a novel human DNA glycosylase for repair of cytosine-derived lesions. J. Biol. Chem. *277*, 30417–30420.

Holt, I.J., Harding, A.E., and Morgan-Hughes, J.A. (1988). Deletions of muscle mitochondrial DNA in patients with mitochondrial myopathies. Nature *331*, 717–719.

Holt, I.J., and Jacobs, H.T. (2014). Unique features of DNA replication in mitochondria: a functional and evolutionary perspective. Bioessays *36*, 1024–1031.

Hornig-Do, H.-T., Montanari, A., Rozanska, A., Tuppen, H.A., Almalki, A.A., Abg-Kamaludin, D.P., Frontali, L., Francisci, S., Lightowlers, R.N., and Chrzanowska-Lightowlers, Z.M. (2014). Human mitochondrial leucyl tRNA synthetase can suppress non cognate pathogenic mt-tRNA mutations. EMBO Mol Med *6*, 183–193.

Howell, N., Bindoff, L.A., McCullough, D.A., Kubacka, I., Poulton, J., Mackey, D., Taylor, L., and Turnbull, D.M. (1991). Leber hereditary optic neuropathy: identification of the same mitochondrial ND1 mutation in six pedigrees. Am. J. Hum. Genet. *49*, 939–950.

Hu, J., de Souza-Pinto, N.C., Haraguchi, K., Hogue, B.A., Jaruga, P., Greenberg, M.M., Dizdaroglu, M., and Bohr, V.A. (2005). Repair of formamidopyrimidines in DNA involves different glycosylases: role of the OGG1, NTH1, and NEIL1 enzymes. J. Biol. Chem. *280*, 40544–40551.

Humphries, A., and Wright, N.A. (2008). Colonic crypt organization and tumorigenesis. Nat. Rev. Cancer *8*, 415–424.

Ichinoe, A., Behmanesh, M., Tominaga, Y., Ushijima, Y., Hirano, S., Sakai, Y., Tsuchimoto, D., Sakumi, K., Wake, N., and Nakabeppu, Y. (2004). Identification and characterization of two forms of mouse MUTYH proteins encoded by alternatively spliced transcripts. Nucleic Acids Res. *32*, 477–487.

Ikeda, S., Biswas, T., Roy, R., IZUMI, T., Boldogh, I., Kurosky, A., Sarker, A.H., Seki, S., and Mitra, S. (1998). Purification and characterization of human NTH1, a homolog of Escherichia coli endonuclease III - Direct identification of Lys-212 as the active nucleophilic residue. J. Biol. Chem. *273*, 21585–21593.

Ikeda, S., Kohmoto, T., Tabata, R., and Seki, Y. (2002). Differential intracellular localization of the human and mouse endonuclease III homologs and analysis of the sorting signals. DNA Repair *1*, 847–854.

Inoue, K., Nakada, K., Ogura, A., Isobe, K., Goto, Y., Nonaka, I., and Hayashi, J.I. (2000). Generation of mice with mitochondrial dysfunction by introducing mouse mtDNA carrying a deletion into zygotes. Nature Genet. *26*, 176–181.

Itsara, L.S., Kennedy, S.R., Fox, E.J., Yu, S., Hewitt, J.J., Sanchez-Contreras, M., Cardozo-Pelaez, F., and Pallanck, L.J. (2014). Oxidative stress is not a major contributor to somatic mitochondrial DNA mutations. PLoS Genet *10*, e1003974.

Jia, W., and Higgs, P.G. (2008). Codon usage in mitochondrial genomes: distinguishing context-dependent mutation from translational selection. Mol. Biol. Evol. *25*, 339–351.

Johnson, A.A., and Johnson, K.A. (2001). Exonuclease proofreading by human mitochondrial DNA polymerase. J. Biol. Chem. *276*, 38097–38107.

Johnson, A.A., Tsai, Y.C., Graves, S.W., and Johnson, K.A. (2000). Human mitochondrial DNA polymerase holoenzyme: reconstitution and characterization. Biochemistry *39*, 1702–1708.

Johnston, I.G., and Williams, B.P. (2016). Evolutionary Inference across Eukaryotes Identifies Specific Pressures Favoring Mitochondrial Gene Retention. Cell Syst *2*, 101–111.

Ju, Y.S., Alexandrov, L.B., Gerstung, M., Martincorena, I., Nik-Zainal, S., Ramakrishna, M., Davies, H.R., Papaemmanuil, E., Gundem, G., Shlien, A., et al. (2014). Origins and functional consequences of somatic mitochondrial DNA mutations in human cancer. Elife *3*, 415.

Kaguni, L.S. (2004). DNA polymerase gamma, the mitochondrial replicase. Annu. Rev. Biochem. *73*, 293–320.

Karahalil, B., de Souza-Pinto, N.C., Parsons, J.L., Elder, R.H., and Bohr, V.A. (2003). Compromised incision of oxidized pyrimidines in liver mitochondria of mice deficient in NTH1 and OGG1 glycosylases. J. Biol. Chem. *278*, 33701–33707.

Kasiviswanathan, R., and Copeland, W.C. (2011). Ribonucleotide Discrimination and Reverse Transcription by the Human Mitochondrial DNA Polymerase. J. Biol. Chem. *286*, 31490–31500.

Kasiviswanathan, R., Minko, I.G., Lloyd, R.S., and Copeland, W.C. (2013). Translesion synthesis past acrolein-derived DNA adducts by human mitochondrial DNA polymerase γ. J. Biol. Chem. *288*, 14247–14255.

Kaufman, B.A., Durisic, N., Mativetsky, J.M., Costantino, S., Hancock, M.A., Grutter, P., and Shoubridge, E.A. (2007). The mitochondrial transcription factor TFAM coordinates the assembly of multiple DNA molecules into nucleoid-like structures. Mol. Biol. Cell *18*, 3225–3236.

Kazak, L., Reyes, A., and Holt, I.J. (2012). Minimizing the damage: repair pathways keep mitochondrial DNA intact. Nat. Rev. Mol. Cell Biol. *13*, 659–671.

Kennedy, S.R., Salk, J.J., Schmitt, M.W., and Loeb, L.A. (2013). Ultra-sensitive sequencing reveals an age-related increase in somatic mitochondrial mutations that are inconsistent with oxidative damage. PLoS Genet *9*, e1003794.

Khrapko, K., Coller, H.A., André, P.C., Li, X.C., Hanekamp, J.S., and Thilly, W.G. (1997). Mitochondrial mutational spectra in human cells and tissues. Proc Natl Acad Sci USA *94*, 13798–13803.

Kirkwood, T.B. (1977). Evolution of ageing. Nature *270*, 301–304.

Klungland, A., Rosewell, I., Hollenbach, S., Larsen, E., Daly, G., Epe, B., Seeberg, E., Lindahl, T., and Barnes, D.E. (1999). Accumulation of premutagenic DNA lesions in mice defective in removal of oxidative base damage. Proc. Natl. Acad. Sci. U.S.a. *96*, 13300–13305.

Kolesar, J.E., Wang, C.Y., Taguchi, Y.V., Chou, S.-H., and Kaufman, B.A. (2013). Two-dimensional intact mitochondrial DNA agarose electrophoresis reveals the structural complexity of the mammalian mitochondrial genome. Nucleic Acids Res. *41*, e58–e58.

Korhonen, J.A., Gaspari, M., and Falkenberg, M. (2003). TWINKLE Has 5" -> 3" DNA helicase activity and is specifically stimulated by mitochondrial single-stranded DNA-binding protein. J. Biol. Chem. *278*, 48627–48632.

Kornblum, C., Nicholls, T.J., Haack, T.B., Schöler, S., Peeva, V., Danhauser, K., Hallmann, K., Zsurka, G., Rorbach, J., Iuso, A., et al. (2013). Loss-of-function mutations in MGME1 impair mtDNA replication and cause multisystemic mitochondrial disease. Nature Genet. *45*, 214–219.

Kouchakdjian, M., Bodebudi, V., Shibutani, S., Eisenberg, M., Johnson, F., Grollman, A.P., and Patel, D.J. (1991). Nmr Structural Studies of the Ionizing-Radiation Adduct 7-Hydro-8-Oxodeoxyguanosine (8-Oxo-7h-Dg) Opposite Deoxyadenosine in a Dna Duplex - 8-Oxo-7h-Dg(Syn).Da(Anti) Alignment at Lesion Site. Biochemistry *30*, 1403–1412.

Kujoth, G.C., Hiona, A., Pugh, T.D., Someya, S., Panzer, K., Wohlgemuth, S.E., Hofer, T., Seo, A.Y., Sullivan, R., Jobling, W.A., et al. (2005). Mitochondrial DNA mutations, oxidative stress, and apoptosis in mammalian aging. Science *309*, 481–484.

Kukat, C., Davies, K.M., Wurm, C.A., Spåhr, H., Bonekamp, N.A., Kühl, I., Joos, F., Polosa, P.L., Park, C.B., Posse, V., et al. (2015). Cross-strand binding of TFAM to a single mtDNA molecule forms the mitochondrial nucleoid. Proc. Natl. Acad. Sci. U.S.a. *112*, 11288–11293.

Kunkel, T.A. (1985). The mutational specificity of DNA polymerases-alpha and -gamma during in vitro DNA synthesis. J. Biol. Chem. *260*, 12866–12874.

Kunkel, T.A., and Loeb, L.A. (1981). Fidelity of mammalian DNA polymerases. Science *213*, 765–767.

Kunkel, T.A., and Erie, D.A. (2005). DNA mismatch repair. Annu. Rev. Biochem. *74*, 681–710.

Kühl, I., Kukat, C., Ruzzenente, B., Milenkovic, D., Mourier, A., Miranda, M., Koolmeister, C., Falkenberg, M., and Larsson, N.-G. (2014). POLRMT does not transcribe nuclear genes. Nature *514*, E7–E11.

Lakshmipathy, U., and Campbell, C. (1999a). The human DNA ligase III gene encodes nuclear and mitochondrial proteins. Mol. Cell. Biol. *19*, 3869–3876.

Lakshmipathy, U., and Campbell, C. (1999b). Double strand break rejoining by mammalian mitochondrial extracts. Nucleic Acids Res. *27*, 1198–1204.

Larsson, N.G., and Clayton, D.A. (1995). Molecular genetic aspects of human mitochondrial disorders. Annu. Rev. Genet. *29*, 151–178.

Larsson, N.G., Tulinius, M.H., Holme, E., Oldfors, A., Andersen, O., Wahlström, J., and Aasly, J. (1992). Segregation and manifestations of the mtDNA tRNA(Lys) A-->G(8344) mutation of myoclonus epilepsy and ragged-red fibers (MERRF) syndrome. Am. J. Hum. Genet. *51*, 1201–1212.

Larsson, N.G., Wang, J., Wilhelmsson, H., Oldfors, A., Rustin, P., Lewandoski, M., Barsh, G.S., and Clayton, D.A. (1998). Mitochondrial transcription factor A is necessary for mtDNA maintenance and embryogenesis in mice. Nature Genet. *18*, 231–236.

Larsson, N.-G. (2010). Somatic mitochondrial DNA mutations in mammalian aging. Annu. Rev. Biochem. *79*, 683–706.

Lavrov, D.V., and Pett, W. (2016). Animal Mitochondrial DNA as We Do Not Know It: mt-Genome Organization and Evolution in Nonbilaterian Lineages. Genome Biol Evol *8*, 2896–2913.

Ledoux, S.P., Wilson, G.L., Beecham, E.J., Stevnsner, T., Wassermann, K., and Bohr, V.A. (1992). Repair of Mitochondrial-Dna After Various Types of Dna Damage in Chinese-Hamster Ovary Cells. Carcinogenesis *13*, 1967–1973.

Lei, X.G., Zhu, J.-H., Cheng, W.-H., Bao, Y., Ho, Y.-S., Reddi, A.R., Holmgren, A., and Arnér, E.S.J. (2016). Paradoxical Roles of Antioxidant Enzymes: Basic Mechanisms and Health Implications. Physiol. Rev. *96*, 307–364.

Leman, G., Gueguen, N., Desquiret-Dumas, V., Kane, M.S., Wettervald, C., Chupin, S., Chevrollier, A., Lebre, A.-S., Bonnefont, J.-P., Barth, M., et al. (2015). Assembly defects induce oxidative stress in inherited mitochondrial complex I deficiency. Int. J. Biochem. Cell Biol. *65*, 91–103.

Leshinsky-Silver, E., Lev, D., Malinger, G., Shapira, D., Cohen, S., Lerman-Sagie, T., and Saada, A. (2010). Leigh disease presenting in utero due to a novel missense mutation in the mitochondrial DNA-ND3. Mol. Genet. Metab. *100*, 65–70.

Levy, S.E., Waymire, K.G., Kim, Y.L., MacGregor, G.R., and Wallace, D.C. (1999). Transfer of chloramphenicol-resistant mitochondrial DNA into the chimeric mouse. Transgenic Res. *8*, 137–145.

Li, H., and Durbin, R. (2009). Fast and accurate short read alignment with Burrows-Wheeler transform. Bioinformatics *25*, 1754–1760.

Li, H., Handsaker, B., Wysoker, A., Fennell, T., Ruan, J., Homer, N., Marth, G., Abecasis, G., Durbin, R., 1000 Genome Project Data Processing Subgroup (2009). The Sequence Alignment/Map format and SAMtools. Bioinformatics *25*, 2078–2079.

Li, K., and Williams, R.S. (1997). Tetramerization and single-stranded DNA binding properties of native and mutated forms of murine mitochondrial single-stranded DNA-binding proteins. J. Biol. Chem. *272*, 8686–8694.

Li, Y., Huang, T.T., Carlson, E.J., Melov, S., Ursell, P.C., Olson, J.L., Noble, L.J., Yoshimura, M.P., Berger, C., Chan, P.H., et al. (1995). Dilated cardiomyopathy and neonatal lethality in mutant mice lacking manganese superoxide dismutase. Nature Genet. *11*, 376–381.

Lightowlers, R.N., Taylor, R.W., and Turnbull, D.M. (2015). Mutations causing mitochondrial disease: What is new and what challenges remain? Science *349*, 1494–1499.

Lim, K.S., Jeyaseelan, K., Whiteman, M., Jenner, A., and Halliwell, B. (2005). Oxidative damage in mitochondrial DNA is not extensive. Annals of the New York Academy of Sciences *1042*, 210–220.

Lim, S.E., Longley, M.J., and Copeland, W.C. (1999). The mitochondrial p55 accessory subunit of human DNA polymerase gamma enhances DNA binding, promotes processive DNA synthesis, and confers N-ethylmaleimide resistance. J. Biol. Chem. *274*, 38197–38203.

Lim, S.C., Hroudová, J., Van Bergen, N.J., Lopez Sanchez, M.I.G., Trounce, I.A., and McKenzie, M. (2016). Loss of mitochondrial DNA-encoded protein ND1 results in disruption of complex I biogenesis during early stages of assembly. Faseb J. fj.201500137R.

Lin, C.S., Sharpley, M.S., Fan, W., Waymire, K.G., Sadun, A.A., Carelli, V., Ross-Cisneros, F.N., Baciu, P., Sung, E., McManus, M.J., et al. (2012). Mouse mtDNA mutant model of Leber hereditary optic neuropathy. Proc. Natl. Acad. Sci. U.S.a. *109*, 20065–20070.

Lindahl, T. (1993). Instability and decay of the primary structure of DNA. Nature *362*, 709–715.

Liu, P., Qian, L., Sung, J.-S., de Souza-Pinto, N.C., Zheng, L., Bogenhagen, D.F., Bohr, V.A., Wilson, D.M., Shen, B., and Demple, B. (2008). Removal of oxidative DNA damage via FEN1-dependent long-patch base excision repair in human cell mitochondria. Mol. Cell. Biol. *28*, 4975–4987.

Logan, A., Shabalina, I.G., Prime, T.A., Rogatti, S., Kalinovich, A.V., Hartley, R.C., Budd, R.C., Cannon, B., and Murphy, M.P. (2014). In vivo levels of mitochondrial hydrogen peroxide increase with age in mtDNA mutator mice. Aging Cell *13*, 765–768.

Longley, M.J., Nguyen, D., Kunkel, T.A., and Copeland, W.C. (2001). The fidelity of human DNA polymerase gamma with and without exonucleolytic proofreading and the p55 accessory subunit. J. Biol. Chem. *276*, 38555–38562.

Longley, M.J., Prasad, R., Srivastava, D.K., Wilson, S.H., and Copeland, W.C. (1998). Identification of 5 '-deoxyribose phosphate lyase activity in human DNA polymerase gamma and its role in mitochondrial base excision repair in vitro. Proc Natl Acad Sci USA *95*, 12244–12248.

López-Otín, C., Blasco, M.A., Partridge, L., Serrano, M., and Kroemer, G. (2013). The hallmarks of aging. Cell *153*, 1194–1217.

Lustgarten, M.S., Jang, Y.C., Liu, Y., Muller, F.L., Qi, W., Steinhelper, M., Brooks, S.V., Larkin, L., Shimizu, T., Shirasawa, T., et al. (2009). Conditional knockout of Mn-SOD targeted to type IIB skeletal muscle fibers increases oxidative stress and is sufficient to alter aerobic exercise capacity. Am. J. Physiol., Cell Physiol. *297*, C1520–C1532.

Lynch, M. (2010). Rate, molecular spectrum, and consequences of human mutation. Proc. Natl. Acad. Sci. U.S.a. *107*, 961–968.

Lynch, M. (2011). The lower bound to the evolution of mutation rates. Genome Biol Evol *3*, 1107–1118.

Macao, B., Uhler, J.P., Siibak, T., Zhu, X., Shi, Y., Sheng, W., Olsson, M., Stewart, J.B., Gustafsson, C.M., and Falkenberg, M. (2015). The exonuclease activity of DNA polymerase γ is required for ligation during mitochondrial DNA replication. Nat Commun *6*, 7303.

Mandal, S.M., Hegde, M.L., Chatterjee, A., Hegde, P.M., Szczesny, B., Banerjee, D., Boldogh, I., Gao, R., Falkenberg, M., Gustafsson, C.M., et al. (2012). Role of human DNA glycosylase Nei-like 2 (NEIL2) and single strand break repair protein polynucleotide kinase 3'-phosphatase in maintenance of mitochondrial genome. J. Biol. Chem. *287*, 2819–2829.

Marcelino, L.A., André, P.C., Khrapko, K., Coller, H.A., Griffith, J., and Thilly, W.G. (1998). Chemically induced mutations in mitochondrial DNA of human cells: mutational spectrum of N-methyl-N'-nitro-N-nitrosoguanidine. Cancer Res. *58*, 2857–2862.

Marchington, D.R., Barlow, D., and Poulton, J. (1999). Transmitochondrial mice carrying resistance to chloramphenicol on mitochondrial DNA: developing the first mouse model of mitochondrial DNA disease. Nat. Med. *5*, 957–960.

Martin, W., and Müller, M. (1998). The hydrogen hypothesis for the first eukaryote. Nature *392*, 37–41.

Mason, P.A., Matheson, E.C., Hall, A.G., and Lightowlers, R.N. (2003). Mismatch repair activity in mammalian mitochondria. Nucleic Acids Res. *31*, 1052–1058.

McDonald, S.A.C., Greaves, L.C., Gutierrez-Gonzalez, L., Rodriguez-Justo, M., Deheragoda, M., Leedham, S.J., Taylor, R.W., Lee, C.Y., Preston, S.L., Lovell, M., et al. (2008). Mechanisms of field cancerization in the human stomach: the expansion and spread of mutated gastric stem cells. Gastroenterology *134*, 500–510.

McFarland, R., Chinnery, P.F., Blakely, E.L., Schaefer, A.M., Morris, A.A.M., Foster, S.M., Tuppen, H.A.L., Ramesh, V., Dorman, P.J., Turnbull, D.M., et al. (2007). Homoplasmy, heteroplasmy, and mitochondrial dystonia. Neurology *69*, 911–916.

McFarland, R., Swalwell, H., Blakely, E.L., He, L., Groen, E.J., Turnbull, D.M., Bushby, K.M., and Taylor, R.W. (2008). The m.5650G>A mitochondrial tRNAAla mutation is pathogenic and causes a phenotype of pure myopathy. Neuromuscular Disorders *18*, 63–67.

McNulty, J.M., Jerkovic, B., Bolton, P.H., and Basu, A.K. (1998). Replication inhibition and miscoding properties of DNA templates containing a site-specific cis-thymine glycol or urea residue. Chem. Res. Toxicol. *11*, 666–673.

Meitzler, J.L., Antony, S., Wu, Y., Juhasz, A., Liu, H., Jiang, G., Lu, J., Roy, K., and Doroshow, J.H. (2014). NADPH oxidases: a perspective on reactive oxygen species production in tumor biology. Antioxid. Redox Signal. *20*, 2873–2889.

Milenkovic, D., Blaza, J.N., Larsson, N.-G., and Hirst, J. (2017). The Enigma of the Respiratory Chain Supercomplex. Cell Metab. *25*, 765–776.

Milenkovic, D., Matic, S., Kühl, I., Ruzzenente, B., Freyer, C., Jemt, E., Park, C.B., Falkenberg, M., and Larsson, N.-G. (2013). TWINKLE is an essential mitochondrial helicase required for synthesis of nascent D-loop strands and complete mtDNA replication. Hum. Mol. Gen. *22*, 1983–1993.

Minczuk, M., He, J., Duch, A.M., Ettema, T.J., Chlebowski, A., Dzionek, K., Nijtmans, L.G.J., Huynen, M.A., and Holt, I.J. (2011). TEFM (c17orf42) is necessary for transcription of human mtDNA. Nucleic Acids Res. *39*, 4284–4299.

Minczuk, M., Papworth, M.A., Kolasinska, P., Murphy, M.P., and Klug, A. (2006). Sequence-specific modification of mitochondrial DNA using a chimeric zinc finger methylase. Proc. Natl. Acad. Sci. U.S.a. *103*, 19689–19694.

Minowa, O., Arai, T., Hirano, M., Monden, Y., Nakai, S., Fukuda, M., Itoh, M., Takano, H., Hippou, Y., Aburatani, H., et al. (2000). Mmh/Ogg1 gene inactivation results in accumulation of 8-hydroxyguanine in mice. Proc. Natl. Acad. Sci. U.S.a. *97*, 4156–4161.

Miquel, J., Economos, A.C., Fleming, J., and Johnson, J.E. (1980). Mitochondrial role in cell aging. Exp. Gerontol. *15*, 575–591.

Miralles Fusté, J., Shi, Y., Wanrooij, S., Zhu, X., Jemt, E., Persson, Ö., Sabouri, N., Gustafsson, C.M., and Falkenberg, M. (2014). In Vivo Occupancy of Mitochondrial Single-Stranded DNA Binding Protein Supports the Strand Displacement Mode of DNA Replication. PLoS Genet *10*, e1004832.

Montanari, A., De Luca, C., Frontali, L., and Francisci, S. (2010). Aminoacyl-tRNA synthetases are multivalent suppressors of defects due to human equivalent mutations in yeast mt tRNA genes. Biochim. Biophys. Acta *1803*, 1050–1057.

Moraes, C.T., Ricci, E., Bonilla, E., DiMauro, S., and Schon, E.A. (1992). The mitochondrial tRNA(Leu(UUR)) mutation in mitochondrial encephalomyopathy, lactic acidosis, and strokelike episodes (MELAS): genetic, biochemical, and morphological correlations in skeletal muscle. Am. J. Hum. Genet. *50*, 934–949.

Moretton, A., Morel, F., Macao, B., Lachaume, P., Ishak, L., Lefebvre, M., Garreau-Balandier, I., Vernet, P., Falkenberg, M., and Farge, G. (2017). Selective mitochondrial DNA degradation following double-strand breaks. PLoS ONE *12*, e0176795.

Morozov, Y.I., Agaronyan, K., Cheung, A.C.M., Anikin, M., Cramer, P., and Temiakov, D. (2014). A novel intermediate in transcription initiation by human mitochondrial RNA polymerase. Nucleic Acids Res. *42*, 3884–3893.

Morozov, Y.I., Parshin, A.V., Agaronyan, K., Cheung, A.C.M., Anikin, M., Cramer, P., and Temiakov, D. (2015). A model for transcription initiation in human mitochondria. Nucleic Acids Res. *43*, 3726–3735.

Mourier, A., Motori, E., Brandt, T., Lagouge, M., Atanassov, I., Galinier, A., Rappl, G., Brodesser, S., Hultenby, K., Dieterich, C., et al. (2015). Mitofusin 2 is required to maintain mitochondrial coenzyme Q levels. J. Cell Biol. *208*, 429–442.

Muller, H.J. (1964). THE RELATION OF RECOMBINATION TO MUTATIONAL ADVANCE. Mutat. Res. *106*, 2–9.

Murakami, E., Feng, J.Y., Lee, H., Hanes, J., Johnson, K.A., and Anderson, K.S. (2003). Characterization of Novel Reverse Transcriptase and Other RNA-associated Catalytic Activities by Human DNA Polymerase : IMPORTANCE IN MITOCHONDRIAL DNA REPLICATION. J. Biol. Chem. *278*, 36403–36409.

Murphy, M.P. (2009). How mitochondria produce reactive oxygen species. Biochem. J. *417*, 1–13.

Murphy, M.P. (2012). Mitochondrial thiols in antioxidant protection and redox signaling: distinct roles for glutathionylation and other thiol modifications. Antioxid. Redox Signal. *16*, 476–495.

Murphy, M.P., Holmgren, A., Larsson, N.-G., Halliwell, B., Chang, C.J., Kalyanaraman, B., Rhee, S.G., Thornalley, P.J., Partridge, L., Gems, D., et al. (2011). Unraveling the biological roles of reactive oxygen species. Cell Metab. *13*, 361–366.

Müller-Höcker, J. (1989). Cytochrome-c-oxidase deficient cardiomyocytes in the human heart--an age-related phenomenon. A histochemical ultracytochemical study. Am. J. Pathol. *134*, 1167–1173.

Nagaike, T., Suzuki, T., Tomari, Y., Takemoto-Hori, C., Negayama, F., Watanabe, K., and Ueda, T. (2001). Identification and characterization of mammalian mitochondrial tRNA nucleotidyltransferases. J. Biol. Chem. *276*, 40041–40049.

Nakada, K., Sato, A., Sone, H., Kasahara, A., Ikeda, K., Kagawa, Y., Yonekawa, H., and Hayashi, J.-I. (2004). Accumulation of pathogenic DeltamtDNA induced deafness but not diabetic phenotypes in mito-mice. Biochem. Biophys. Res. Commun. *323*, 175–184.

Nakanishi, N., Fukuoh, A., Kang, D., Iwai, S., and Kuraoka, I. (2013). Effects of DNA lesions on the transcription reaction of mitochondrial RNA polymerase: implications for bypass RNA synthesis on oxidative DNA lesions. Mutagenesis *28*, 117–123.

Nass, M.M., and Nass, S. (1963). Intramitochondrial fibers with DNA characteristics. I. Fixation and electron staining reactions. J. Cell Biol. *19*, 593–611.

Nass, M.M., Nass, S., and Afzelius, B.A. (1965). The general occurence of mitochondrial DNA. Exp. Cell Res. *37*, 516–539.

Nesbitt, V., Pitceathly, R.D.S., Turnbull, D.M., Taylor, R.W., Sweeney, M.G., Mudanohwo, E.E., Rahman, S., Hanna, M.G., and McFarland, R. (2013). The UK MRC Mitochondrial Disease Patient Cohort Study: clinical phenotypes associated with the m.3243A>G mutation--implications for diagnosis and management. J. Neurol. Neurosurg. Psychiatr. *84*, 936–938.

Nicholls, T.J., Nadalutti, C.A., Motori, E., Sommerville, E.W., Gorman, G.S., Basu, S., Hoberg, E., Turnbull, D.M., Chinnery, P.F., Larsson, N.-G., et al. (2018). Topoisomerase 3α Is Required for Decatenation and Segregation of Human mtDNA. Molecular Cell *69*, 9–23.e6.

Nielsen, H., Engelbrecht, J., Brunak, S., and Heijne, von, G. (1997). Identification of prokaryotic and eukaryotic signal peptides and prediction of their cleavage sites. Protein Eng. *10*, 1–6.

Nilsen, H., Otterlei, M., Haug, T., Solum, K., Nagelhus, T.A., Skorpen, F., and Krokan, H.E. (1997). Nuclear and mitochondrial uracil-DNA glycosylases are generated by alternative splicing and transcription from different positions in the UNG gene. Nucleic Acids Res. *25*, 750–755.

Nishioka, K., Ohtsubo, T., Oda, H., Fujiwara, T., Kang, D.C., Sugimachi, K., and Nakabeppu, Y. (1999). Expression and differential intracellular localization of two major forms of human 8-oxoguanine DNA glycosylase encoded by alternatively spliced OGG1 mRNAs. Mol. Biol. Cell *10*, 1637–1652.

Nojiri, H., Shimizu, T., Funakoshi, M., Yamaguchi, O., Zhou, H., Kawakami, S., Ohta, Y., Sami, M., Tachibana, T., Ishikawa, H., et al. (2006). Oxidative stress causes heart failure with impaired mitochondrial respiration. J. Biol. Chem. *281*, 33789–33801.

Ohtsubo, T., Nishioka, K., Imaiso, Y., Iwai, S., Shimokawa, H., Oda, H., Fujiwara, T., and Nakabeppu, Y. (2000). Identification of human MutY homolog (hMYH) as a repair enzyme for 2-hydroxyadenine in DNA and detection of multiple forms of hMYH located in nuclei and mitochondria. Nucleic Acids Res. *28*, 1355–1364.

Ojala, D., Montoya, J., and Attardi, G. (1981). tRNA punctuation model of RNA processing in human mitochondria. Nature *290*, 470–474.

Oliveira, M.T., and Kaguni, L.S. (2011). Reduced stimulation of recombinant DNA polymerase γ and mitochondrial DNA (mtDNA) helicase by variants of mitochondrial single-stranded DNA-

binding protein (mtSSB) correlates with defects in mtDNA replication in animal cells. J. Biol. Chem. *286*, 40649–40658.

Olivo, P.D., Van de Walle, M.J., Laipis, P.J., and Hauswirth, W.W. (1983). Nucleotide sequence evidence for rapid genotypic shifts in the bovine mitochondrial DNA D-loop. Nature *306*, 400–402.

Page, M.M., and Stuart, J.A. (2009). In vitro measurement of DNA base excision repair in isolated mitochondria. Methods Mol. Biol. *554*, 213–231.

Pagliarini, D.J., Calvo, S.E., Chang, B., Sheth, S.A., Vafai, S.B., Ong, S.-E., Walford, G.A., Sugiana, C., Boneh, A., Chen, W.K., et al. (2008). A mitochondrial protein compendium elucidates complex I disease biology. Cell *134*, 112–123.

Pascucci, B., Versteegh, A., vanHoffen, A., vanZeeland, A.A., Mullenders, L., and Dogliotti, E. (1997). DNA repair of UV photoproducts and mutagenesis in human mitochondrial DNA. J. Mol. Biol. *273*, 417–427.

Pata, J.D. (2010). Structural diversity of the Y-family DNA polymerases. Biochim. Biophys. Acta *1804*, 1124–1135.

Perli, E., Giordano, C., Pisano, A., Montanari, A., Campese, A.F., Reyes, A., Ghezzi, D., Nasca, A., Tuppen, H.A., Orlandi, M., et al. (2014). The isolated carboxy-terminal domain of human mitochondrial leucyl-tRNA synthetase rescues the pathological phenotype of mitochondrial tRNA mutations in human cells. EMBO Mol Med *6*, 169–182.

Pérez, V.I., Bokov, A., Van Remmen, H., Mele, J., Ran, Q., Ikeno, Y., and Richardson, A. (2009a). Is the oxidative stress theory of aging dead? Biochim. Biophys. Acta *1790*, 1005–1014.

Pérez, V.I., Van Remmen, H., Bokov, A., Epstein, C.J., Vijg, J., and Richardson, A. (2009b). The overexpression of major antioxidant enzymes does not extend the lifespan of mice. Aging Cell *8*, 73–75.

Pinz, K.G., and Bogenhagen, D.F. (2000). Characterization of a catalytically slow AP lyase activity in DNA polymerase gamma and other family A DNA polymerases. J. Biol. Chem. *275*, 12509–12514.

Pogozelski, W.K., and Tullius, T.D. (1998). Oxidative Strand Scission of Nucleic Acids: Routes Initiated by Hydrogen Abstraction from the Sugar Moiety. Chem. Rev. *98*, 1089–1108.

Polyak, K., Li, Y., Zhu, H., Lengauer, C., Willson, J.K., Markowitz, S.D., Trush, M.A., Kinzler, K.W., and Vogelstein, B. (1998). Somatic mutations of the mitochondrial genome in human colorectal tumours. Nature Genet. *20*, 291–293.

Ponamarev, M.V., Longley, M.J., Nguyen, D., Kunkel, T.A., and Copeland, W.C. (2002). Active site mutation in DNA polymerase gamma associated with progressive external ophthalmoplegia causes error-prone DNA synthesis. J. Biol. Chem. *277*, 15225–15228.

Popot, J.L., and de Vitry, C. (1990). On the microassembly of integral membrane proteins. Annu Rev Biophys Biophys Chem *19*, 369–403.

Posse, V., Hoberg, E., Dierckx, A., Shahzad, S., Koolmeister, C., Larsson, N.-G., Wilhelmsson, L.M., Hallberg, B.M., and Gustafsson, C.M. (2014). The amino terminal extension of mammalian mitochondrial RNA polymerase ensures promoter specific transcription initiation. Nucleic Acids Res. *42*, 3638–3647.

Posse, V., Shahzad, S., Falkenberg, M., Hallberg, B.M., and Gustafsson, C.M. (2015). TEFM is a potent stimulator of mitochondrial transcription elongation in vitro. Nucleic Acids Res. *43*, 2615–2624.

Pursell, Z.F., McDonald, J.T., Mathews, C.K., and Kunkel, T.A. (2008). Trace amounts of 8-oxo-dGTP in mitochondrial dNTP pools reduce DNA polymerase gamma replication fidelity. Nucleic Acids Res. *36*, 2174–2181.

Quinlan, A.R., and Hall, I.M. (2010). BEDTools: a flexible suite of utilities for comparing genomic features. Bioinformatics *26*, 841–842.

Raina, S.Z., Faith, J.J., Disotell, T.R., Seligmann, H., Stewart, C.-B., and Pollock, D.D. (2005). Evolution of base-substitution gradients in primate mitochondrial genomes. Genome Res. *15*, 665–673.

Rappsilber, J., Ishihama, Y., and Mann, M. (2003). Stop and go extraction tips for matrix-assisted laser desorption/ionization, nanoelectrospray, and LC/MS sample pretreatment in proteomics. Anal. Chem. *75*, 663–670.

Reddy, P., Ocampo, A., Suzuki, K., Luo, J., Bacman, S.R., Williams, S.L., Sugawara, A., Okamura, D., Tsunekawa, Y., Wu, J., et al. (2015). Selective elimination of mitochondrial mutations in the germline by genome editing. Cell *161*, 459–469.

Reijns, M.A.M., Rabe, B., Rigby, R.E., Mill, P., Astell, K.R., Lettice, L.A., Boyle, S., Leitch, A., Keighren, M., Kilanowski, F., et al. (2012). Enzymatic Removal of Ribonucleotides from DNA Is Essential for Mammalian Genome Integrity and Development. Cell *149*, 1008–1022.

Reyes, A., Gissi, C., Pesole, G., and Saccone, C. (1998). Asymmetrical directional mutation pressure in the mitochondrial genome of mammals. Mol. Biol. Evol. *15*, 957–966.

Richman, T.R., Ermer, J.A., Davies, S.M.K., Perks, K.L., Viola, H.M., Shearwood, A.-M.J., Hool, L.C., Rackham, O., and Filipovska, A. (2015). Mutation in MRPS34 compromises protein synthesis and causes mitochondrial dysfunction. PLoS Genet *11*, e1005089.

Richter, C., Park, J.W., and Ames, B.N. (1988). Normal Oxidative Damage to Mitochondrial and Nuclear-Dna Is Extensive. Proc. Natl. Acad. Sci. U.S.a. *85*, 6465–6467.

Richter, U., Lahtinen, T., Marttinen, P., Myöhänen, M., Greco, D., Cannino, G., Jacobs, H.T., Lietzén, N., Nyman, T.A., and Battersby, B.J. (2013). A mitochondrial ribosomal and RNA decay pathway blocks cell proliferation. Curr. Biol. *23*, 535–541.

Rocha, M.C., Grady, J.P., Grünewald, A., Vincent, A., Dobson, P.F., Taylor, R.W., Turnbull, D.M., and Rygiel, K.A. (2015). A novel immunofluorescent assay to investigate oxidative phosphorylation deficiency in mitochondrial myopathy: understanding mechanisms and improving diagnosis. Sci Rep *5*, 15037.

Roginskaya, M., Bernhard, W.A., Marion, R.T., and Razskazovskiy, Y. (2005). The release of 5-methylene-2-furanone from irradiated DNA catalyzed by cationic polyamines and divalent metal cations. Radiation Research *163*, 85–89.

Roginskaya, M., Mohseni, R., Moore, T.J., Bernhard, W.A., and Razskazovskiy, Y. (2014). Identification of the C4'-oxidized abasic site as the most abundant 2-deoxyribose lesion in radiation-damaged DNA using a novel HPLC-based approach. Radiation Research *181*, 131–137.

Rohlin, A., Wernersson, J., Engwall, Y., Wiklund, L., Björk, J., and Nordling, M. (2009). Parallel sequencing used in detection of mosaic mutations: comparison with four diagnostic DNA screening techniques. Hum. Mutat. *30*, 1012–1020.

Rorbach, J., Yusoff, A.A., Tuppen, H., Abg-Kamaludin, D.P., Chrzanowska-Lightowlers, Z.M.A., Taylor, R.W., Turnbull, D.M., McFarland, R., and Lightowlers, R.N. (2008). Overexpression of human mitochondrial valyl tRNA synthetase can partially restore levels of cognate mt-tRNAVal carrying the pathogenic C25U mutation. Nucleic Acids Res. *36*, 3065–3074.

Rosenquist, T.A., Zharkov, D.O., and Grollman, A.P. (1997). Cloning and characterization of a mammalian 8-oxoguanine DNA glycosylase. Proc. Natl. Acad. Sci. U.S.a. *94*, 7429–7434.

Ross, J.M., Coppotelli, G., Hoffer, B.J., and Olson, L. (2014). Maternally transmitted mitochondrial DNA mutations can reduce lifespan. Sci Rep *4*, 6569.

Ross, J.M., Stewart, J.B., Hagström, E., Brené, S., Mourier, A., Coppotelli, G., Freyer, C., Lagouge, M., Hoffer, B.J., Olson, L., et al. (2013). Germline mitochondrial DNA mutations aggravate ageing and can impair brain development. Nature *501*, 412–415.

Rossignol, R., Faustin, B., Rocher, C., Malgat, M., Mazat, J.P., and Letellier, T. (2003). Mitochondrial threshold effects. Biochem. J. *370*, 751–762.

Russell, O., and Turnbull, D. (2014). Mitochondrial DNA disease-molecular insights and potential routes to a cure. Exp. Cell Res. *325*, 38–43.

Schägger, H., and Pfeiffer, K. (2000). Supercomplexes in the respiratory chains of yeast and mammalian mitochondria. Embo J. *19*, 1777–1783.

Schmitt, M.W., Kennedy, S.R., Salk, J.J., Fox, E.J., Hiatt, J.B., and Loeb, L.A. (2012). Detection of ultra-rare mutations by next-generation sequencing. Proc. Natl. Acad. Sci. U.S.a. *109*, 14508–14513.

Schultz, B.E., and Chan, S.I. (2001). Structures and proton-pumping strategies of mitochondrial respiratory enzymes. Annu Rev Biophys Biomol Struct *30*, 23–65.

Shimizu, A., Mito, T., Hashizume, O., Yonekawa, H., Ishikawa, K., Nakada, K., and Hayashi, J.-I. (2015). G7731A mutation in mouse mitochondrial tRNALys regulates late-onset disorders in transmitochondrial mice. Biochem. Biophys. Res. Commun. *459*, 66–70.

Shimizu, A., Mito, T., Hayashi, C., Ogasawara, E., Koba, R., Negishi, I., Takenaga, K., Nakada, K., and Hayashi, J.-I. (2014). Transmitochondrial mice as models for primary prevention of diseases caused by mutation in the tRNA(Lys) gene. Proc. Natl. Acad. Sci. U.S.a. *111*, 3104–3109.

Shokolenko, I., Venediktova, N., Bochkareva, A., Wilson, G.L., and Alexeyev, M.F. (2009). Oxidative stress induces degradation of mitochondrial DNA. Nucleic Acids Res. *37*, 2539–2548.

Shokolenko, I.N., Fayzulin, R.Z., Katyal, S., McKinnon, P.J., Wilson, G.L., and Alexeyev, M.F. (2013). Mitochondrial DNA ligase is dispensable for the viability of cultured cells but essential for mtDNA maintenance. J. Biol. Chem. *288*, 26594–26605.

Shutt, T.E., and Gray, M.W. (2006). Bacteriophage origins of mitochondrial replication and transcription proteins. Trends Genet. *22*, 90–95.

Sligh, J.E., Levy, S.E., Waymire, K.G., Allard, P., Dillehay, D.L., Nusinowitz, S., Heckenlively, J.R., MacGregor, G.R., and Wallace, D.C. (2000). Maternal germ-line transmission of mutant mtDNAs from embryonic stem cell-derived chimeric mice. Proc. Natl. Acad. Sci. U.S.a. *97*, 14461–14466.

Slupphaug, G., Eftedal, I., Kavli, B., Bharati, S., Helle, N.M., Haug, T., Levine, D.W., and Krokan, H.E. (1995). Properties of a Recombinant Human Uracil-Dna Glycosylase From the Ung Gene and Evidence That Ung Encodes the Major Uracil-Dna Glycosylase. Biochemistry *34*, 128–138.

Slupska, M.M., Luther, W.M., Chiang, J.H., Yang, H.J., and Miller, J.H. (1999). Functional expression of hMYH, a human homolog of the Escherichia coli MutY protein. J. Bacteriol. *181*, 6210–6213.

Smith, D.R., and Keeling, P.J. (2015). Mitochondrial and plastid genome architecture: Reoccurring themes, but significant differences at the extremes. Proc. Natl. Acad. Sci. U.S.a. *112*, 10177–10184.

Sobek, S., Dalla Rosa, I., Pommier, Y., Bornholz, B., Kalfalah, F., Zhang, H., Wiesner, R.J., Kleist-Retzow, von, J.-C., Hillebrand, F., Schaal, H., et al. (2013). Negative regulation of mitochondrial transcription by mitochondrial topoisomerase I. Nucleic Acids Res. *41*, 9848–9857.

Song, S., Pursell, Z.F., Copeland, W.C., Longley, M.J., Kunkel, T.A., and Mathews, C.K. (2005). DNA precursor asymmetries in mammalian tissue mitochondria and possible contribution to mutagenesis through reduced replication fidelity. Proc Natl Acad Sci USA *102*, 4990–4995.

Srivastava, S., and Moraes, C.T. (2001). Manipulating mitochondrial DNA heteroplasmy by a mitochondrially targeted restriction endonuclease. Hum. Mol. Gen. *10*, 3093–3099.

Stadtman, E.R. (2006). Protein oxidation and aging. Free Radic. Res. *40*, 1250–1258.

Stevnsner, T., Nyaga, S., de Souza-Pinto, N.C., van der Horst, G., Gorgels, T., Hogue, B.A., Thorslund, T., and Bohr, V.A. (2002). Mitochondrial repair of 8-oxoguanine is deficient in Cockayne syndrome group B. Oncogene *21*, 8675–8682.

Stewart, J.B., and Chinnery, P.F. (2015). The dynamics of mitochondrial DNA heteroplasmy: implications for human health and disease. Nat. Rev. Genet. *16*, 530–542.

Stewart, J.B., and Larsson, N.-G. (2014). Keeping mtDNA in Shape between Generations. PLoS Genet *10*, e1004670.

Stewart, J.B., Alaei-Mahabadi, B., Sabarinathan, R., Samuelsson, T., Gorodkin, J., Gustafsson, C.M., and Larsson, E. (2015). Simultaneous DNA and RNA Mapping of Somatic Mitochondrial Mutations across Diverse Human Cancers. PLoS Genet *11*, e1005333.

Stewart, J.B., Freyer, C., Elson, J.L., and Larsson, N.-G. (2008a). Purifying selection of mtDNA and its implications for understanding evolution and mitochondrial disease. Nat. Rev. Genet. *9*, 657–662.

Stewart, J.B., Freyer, C., Elson, J.L., Wredenberg, A., Cansu, Z., Trifunovic, A., and Larsson, N.-G. (2008b). Strong purifying selection in transmission of mammalian mitochondrial DNA. PLoS Biol. *6*, e10.

Stojkovič, G., Makarova, A.V., Wanrooij, P.H., Forslund, J., Burgers, P.M., and Wanrooij, S. (2016). Oxidative DNA damage stalls the human mitochondrial replisome. Sci Rep *6*, 28942.

Strassburger, M., Bloch, W., Sulyok, S., Schüller, J., Keist, A.F., Schmidt, A., Wenk, J., Peters, T., Wlaschek, M., Lenart, J., et al. (2005). Heterozygous deficiency of manganese superoxide dismutase results in severe lipid peroxidation and spontaneous apoptosis in murine myocardium in vivo. Free Radic. Biol. Med. *38*, 1458–1470.

Stuart, J.A., Bourque, B.M., de Souza-Pinto, N.C., and Bohr, V.A. (2005). No evidence of mitochondrial respiratory dysfunction in OGG1-null mice deficient in removal of 8-oxodeoxyguanine from mitochondrial DNA. Free Radic. Biol. Med. *38*, 737–745.

Sun, F., Huo, X., Zhai, Y., Wang, A., Xu, J., Su, D., Bartlam, M., and Rao, Z. (2005). Crystal structure of mitochondrial respiratory membrane protein complex II. Cell *121*, 1043–1057.

Sung, J.-S., DeMott, M.S., and Demple, B. (2005). Long-patch base excision DNA repair of 2-deoxyribonolactone prevents the formation of DNA-protein cross-links with DNA polymerase beta. J. Biol. Chem. *280*, 39095–39103.

Suter, M., and Richter, C. (1999). Fragmented mitochondrial DNA is the predominant carrier of oxidized DNA bases. Biochemistry *38*, 459–464.

Suzuki, T., Nagao, A., and Suzuki, T. (2011). Human mitochondrial tRNAs: biogenesis, function, structural aspects, and diseases. Annu. Rev. Genet. *45*, 299–329.

Szczesny, B., Tann, A.W., Longley, M.J., Copeland, W.C., and Mitra, S. (2008). Long patch base excision repair in mammalian mitochondrial genomes. J. Biol. Chem. *283*, 26349–26356.

Tahbaz, N., Subedi, S., and Weinfeld, M. (2012). Role of polynucleotide kinase/phosphatase in mitochondrial DNA repair. Nucleic Acids Res. *40*, 3484–3495.

Takao, M., Aburatani, H., Kobayashi, K., and Yasui, A. (1998). Mitochondrial targeting of human DNA glycosylases for repair of oxidative DNA damage. Nucleic Acids Res. *26*, 2917–2922.

Takao, M., Zhang, Q.M., Yonei, S., and Yasui, A. (1999). Differential subcellular localization of human MutY homolog (hMYH) and the functional activity of adenine : 8-oxoguanine DNA glycosylase. Nucleic Acids Res. *27*, 3638–3644.

Tann, A.W., Boldogh, I., Meiss, G., Qian, W., Van Houten, B., Mitra, S., and Szczesny, B. (2011). Apoptosis Induced by Persistent Single-strand Breaks in Mitochondrial Genome CRITICAL ROLE OF EXOG (5 '-EXO/ENDONUCLEASE) IN THEIR REPAIR. J. Biol. Chem. *286*, 31975–31983.

Tarpey, M.M., Wink, D.A., and Grisham, M.B. (2004). Methods for detection of reactive metabolites of oxygen and nitrogen: in vitro and in vivo considerations. Am. J. Physiol. Regul. Integr. Comp. Physiol. *286*, R431–R444.

Taylor, R.W., Barron, M.J., Borthwick, G.M., Gospel, A., Chinnery, P.F., Samuels, D.C., Taylor, G.A., Plusa, S.M., Needham, S.J., Greaves, L.C., et al. (2003). Mitochondrial DNA mutations in human colonic crypt stem cells. J. Clin. Invest. *112*, 1351–1360.

Terzioglu, M., Ruzzenente, B., Harmel, J., Mourier, A., Jemt, E., López, M.D., Kukat, C., Stewart, J.B., Wibom, R., Meharg, C., et al. (2013). MTERF1 binds mtDNA to prevent transcriptional interference at the light-strand promoter but is dispensable for rRNA gene transcription regulation. Cell Metab. *17*, 618–626.

Tomasetti, C., Li, L., and Vogelstein, B. (2017). Stem cell divisions, somatic mutations, cancer etiology, and cancer prevention. Science *355*, 1330–1334.

Tovar, J., León-Avila, G., Sánchez, L.B., Sutak, R., Tachezy, J., van der Giezen, M., Hernández, M., Müller, M., and Lucocq, J.M. (2003). Mitochondrial remnant organelles of Giardia function in iron-sulphur protein maturation. Nature *426*, 172–176.

Trapp, C., McCullough, A.K., and Epe, B. (2007). The basal levels of 8-oxoG and other oxidative modifications in intact mitochondrial DNA are low even in repair-deficient (Ogg1(-/-)/Csb(-/-)) mice. Mutat. Res. *625*, 155–163.

Trifunovic, A., Hansson, A., Wredenberg, A., Rovio, A.T., Dufour, E., Khvorostov, I., Spelbrink, J.N., Wibom, R., Jacobs, H.T., and Larsson, N.-G. (2005). Somatic mtDNA mutations cause aging phenotypes without affecting reactive oxygen species production. Proc. Natl. Acad. Sci. U.S.a. *102*, 17993–17998.

Trifunovic, A., Wredenberg, A., Falkenberg, M., Spelbrink, J.N., Rovio, A.T., Bruder, C.E., Bohlooly-Y, M., Gidlöf, S., Oldfors, A., Wibom, R., et al. (2004). Premature ageing in mice expressing defective mitochondrial DNA polymerase. Nature *429*, 417–423.

Tsukihara, T., Aoyama, H., Yamashita, E., Tomizaki, T., Yamaguchi, H., Shinzawa-Itoh, K., Nakashima, R., Yaono, R., and Yoshikawa, S. (1996). The whole structure of the 13-subunit oxidized cytochrome c oxidase at 2.8 A. Science *272*, 1136–1144.

Tyynismaa, H., and Suomalainen, A. (2009). Mouse models of mitochondrial DNA defects and their relevance for human disease. EMBO Rep. *10*, 137–143.

Ugalde, C., Hinttala, R., Timal, S., Smeets, R., Rodenburg, R.J.T., Uusimaa, J., van Heuvel, L.P., Nijtmans, L.G.J., Majamaa, K., and Smeitink, J.A.M. (2007). Mutated ND2 impairs mitochondrial complex I assembly and leads to Leigh syndrome. Mol. Genet. Metab. *90*, 10–14.

Valente, W.J., Ericson, N.G., Long, A.S., White, P.A., Marchetti, F., and Bielas, J.H. (2016). Mitochondrial DNA exhibits resistance to induced point and deletion mutations. Nucleic Acids Res. *44*, 8513–8524.

Van Remmen, H., Ikeno, Y., Hamilton, M., Pahlavani, M., Wolf, N., Thorpe, S.R., Alderson, N.L., Baynes, J.W., Epstein, C.J., Huang, T.-T., et al. (2003). Life-long reduction in MnSOD activity results in increased DNA damage and higher incidence of cancer but does not accelerate aging. Physiol. Genomics *16*, 29–37.

Vartanian, V., Lowell, B., Minko, I.G., Wood, T.G., Ceci, J.D., George, S., Ballinger, S.W., Corless, C.L., McCullough, A.K., and Lloyd, R.S. (2006). The metabolic syndrome resulting from a knockout of the NEIL1 DNA glycosylase. Proc. Natl. Acad. Sci. U.S.a. *103*, 1864–1869.

Vermulst, M., Bielas, J.H., Kujoth, G.C., Ladiges, W.C., Rabinovitch, P.S., Prolla, T.A., and Loeb, L.A. (2007). Mitochondrial point mutations do not limit the natural lifespan of mice. Nature Genet. *39*, 540–543.

Vilardo, E., Nachbagauer, C., Buzet, A., Taschner, A., Holzmann, J., and Rossmanith, W. (2012). A subcomplex of human mitochondrial RNase P is a bifunctional methyltransferase--extensive moonlighting in mitochondrial tRNA biogenesis. Nucleic Acids Res. *40*, 11583–11593.

Vögtle, F.-N., Wortelkamp, S., Zahedi, R.P., Becker, D., Leidhold, C., Gevaert, K., Kellermann, J., Voos, W., Sickmann, A., Pfanner, N., et al. (2009). Global analysis of the mitochondrial N-proteome identifies a processing peptidase critical for protein stability. Cell *139*, 428–439.

Wallace, D.C., Singh, G., Lott, M.T., Hodge, J.A., Schurr, T.G., Lezza, A.M., Elsas, L.J., and Nikoskelainen, E.K. (1988). Mitochondrial DNA mutation associated with Leber's hereditary optic neuropathy. Science *242*, 1427–1430.

Wang, D., Kreutzer, D.A., and Essigmann, J.M. (1998). Mutagenicity and repair of oxidative DNA damage: insights from studies using defined lesions. Mutat. Res. *400*, 99–115.

Wang, J., Wilhelmsson, H., Graff, C., Li, H., Oldfors, A., Rustin, P., Brüning, J.C., Kahn, C.R., Clayton, D.A., Barsh, G.S., et al. (1999). Dilated cardiomyopathy and atrioventricular conduction blocks induced by heart-specific inactivation of mitochondrial DNA gene expression. Nature Genet. *21*, 133–137.

Wang, X., and Lavrov, D.V. (2008). Seventeen new complete mtDNA sequences reveal extensive mitochondrial genome evolution within the Demospongiae. PLoS ONE *3*, e2723.

Wanrooij, S., Fusté, J.M., Farge, G., Shi, Y., Gustafsson, C.M., and Falkenberg, M. (2008). Human mitochondrial RNA polymerase primes lagging-strand DNA synthesis in vitro. Proc. Natl. Acad. Sci. U.S.a. *105*, 11122–11127.

Wanrooij, S., Miralles Fusté, J., Stewart, J.B., Wanrooij, P.H., Samuelsson, T., Larsson, N.-G., Gustafsson, C.M., and Falkenberg, M. (2012). In vivo mutagenesis reveals that OriL is essential for mitochondrial DNA replication. EMBO Rep. *13*, 1130–1137.

Watanabe, T., Dewey, M.J., and Mintz, B. (1978). Teratocarcinoma cells as vehicles for introducing specific mutant mitochondrial genes into mice. Proc. Natl. Acad. Sci. U.S.a. *75*, 5113–5117.

Weisiger, R.A., and Fridovich, I. (1973). Mitochondrial superoxide simutase. Site of synthesis and intramitochondrial localization. J. Biol. Chem. *248*, 4793–4796.

Wheeler, L.J., and Mathews, C.K. (2011). Nucleoside Triphosphate Pool Asymmetry in Mammalian Mitochondria. J. Biol. Chem. *286*, 16992–16996.

Wieckowski, M.R., Giorgi, C., Lebiedzinska, M., Duszynski, J., and Pinton, P. (2009). Isolation of mitochondria-associated membranes and mitochondria from animal tissues and cells. Nat Protoc *4*, 1582–1590.

Wiedemann, N., and Pfanner, N. (2017). Mitochondrial Machineries for Protein Import and Assembly. Annu. Rev. Biochem. *86*, 685–714.

Williams, M.D., Van Remmen, H., Conrad, C.C., Huang, T.T., Epstein, C.J., and Richardson, A. (1998). Increased oxidative damage is correlated to altered mitochondrial function in heterozygous manganese superoxide dismutase knockout mice. J. Biol. Chem. *273*, 28510–28515.

Williams, S.L., Mash, D.C., Züchner, S., and Moraes, C.T. (2013). Somatic mtDNA mutation spectra in the aging human putamen. PLoS Genet *9*, e1003990.

Wilm, A., Aw, P.P.K., Bertrand, D., Yeo, G.H.T., Ong, S.H., Wong, C.H., Khor, C.C., Petric, R., Hibberd, M.L., and Nagarajan, N. (2012). LoFreq: a sequence-quality aware, ultra-sensitive variant caller for uncovering cell-population heterogeneity from high-throughput sequencing datasets. Nucleic Acids Res. *40*, 11189–11201.

Wirth, C., Brandt, U., Hunte, C., and Zickermann, V. (2016). Structure and function of mitochondrial complex I. Biochim. Biophys. Acta *1857*, 902–914.

Wittig, I., Carrozzo, R., Santorelli, F.M., and Schägger, H. (2007). Functional assays in high-resolution clear native gels to quantify mitochondrial complexes in human biopsies and cell lines. Electrophoresis *28*, 3811–3820.

Wonnapinij, P., Chinnery, P.F., and Samuels, D.C. (2008). The distribution of mitochondrial DNA heteroplasmy due to random genetic drift. Am. J. Hum. Genet. *83*, 582–593.

Xie, Y.L., Yang, H.J., Cunanan, C., Okamoto, K., Shibata, D., Pan, J., Barnes, D.E., Lindahl, T., McIlhatton, M., Fishel, R., et al. (2004). Deficiencies in mouse Myh and Ogg1 result in tumor predisposition and G to T mutations in codon 12 of the K-Ras oncogene in lung tumors. Cancer Res. *64*, 3096–3102.

Yakes, F.M., and VanHouten, B. (1997). Mitochondrial DNA damage is more extensive and persists longer than nuclear DNA damage in human cells following oxidative stress. Proc. Natl. Acad. Sci. U.S.a. *94*, 514–519.

Yakubovskaya, E., Guja, K.E., Eng, E.T., Choi, W.S., Mejia, E., Beglov, D., Lukin, M., Kozakov, D., and Garcia-Diaz, M. (2014). Organization of the human mitochondrial transcription initiation complex. Nucleic Acids Res. *42*, 4100–4112.

Yang, C., Curth, U., Urbanke, C., and Kang, C. (1997). Crystal structure of human mitochondrial single-stranded DNA binding protein at 2.4 A resolution. Nat. Struct. Biol. *4*, 153–157.

Yasukawa, T., Reyes, A., Cluett, T.J., Yang, M.Y., Bowmaker, M., Jacobs, H.T., and Holt, I.J. (2006). Replication of vertebrate mitochondrial DNA entails transient ribonucleotide incorporation throughout the lagging strand. Embo J. *25*, 5358–5371.

Zhang, H., Meng, L.-H., and Pommier, Y. (2007). Mitochondrial topoisomerases and alternative splicing of the human TOP1mt gene. Biochimie *89*, 474–481.

Zheng, W., Khrapko, K., Coller, H.A., Thilly, W.G., and Copeland, W.C. (2006). Origins of human mitochondrial point mutations as DNA polymerase γ-mediated errors. Mutat. Res. *599*, 11–20.

SUPPLEMENT

A
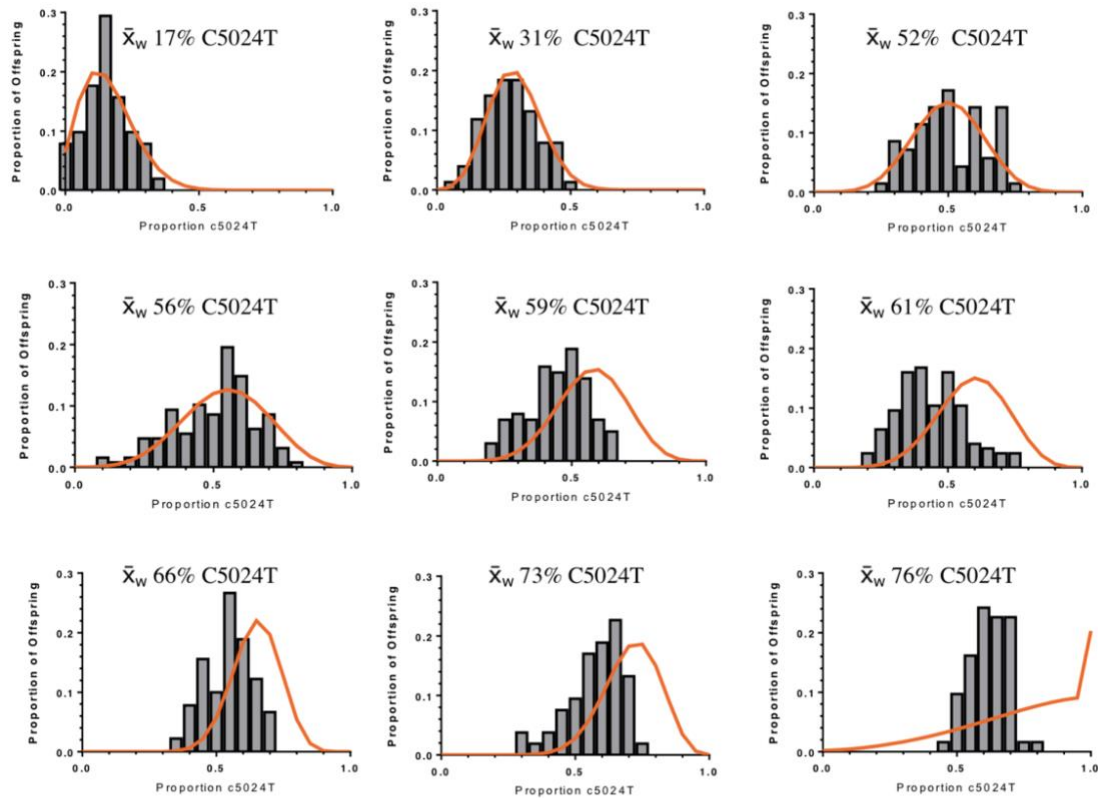
B

Weighted Mean of Mothers ($\bar{x}_w$)	Number of Data Points	Sample Variance	p value
0.174	56	0.00978	0.838
0.308	81	0.00940	0.538
0.515	75	0.01608	0.520
0.559	75	0.02251	0.033
0.590	106	0.01550	< 0.000001
0.608	130	0.01628	< 0.000001
0.663	95	0.00774	< 0.000001
0.725	58	0.01057	< 0.000001
0.756	67	0.00493	< 0.000001

Adapted from Kauppila et al., 2016

Segregation of the C5024T mutation

Test to study the deviation of C5024T mutation segregation from the neutral model with Kimura distribution in pups born to mice with varying levels of C5024T mutation. Orange line represents the expected levels of mutation with neutral distribution and the grey bars represents the observed levels. $\bar{x}_w$ depicts the mother's weighted means. **B** Summary of statistics and variables in the Kimura distribution tests.

114

Mutation loads in Illumina DNA sequencing data. MT.nofilter refers to only quality filtered data and MT.minAF refers to quality filtered data with minimum variant allele frequency threshold of 0.5%.

Sample	Sequenced bp genome	Filtering	Unique variants	Total variant reads	Unique load	Total load
DDDD_2255_L_DNA	990743299	MT.nofilter	287	193602	2.90E-07	0.00019541
DDDD_2255_L_DNA	990743299	MT.minAF	1	751	1.01E-09	7.58E-07
DDDD_2259_L_DNA	1024995331	MT.nofilter	310	231404	3.02E-07	0.00022576
DDDD_2259_L_DNA	1024995331	MT.minAF	2	1074	1.95E-09	1.05E-06
DDDD_2261_L_DNA	996309681	MT.nofilter	153	145441	1.54E-07	0.00014598
DDDD_2261_L_DNA	996309681	MT.minAF	2	3713	2.01E-09	3.73E-06
DDDD_2264_L_DNA	1052633109	MT.nofilter	263	212891	2.50E-07	0.00020225
DDDD_2264_L_DNA	1052633109	MT.minAF	4	14206	3.80E-09	1.35E-05
DDDD_2440_L_DNA	656076857	MT.nofilter	150	89351	2.29E-07	0.00013619
DDDD_2440_L_DNA	656076857	MT.minAF	3	7522	4.57E-09	1.15E-05
DDDD_2443_L_DNA	995720254	MT.nofilter	113	102307	1.13E-07	0.00010275
DDDD_2443_L_DNA	995720254	MT.minAF	2	3251	2.01E-09	3.26E-06
DDDD_2492_L_DNA	938837376	MT.nofilter	102	113580	1.09E-07	0.00012098
DDDD_2492_L_DNA	938837376	MT.minAF	2	1538	2.13E-09	1.64E-06
DDDD_2496_L_DNA	905756315	MT.nofilter	47	90811	5.19E-08	0.00010026
DDDD_2496_L_DNA	905756315	MT.minAF	2	2233	2.21E-09	2.47E-06
PP_2206_H_DNA	471667665	MT.nofilter	72	23653	1.53E-07	5.01E-05
PP_2206_H_DNA	471667665	MT.minAF	3	1156	6.36E-09	2.45E-06
PP_2207_H_DNA	519984130	MT.nofilter	17	6802	3.27E-08	1.31E-05
PP_2207_H_DNA	519984130	MT.minAF	1	420	1.92E-09	8.08E-07
PP_2218_H_DNA	515659450	MT.nofilter	53	17299	1.03E-07	3.35E-05
PP_2218_H_DNA	515659450	MT.minAF	1	407	1.94E-09	7.89E-07
PP_2219_H_DNA	385499623	MT.nofilter	102	22029	2.65E-07	5.71E-05
PP_2219_H_DNA	385499623	MT.minAF	1	269	2.59E-09	6.98E-07
++_2562_H_DNA	667494215	MT.nofilter	102	51532	1.53E-07	7.72E-05
++_2562_H_DNA	667494215	MT.minAF	2	3183	3.00E-09	4.77E-06
++_2583_H_DNA	475485357	MT.nofilter	73	61498	1.54E-07	0.00012934
++_2583_H_DNA	475485357	MT.minAF	2	961	4.21E-09	2.02E-06
PPcreDD_2199_H_DNA	751653946	MT.nofilter	94	36126	1.25E-07	4.81E-05
PPcreDD_2199_H_DNA	751653946	MT.minAF	2	805	2.66E-09	1.07E-06
PPcreDD_2200_H_DNA	775460824	MT.nofilter	101	39181	1.30E-07	5.05E-05
PPcreDD_2200_H_DNA	775460824	MT.minAF	1	540	1.29E-09	6.96E-07
PPcreDD_2201_H_DNA	503892768	MT.nofilter	77	23957	1.53E-07	4.75E-05
PPcreDD_2201_H_DNA	503892768	MT.minAF	1	284	1.98E-09	5.64E-07
PPcreDD_2205_H_DNA	581940318	MT.nofilter	89	24699	1.53E-07	4.24E-05
PPcreDD_2205_H_DNA	581940318	MT.minAF	1	423	1.72E-09	7.27E-07
PPcreDD_2568_H_DNA	752665548	MT.nofilter	453	74776	6.02E-07	9.93E-05
PPcreDD_2568_H_DNA	752665548	MT.minAF	2	1019	2.66E-09	1.35E-06
PPcreDD_2572_H_DNA	792214769	MT.nofilter	54	55529	6.82E-08	7.01E-05
PPcreDD_2572_H_DNA	792214769	MT.minAF	1	560	1.26E-09	7.07E-07
PPcreDD_2573_H_DNA	682734582	MT.nofilter	381	93507	5.58E-07	0.00013696
PPcreDD_2573_H_DNA	682734582	MT.minAF	1	558	1.46E-09	8.17E-07
PPDD_2202_H_DNA	554979413	MT.nofilter	95	30833	1.71E-07	5.56E-05
PPDD_2202_H_DNA	554979413	MT.minAF	2	1474	3.60E-09	2.66E-06
PPDD_2203_H_DNA	269815528	MT.nofilter	35	7868	1.30E-07	2.92E-05
PPDD_2203_H_DNA	269815528	MT.minAF	1	180	3.71E-09	6.67E-07
PPDD_2211_H_DNA	526520976	MT.nofilter	67	19470	1.27E-07	3.70E-05
PPDD_2211_H_DNA	526520976	MT.minAF	1	297	1.90E-09	5.64E-07
PPDD_2212_H_DNA	441553080	MT.nofilter	59	16888	1.34E-07	3.82E-05
PPDD_2212_H_DNA	441553080	MT.minAF	1	231	2.26E-09	5.23E-07
+PDD_2528_H_DNA	601080024	MT.nofilter	376	69024	6.26E-07	0.00011483
+PDD_2528_H_DNA	601080024	MT.minAF	1	516	1.66E-09	8.58E-07
+PDD_2567_H_DNA	483870548	MT.nofilter	90	45230	1.86E-07	9.35E-05
+PDD_2567_H_DNA	483870548	MT.minAF	3	1269	6.20E-09	2.62E-06
+PcreDD_2569_H_DNA	447731038	MT.nofilter	75	44367	1.68E-07	9.91E-05
+PcreDD_2569_H_DNA	447731038	MT.minAF	1	346	2.23E-09	7.73E-07
++_2228_L_DNA	1028043407	MT.nofilter	302	234783	2.94E-07	0.00022838
++_2228_L_DNA	1028043407	MT.minAF	3	2291	2.92E-09	2.23E-06
++_2229_L_DNA	1031260141	MT.nofilter	290	212808	2.81E-07	0.00020636
++_2229_L_DNA	1031260141	MT.minAF	1	771	9.70E-10	7.48E-07

Sample	Sequenced bp genome	Filtering	Unique variants	Total variant reads	Unique load	Total load
++_2235_L_DNA	993407526	MT.nofilter	266	175661	2.68E-07	0.00017683
++_2235_L_DNA	993407526	MT.minAF	1	682	1.01E-09	6.87E-07
++_2267_L_DNA	1017895781	MT.nofilter	271	202164	2.66E-07	0.00019861
++_2267_L_DNA	1017895781	MT.minAF	2	5462	1.96E-09	5.37E-06
PP_2553_L_DNA	964429089	MT.nofilter	100	138828	1.04E-07	0.00014395
PP_2553_L_DNA	964429089	MT.minAF	3	21649	3.11E-09	2.24E-05
PP_2554_L_DNA	946173208	MT.nofilter	98	109803	1.04E-07	0.00011605
PP_2554_L_DNA	946173208	MT.minAF	3	20256	3.17E-09	2.14E-05
++_2558_L_DNA	969596160	MT.nofilter	88	111931	9.08E-08	0.00011544
++_2558_L_DNA	969596160	MT.minAF	1	845	1.03E-09	8.71E-07
++_2559_L_DNA	857623065	MT.nofilter	95	97517	1.11E-07	0.00011371
++_2559_L_DNA	857623065	MT.minAF	1	756	1.17E-09	8.82E-07
++_2561_H_DNA	475554547	MT.nofilter	415	56919	8.73E-07	0.00011969
++_2561_H_DNA	475554547	MT.minAF	1	431	2.10E-09	9.06E-07

Mutation loads in Illumina RNA sequencing data. MT.nofilter refers to only quality filtered data and MT.minAF refers to quality filtered data with minimum variant allele frequency threshold of 0.5%.

Sample	Sequenced bp genome	Filtering	Unique variants	Total variant reads	Unique load	Total load
PP_809_H_RNA	2240608049	MT.nofilter	1362	444934	6.08E-07	0.00019858
PP_809_H_RNA	2240608049	MT.minAF	40	29571	1.79E-08	1.32E-05
PP_904_H_RNA	2490940364	MT.nofilter	1315	440631	5.28E-07	0.00017689
PP_904_H_RNA	2490940364	MT.minAF	37	29677	1.49E-08	1.19E-05
+P_991_H_RNA	2060176685	MT.nofilter	1450	508725	7.04E-07	0.00024693
+P_991_H_RNA	2060176685	MT.minAF	40	37002	1.94E-08	1.80E-05
PPcre_876_H_RNA	2594964539	MT.nofilter	1467	501776	5.65E-07	0.00019337
PPcre_876_H_RNA	2594964539	MT.minAF	46	49972	1.77E-08	1.93E-05
PPcre_879_H_RNA	2736516925	MT.nofilter	1509	491776	5.51E-07	0.00017971
PPcre_879_H_RNA	2736516925	MT.minAF	43	39829	1.57E-08	1.46E-05
PPcre_881_H_RNA	2392594731	MT.nofilter	1357	506637	5.67E-07	0.00021175
PPcre_881_H_RNA	2392594731	MT.minAF	41	35340	1.71E-08	1.48E-05
PPcreDD_1932_H_RNA	1937041377	MT.nofilter	1053	364487	5.44E-07	0.00018817
PPcreDD_1932_H_RNA	1937041377	MT.minAF	35	38934	1.81E-08	2.01E-05
PPcreDD_2021_H_RNA	2388338567	MT.nofilter	1055	336818	4.42E-07	0.00014103
PPcreDD_2021_H_RNA	2388338567	MT.minAF	33	42949	1.38E-08	1.80E-05
PPcreDD_2024_H_RNA	2026299580	MT.nofilter	1048	352328	5.17E-07	0.00017388
PPcreDD_2024_H_RNA	2026299580	MT.minAF	32	41361	1.58E-08	2.04E-05
PPcreDD_2307_H_RNA	2350475233	MT.nofilter	1162	435370	4.94E-07	0.00018523
PPcreDD_2307_H_RNA	2350475233	MT.minAF	35	44365	1.49E-08	1.89E-05
PPDD_1934_H_RNA	1919742567	MT.nofilter	1049	385624	5.46E-07	0.00020087
PPDD_1934_H_RNA	1919742567	MT.minAF	35	40767	1.82E-08	2.12E-05
PPDD_2022_H_RNA	1441985383	MT.nofilter	930	282484	6.45E-07	0.0001959
PPDD_2022_H_RNA	1441985383	MT.minAF	36	38181	2.50E-08	2.65E-05
PPDD_2290_H_RNA	1755139522	MT.nofilter	1055	348177	6.01E-07	0.00019838
PPDD_2290_H_RNA	1755139522	MT.minAF	42	43844	2.39E-08	2.50E-05
PPDD_2306_H_RNA	1952218570	MT.nofilter	1099	371281	5.63E-07	0.00019018
PPDD_2306_H_RNA	1952218570	MT.minAF	38	46342	1.95E-08	2.37E-05

ACKNOWLEDGEMENTS

ERKLÄRUNG

Ich versichere, dass ich die von mir vorgelegte Dissertation selbständig angefertigt, die benutzten Quellen und Hilfsmittel vollständig angegeben und die Stellen der Arbeit − einschließlich Tabellen, Karten und Abbildungen −, die anderen Werken im Wortlaut oder dem Sinn nach entnommen sind, in jedem Einzelfall als Entlehnung kenntlich gemacht habe; dass diese Dissertation noch keiner anderen Fakultät oder Universität zur Prüfung vorgelegen hat; dass sie − abgesehen von unten angegebenen Teilpublikationen − noch nicht veröffentlicht worden ist sowie, dass ich eine solche Veröffentlichung vor Abschluss des Promotionsverfahrens nicht vornehmen werde. Die Bestimmungen der Promotionsordnung sind mir bekannt. Die von mir vorgelegte Dissertation ist von Prof. Dr. Nils-Göran Larsson betreut worden.

Köln, 16.4.2018

_____

Johanna Kauppila

TEILPUBLIKATIONEN

Teilpublikationen

Kauppila JHK*, Baines HL*, Bratic A, Simard ML, Freyer C, Mourier A, Stamp C, Filograna R, Larsson NG, Greaves LC, Stewart JB. (2016) A Phenotype-Driven Approach to Generate Mouse Models with Pathogenic mtDNA Mutations Causing Mitochondrial Disease. *Cell Rep.* 2016 Sep 13;16(11):2980-2990. (*Authors contributed equally to this work)

Kauppila JHK, Bonekamp NA, Mourier A, Isokallio MA, Just A, Kauppila TES, Stewart JB, Larsson NG. Base-excision repair deficiency alone or combined with increased oxidative stress does not lead to an increase in mtDNA point mutations in mice. Submitted.

Weitere Publikationen

Kauppila JH, Stewart JB. Mitochondrial DNA: Radically free of free-radical driven mutations. *Biochim Biophys Acta.* 2015 Nov;1847(11):1354-61.

Kauppila TES, Kauppila JHK, Larsson NG. Mammalian Mitochondria and Aging: An Update. *Cell Metab.* 2017 Jan 10;25(1):57-71.